

Chaperone-mediated protein folding at the nanoscale

Moayed, Fatemeh

DOI

[10.4233/uuid:3447970a-b1e1-4326-b008-679c2cd7e1f8](https://doi.org/10.4233/uuid:3447970a-b1e1-4326-b008-679c2cd7e1f8)

Publication date

2016

Document Version

Final published version

Citation (APA)

Moayed, F. (2016). *Chaperone-mediated protein folding at the nanoscale*. [Dissertation (TU Delft), Delft University of Technology]. <https://doi.org/10.4233/uuid:3447970a-b1e1-4326-b008-679c2cd7e1f8>

Important note

To cite this publication, please use the final published version (if applicable).
Please check the document version above.

Copyright

Other than for strictly personal use, it is not permitted to download, forward or distribute the text or part of it, without the consent of the author(s) and/or copyright holder(s), unless the work is under an open content license such as Creative Commons.

Takedown policy

Please contact us and provide details if you believe this document breaches copyrights.
We will remove access to the work immediately and investigate your claim.

Chaperone-mediated protein folding at the nanoscale

Fatemeh Moayed

Chaperone-mediated protein folding at the nanoscale

Proefschrift

ter verkrijging van de graad van doctor

aan de Technische Universiteit Delft,

op gezag van de Rector Magnificus Prof. ir. K.C.A.M. Luyben,

voorzitter van het College voor Promoties,

in het openbaar te verdedigen op dinsdag 13 september 2016, om 12.30 uur

Door

Fatemeh MOAYED

Master of Science in Chemical Engineering,
University of Tehran,
geboren te Iran

This dissertation has been approved by the:
Promotor Prof. dr. S.J. Tans

Promotion committee:

Rector Magnificus
Prof. dr. S.J. Tans

Chairman
Technische Universiteit Delft

Independent members:

Prof. dr. M.P. Mayer	Universitat Heidelberg, Germany
Prof. dr. P. De Los Rios	Ecole polytechnique federale de Lausanne, Switzerland
Prof. dr. T.J. Aartsma	Universiteit Leiden
Dr. W. Boelens	Radboud Universiteit
Prof. dr. N.H. Dekker	Technische Universiteit Delft
Prof. dr. A.H. Engel	Technische Universiteit Delft, reserved



The research described in this thesis was carried out in the FOM institute AMOLF, Science Park 104, 1098 XG, Amsterdam, The Netherlands. This work is part of the research program of the Foundation for Fundamental Research on Matter (FOM), which is financially supported by the Netherlands Organization for Scientific Research (NWO).

©Fateme Moayed 2016
ISBN 978-94-92323-05-7

An electronic version of this thesis is available at <http://www.amolf.nl> and at <http://repository.tudelft.nl/>. Printed copies can be obtained by request via email to library@amolf.nl.

*To F. Chehel Amirani
and her beloved Hamid*

Contents

List of Figures	iii
List of Tables	v
1 Introduction	1
1.1 introduction	3
1.2 Chaperones advance folding reaction	4
1.3 Structural principal of chaperone machinery	7
1.4 Outline of this thesis	17
2 A polypeptide-DNA hybrid for single molecule pulling experiments	21
2.1 Introduction	23
2.2 Materials and Methods	25
2.3 Results and Discussion	27
2.4 CONCLUSIONS	32
3 Hsp42 preserve proteins in native-like conformation	35
3.1 Introduction	37
3.2 Materials and Methods	39
3.3 Results and Discussion	41
4 HspB6 compacts <i>alphasynuclein</i>	47
4.1 Introduction	49
4.2 Materials and Methods	52
4.3 Results and Discussion	53
5 Aggregation suppression by Hsp33	59
5.1 Introduction	61
5.2 Material and Methods	62
5.3 Results	62
5.4 Discussion	67
Supplementary information	71
6 Hsp90-induced conformational changes in a protein chain	83
6.1 Introduction	85

6.2	Material and Methods	86
6.3	Results	87
6.4	Discussion	93
	Supplementary information	95
7	conclusion	99
	Bibliography	105
	Summary	123
	Samenvatting	125
	Acknowledgments	127
	Publications	133

List of Figures

1.1	Possible mechanisms on how chaperones and enzymes act on their substrate	7
1.2	Table of chaperone families and their functions	8
1.3	Thermal stability of <i>E. Coli</i> chaperones in the presence and absence of nucleotide.	10
1.4	Diagram representation of work flow in the protein factory	13
1.5	Hypothetical design models for the cytosolic and ER stress response	16
2.1	Hierarchical synthesis of protein-DNA hybrids.	27
2.2	Specificity of tST-STN interactions	28
2.3	Mechanical stability analysis.	29
2.4	Dig-AntiDig establishment method controls the stability of linkage	31
2.5	Mechanical stability analysis at constant force.	32
3.1	Function and structure of yeast cytosolic sHsps	38
3.2	Hsp42 suppresses inter-domain misfolding	42
3.3	Hsp42 promotes folding	43
3.4	Hsp42 binds folded structures near native states	44
4.1	α Syn structure, propagation and accumulation	50
4.2	Cartoon representation of the functional HspB6 dimeric structure.	51
4.3	Diverse structures form by small oligomers of α Syn.	54
4.4	HspB6 promotes and stabilizes long-range interactions within α Syn oligomeric structures	54
4.5	Effect of HspB6 on α Syn folding pathways.	56
4.6	HspB6 binds and stabilizes MBP folds	57
4.7	STEM imaging of the interaction between HspB6 and mature α Syn fibrils	57
5.1	Hsp33 suppresses misfolding between domains and promotes native-like folds	64
5.2	Hsp33 prevents folding	65
5.3	Hsp33 binds and destabilizes folded structures	66
5.4	A model to predict the 4MBP refolding in the presence of Hsp33	68
S.1	The predictive model computes the 4MBP refolding in the absence of chaperone	73

S.2	Fitting the data set to describe the refolding of 4MBP, using Boltzmann weights.	76
6.1	HtpG compacts protein chains	88
6.2	HtpG induces small steps in the protein structure	90
6.3	HtpG suppresses the misfolding of Luciferase	91
6.4	HtpG-promoted conformational changes are stimulated by ATP hydrolysis	93
S.1	Characterizing the HtpG-induced conformational change in Luciferase .	96
S.2	HtpG suppresses inter-domain misfolding	97

List of Tables

1.1	Cellular pQM strategies and the action plans of different compartments	14
S.1	Schematic distribution of aggregated monomers in the absence of chaperone.	78
S.2	Schematic distribution of aggregated monomers in the presence of chaperone.	78
S.3	Schematic distribution of unfolded monomers in the presence of chaperone.	78
S.4	Schematic distribution of folded monomers in the presence of chaperonee.	79
S.5	Schematics of 11 different micro-states in the fitting model.	80

CHAPTER **1**

**Functional and design
principles of molecular
chaperones**

Abstract

Proteins are the main commodities within the cell that must fold to a precise three-dimensional structure to actively function. To pass the folding process, and after that, to stay functional and cope the environmental alterations, proteins are assisted by molecular chaperones. Here we provide insights into the structural and functional principles of chaperone systems. This chapter starts with formulating protein folding as a reaction and discusses the role of chaperones in this context. It's followed by an overview of structural principles of chaperone machinery and commenting on structural flexibility and stability under stressful conditions. Finally, and in connection with the structural analysis, the functional principles of chaperone actions will be discussed. We attempt to map the tasks of molecular chaperones at different conditions and over different time scales.

1.1 introduction

Proteins are the building blocks of life that experience vast number of changes. They are made by adding components under minimal geometric constraints in which a component is only connected to two neighboring components. This leaves many degrees of freedom to be fixed at a later stage and extends to distinctive specifications, as follows: 1) The system is flexible: one can construct (e.g. for functioning) and deconstruct (e.g. for transport) at wish 2) The system is prone to errors: there is a risk associated with establishing a connection between two components in the minimally connected system. To make the structure according to a desired design, global measures have to be taken, unless assistance is provided externally. 3) The size of the system varies non-monotonically with the construction time: The minimally connected system takes a large space and needs to be compressed to reach the final design. 4) Two neighboring under-construction systems can get mixed because each takes too much space and the degrees of freedom provide inter-system access.

Folding is the process of transforming proteins from an array of flexible hetero-bricks to the 3D functional structure with a precise layout. This process is accompanied with intensive spontaneous compression. For example, Maltose Binding Protein (MBP) is a middle-size model protein that contains 370 aa and longs 120 nm as an unfolded chain. While the natively folded MBP forms a globular compact structure of 4.4 nm in diameter ($R_g=22$ °Å) [174]. It's interesting to remember that compression is usually an expensive energy-consuming process, as it isn't the preferred direction of normal systems that tend to expand. While here the target tends to compress spontaneously and folding is a downhill movement in the energy landscape [44]. Despite this fact that folding doesn't need external energy source, all polypeptide chains could not easily reach their native states. For many proteins, the low number of geometrical constrains makes the formation of many mistaken interactions possible. These interactions don't satisfy the functional constrains and just launch large roughness in folding pathway. The appearance of many hills and valleys on the way to native state that could kinetically trap polypeptides increases the demand of guided compression.

Chaperones are machines that assist proteins during compression (folding) and decompression (unfolding), accompanied with doing the risk management and quality control. In other terms, guiding (de) compression and facilitating a conformational reaction by suppressing risks are two functions of chaperones. The former seems like a motor function of molecular motors (Box I) while the latter resembles catalytic functions of enzymes (Box II) [136, 205]. An immediate question that arises is whether these "superficial" resemblances show a deeper connection between these systems. These questions have not been thoroughly discussed in the literature.

Here we provide insights into the structural and functional principles of chaperone systems. First we will start with formulating protein folding as a reaction and discuss the role of chaperones in this context. Then we will discuss the structural principles of chaperone machinery and comment on structural flexibility and stability under stressful conditions. Finally, and in connection with the structural analysis, the functional principles of chaperone actions will be discussed. We map the tasks of molecular chaperones at different conditions and over different time scales.

Box I. Molecular motors

Molecular motors are systems able of converting the chemical energy, stored in ATP, into directed motion and mechanical work. Structurally, they are molecular entities that have nanoscale moving parts. Molecular motors are capable of performing different types of motions, such as rectilinear (kinesin, dynein, myosin) or rotational (FoF1-ATP synthase, bacterial flagellum) movement. They are in charge of diverse mechanical functions, like compressing (viral DNA packaging motors), assembling (RNA polymerase, DNA polymerase), cutting (Helicases), compacting and packaging (SMC protein), twisting (AAA proteins), unwinding (Topoisomerase), etc [195]. Some basic principles are as follows:

1- Molecular motors have distinguishable features from macroscopic motors. Due to their small size, their motion is dominated by viscous friction and thermal fluctuations. Gravity and inertia are negligible for these motors and the chemical and mechanical efficiencies are not constrained by any Carnot-like relation [6].

2- For ATP-driven motors, ATP hydrolysis cycle (binding, reaction, and release) induces a sequence of conformational states that is associated with nanoscale motions.

3-Two general mechanisms have been identified to explain how chemical energy converts to force and motion, the Brownian ratchet and the power stroke. A ratchet is a motor that is driven by thermal motion but rectified by chemical reactions, while power-stroke motors directly convert chemical energy of ATP hydrolysis into movement and forces. For ratchets, the reaction acts as a barrier that biases the motion in one direction, whereas for power strokes the reaction creates an irreversible shift that makes the process directional. Brownian ratchet and power stroke motors can be considered as two extreme situations [93].

1.2 Chaperones advance folding reaction

1.2.1 Protein folding as a reaction

Protein folding inherently is a conformational reaction that converts a linear chain of aminoacids (reactant) to a compacted native structure (product). To understand this reaction, we need to know the kinetics (transition states and time scales of inter conversion between them) and the dynamics (how dominant intra- and extra-interactions lead the reactants to the products) of reaction. “Energy landscape” plots the change of internal free energy vs. reaction coordinates and it is a conceptual tool helping to understand both the kinetics and dynamics [45]. Internal free energy represents the summation of all forces that work to drive a single protein molecule to fold, i.e. intra-chain enthalpies and solvent interactions. Reaction coordinates stand for degrees of freedom, so the real energy landscape of protein folding is a multi dimensional surface. However for simplicity, energy landscape usually is projected to a three (or two) dimensional function [45]. To follow how the reaction proceeds in a lower dimensional landscape, one could use progress variables as reaction coordinates. Progress variables describe the closeness of transient states to the native state and could be defined as thermodynamic closeness (based on the difference in energy level)

Box II. Enzymes

Enzymes are biological catalysts that reduce the timescale of otherwise slow biochemical reactions. They fight against entropy by positioning reacting molecules (substrates) on their active sites and compulsorily aligning reacting bonds in the proper orientation. Oxidation, reduction, isomerization, transferring functional groups, hydrolysis, and forming-cleaving covalent bonds are examples of chemical transformations that are performed by enzymes. These molecules are highly specific (optimized for a single reaction) and efficient, e.g. handle $10 - 10^7$ [10] substrate molecules by one active site per second (turnover number). Following items briefly explain some important basis of enzymes' functioning:

1- The specificity of enzymes to their substrates has been described by the "lock and key" model which proposes inflexible shape selectivity between a substrate and the active site of an enzyme. Later this model was revised to the "induced-fit" model considering the structural flexibility of enzyme proteins. More recently, it has been advocated that the enzymes' specificity has roots in stereo-electronic complementarity between the active site of an enzyme and the transition state(s) of a reaction [109].

2- The capacity of an enzyme to increase the rate of its catalyzed reaction is correlated with its ability to reduce the free energy of transition state(s) that separate substrates from products (Fig.1.1). Activating functional groups, dehydrating active sites and aligning substrates in an optimal geometry for reaction are other functionalities that control the efficiency of enzymes.

3- The enzymes' functionalities are mostly linked to their conformational dynamics on different timescales [83]. It has been experimentally and theoretically shown that enzymatic functions are coupled to micro- to millisecond domain motions [85], however recent experimental evidences suggest these collective movements physically originate from fast pico- to nanoseconds atomic fluctuations [84].

or kinetic closeness (how quickly a conformation can transform to the native state). Radius of gyration (R_g), fraction of native contacts (Q), and minimum number of necessary moves to transition from one conformation to another (δ) are some examples of progress variables that the formers are thermodynamic and the latter is a kinetic [27].

The kinetics of reaction could be considered as a diffusive motion on the energy landscape [32]. Under physiological condition the motion starts from upper layer of landscape and biasedly continues downhill toward the global minimum of function, to the native state. The complexity of folding kinetics comes from the fact that the motion doesn't have a constant rate and diffusion coefficient varies point to point. The rate inconstancy originates from the roughness of energy surface and means the motion faces with many hills and valleys from different height and width. From physics point of view, the roughness reveals the fact that there are many competing interactions that all cannot be satisfied at once. This competition has been interpreted as "Frustration". Competing between secondary and tertiary structure is an example of interactions frustrating protein folding. At first glance, frustration is a factor decreasing folding rate and protein stability, but on the other hand frustration is a reason that makes

it possible to escape from kinetic traps and overcome high energy barriers. Kinetic traps represent non-native low energy conformations that structurally are compact and sometimes their lifetime is in the order of folding time [91]. Passing a kinetic trap requires reorganization of intra-chain contact points that involves breaking the nonnative interactions (entropically favorable and enthalpically unfavorable) and in parallel forming the native-like interactions (entropically unfavorable and enthalpically favorable). Recent progresses in single molecule techniques provided the ability of specifying kinetic traps and other local extremums of energy function [132].

1.2.2 Do chaperones play enzymatic role for protein folding?

Chaperones can be defined as external agents that guide the folding process, interact with non-native conformations, and assist the transition to the native state whereas ultimately they do not incorporate into the final structure. This definition resembles catalysts and catalysis. To describe the similarities and dissimilarities between catalysis and chaperoning, one could compare how energy landscape would be influenced by a chaperone match up to a biocatalyst, i.e. an enzyme. Briefly the catalytic power of enzymes comes from stabilizing the transition state(s), or in the other words decreasing the height of energy barrier, between the reactants and the products. This accelerates the progress of reaction, but does not change the inter-states equilibrium [BoxII]. However, interacting with enzyme not only lowers the barrier but also roughens its surface [125]. The roughness comes from the fact that enzymes are also protein molecules that undergo many conformational changes during reaction. This adds on an extra dimension to the energy landscape of enzymatic reactions which assimilates the enzyme's conformational changes [16].

How chaperones affect the energy landscape remains poorly understood. Three discrete scenarios may be considered for chaperoning function, although the action of a specific chaperone could be a combination of different scenarios (Fig.1.1c-1.1e). In the first scenario, the chaperone catalyzes folding reaction by decreasing the energy barrier(s) between the on-pathway states (Fig.1.1c). Within this scenario, the folding rate increases, whereas the equilibrium between the states is unchanged. Interestingly, chaperones are also capable of playing the opposite role and slowing down the folding rate ((Fig.1.1d). This is the second scenario where the chaperone stabilizes the protein states and hence, deepens the minima over the landscape. The change in the energy of minima affects the equilibrium and shifts it towards the stabilized state(s). In the above cases, chaperones do not need external energy while different vital ATP-dependent chaperones have been found in cells (Fig.1.2). The action of ATP-dependent chaperones is assumed to be inducing or changing the directionality of the system (Fig.1.1d). Directionality is gained at the expense of continuous energy consumption and if the energy supply stops, the system ends up in an equilibrium state (see section (1.3.3) for more details). Recent single molecule studies are experimentally distinguishing between different roles of chaperones during protein folding [134]. For example, trigger factor has been suggested to stabilize the transient protein intermediates (second scenario)[135] whereas the prokaryotic Hsp60, GroEL seems to combine the first and third scenarios to function [172].

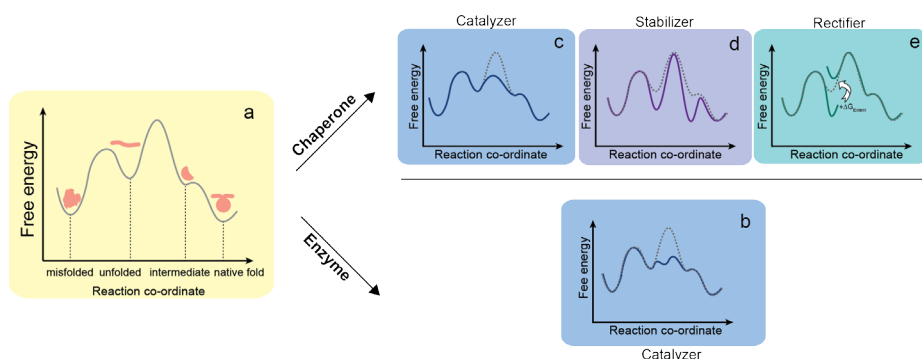


Figure 1.1: Possible mechanisms on how chaperones and enzymes act on their substrate. (a) Schematic representation of a free-energy landscape that proteins explore as they move toward the native-state. (b) Enzymes can influence the energy landscape by changing the energy barriers between the states, while the equilibrium stays unchanged. (c-e) Chaperones may broadly manipulate the energy landscape in different ways. The most common three scenarios are as follows: (c) First, chaperones could act like enzymes and increase the folding rate by lowering the energy barriers between the states. (d) Second, chaperone could slow down folding by deepening energy valleys. In this scenario the equilibrium is changed. (e) Third, chaperones could rectify the protein motion over the energy landscape by using external energy, which moves the system to a non- equilibrium state.

1.3 Structural principal of chaperone machinery

1.3.1 Oligomeric proteins

Chaperones often have quaternary structures [3, 62]. They can be assembled into homo- or hetero-oligomeric configurations and represent diverse symmetrical architectures with two- to seven-fold rotational axis (Fig.1.2). Considering different chaperone families, differentiated based on the molecular weight of subunits, the structures with relatively small and big subunits predominantly function in oligomeric states; whereas the midsize chaperones mainly tend to work monomerically. Small-sized chaperones, like sHsps can gain stability by oligomerization. SHsps mostly interact with substrates via surface and hence, oligomerization may help them to make a tailored multivalent binding surface. The formation of binding sites at the interface of subunits is another advantage of oligomerization that for example is used by the redox regulated chaperone Hsp33.

Oligomerization structurally diversifies the chaperones architectures and provides a basis for functional regulation (Fig.1.2). Some chaperone families oligomerize in different hollow structures, such as clamp-like configurations, pores, and cavities. The clamp-like features, represented by Hsp40s, Prefoldin, and Hsp90s, seem useful for holding non-native protein substrates in a partly protected space until they reach to the native state or are transferred to other chaperone molecules [180]. The internal pores and cavities, represented by Hsp60s and Hsp100s, make chaperones capable of sequestering and encapsulating non-native protein substrates. While confinement in the cavity of Hsp60s kinetically can accelerate folding and thermodynamically

stabilize the native-state, passing through the central pore of Hsp100s results in unfolding and disaggregation. Allosteric regulation and cooperativity effects are other functional rewards for oligomeric proteins. Hsp60s are good examples of oligomeric chaperones with two back-to-back oligomeric rings that show great intra- and inter-ring allosteric regulations [73]. Protein substrates, nucleotides, and co-chaperones are some examples of allosteric effectors for Hsp60 family.

Midsized chaperones, like TF and Hsp70 are commonly assumed to function in monomeric state; however they are also capable of oligomerization [126, 189]. The midsized chaperones may use the same structural principles to interact with protein substrates. Representing clamp-like structures by TF and Hsp70 and allosteric regulation of Hsp70 by ATP binding and hydrolysis are examples of shared principles between monomeric and oligomeric chaperones.

1.3.2 Stability and Flexibility

The capability of chaperones to form oligomeric structures is intimately related to their intrinsic flexibility. Conformational flexibility and dynamic features are more known as the basis for enzymatic catalysis (Box II) and allosteric regulation [68]. As chaperones may complex with diverse protein conformers, it might be important to be flexible. The flexibility usually is obtained at the expense of stability which is paradoxical as they are specialized to function at destabilizing condition, i.e. higher temperatures. Flexible structures appear to be heat sink. They have higher available degrees of freedom that result in an increased uptake of heat energy or higher heat capacity (C_p). Functional proteins, on the other hand, are usually stable folded structures with high molecular packing density and hence smaller degrees of freedom [35]. Within the anti-correlated changes in flexibility and stability [191], unfolded polypeptide chains are extreme examples of having the maximum heat capacities and the minimum functionalities [35]. Here we briefly review the basis of chaperones stability and flexibility.

To estimate the relative stability of chaperones structures, we compared the melting temperature of *E. coli* chaperones with other mesophilic proteins (T_m) (Fig.1.3). Intriguingly, the chaperone molecules do not represent significantly higher stability and even an important chaperone molecule like DnaK is expected to unfold at moderate heat shock temperature ($T_h=42$ °C). However, many studies have shown that binding to the substrates [156] and the nucleotides [129, 155] increase the melting temperature and hence, stabilize the chaperone structures (Fig.1.3). Thus, while stability is not favored structurally, but the external supports are provided to compensate the lack of intrinsic stability and assist chaperones to fulfill the function at higher temperatures.

ATP-dependent chaperone families exhibit a great conformational flexibility. These molecules adopt different conformational states and usually the transitions between the states are coupled with tandem ATPase cycles. This suggests the energy barriers connecting the states are relatively high. Hsp60, Hsp70, and Hsp100 are the main ATP-dependent chaperones whose structural flexibility is apparent from their diverse conformational states and large rotational degrees amongst the domains [139]. Several experimental methods have elucidated different conformational states

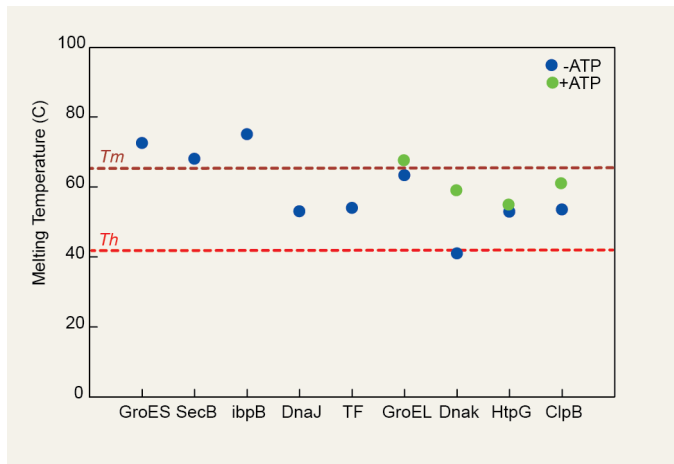


Figure 1.3: Thermal stability of *E. coli* chaperones in the presence and absence of nucleotide. $T_m=65.5$ °C represents the average melting temperature of diverse mesophilic proteins [166], whereas $T_h=42$ °C shows the moderate heat shock temperature. All the melting temperatures have been measured by differential scanning calorimetry [9, 17, 53, 61, 98, 129, 155, 157, 187].

for Hsp90, another ATP-dependent chaperone, that could co-exist in a dynamic equilibrium [111, 177, 183]. This suggests Hsp90 has high structural plasticity and the ATP usage serves to deepen valleys, rather than passing barriers. Section (1.3.3) discusses this subject in detail.

ATP-independent chaperones rather display regulated plastic structures [184]. Dynamic oligomerization and local conformational rearrangements are two examples of structural features of ATP-independent chaperone structures. The role of dynamic oligomerization is best described for the sHsps [77]. IbpB, a sHsp from *E. coli*, forms large oligomers of 100-150 subunits [106] at mild temperatures that dissociate into smaller ones at heat-shock temperatures. The dissociation is reported to be accompanied by an increase in chaperone activity [97]. Yeast Hsp26, similarly undergoes activation (and a conformational change) upon heat stress but the temperature increment does not change its oligomeric state. Hsp26 oligomers are observed to dynamically exchange dimeric subunits with each other [58]. Pea Hsp18.1 transitions from monodisperse dodecamers to polydisperse ensemble of higher-order oligomers (up to 20) when increasing the temperature [179]. Local conformational rearrangements play key role in the functioning of chaperones with clamp-like structural features. An important subset of ATP-independent chaperones including trigger factor (TF), Hsp40, prefoldin, and Skp bind non-native proteins via flexible arm-like binding sites [180]. Using their structural flexibility, the arms rearrange the binding surface to interact with substrates of diverse states and sizes. TF, for example has been shown to interact with unfolded and folded structures [135]. The crystal structures represent an extended TF conformation at the ribosome exit tunnel [55] suitable for interaction with unfolded polypeptide chains [175], whereas it collapses in complex with folded substrates [130] to wrap its arms around them [175].

1.3.3 Energy consumption

Chaperone molecules can be categorized into two classes: active and passive systems. Many questions remain on why these systems use energy (Box I): Do chaperones use ATP binding/hydrolysis or product release to rectify their Brownian motions in one direction or to directly drive the motion? In both scenarios, the motion is coupled by transitions between different conformational states. From the thermodynamics point of view, at equilibrium condition the occupation of each state and the transition rates between them are determined by thermodynamic rules, knowing the depths of valleys and the heights of barriers on energy landscape. However, energy consumption moves these systems to a non-equilibrium state, where the populations of different states are rather controlled by the kinetics of ATP hydrolysis and nucleotide exchange [11]. Deviation from the equilibrium state has different effects on the chaperone functions that are not fully known. Here we discuss the current views of these effects on the function of Hsp60s, Hsp70s, Hsp90s, and Hsp100s families.

Hsp60s or chaperonins are known as complex folding machines (Fig.1.2). The prokaryotic Hsp60, i.e. GroEL is perhaps the most well-known members of chaperonins. It uses the cap-like co-chaperone GroES to encapsulate the substrates within the hollow rings. Each ring of GroEL can adopt at least two allosteric states: a T-state with high affinity for substrates and a R-state with high affinity for nucleotides and GroES. A single molecule study has recently shown in the absence of protein substrate, the populations of T- and R-state are not controlled by the ATP concentration, while the conformational transition between them is triggered by ATP-binding [57]. This study suggests that GroEL slowly releases ADP to tune the population of functional conformers and importantly to ample the cycling time. However, the presence of protein substrate increases the rate of ADP release [70] and, therefore, stabilizes the T-state. The free energy of stabilization of the T-state relative to the R-state has been estimated by Corsepius and Lorimer [36]. They demonstrated that GroEL can do work and overcome a load of 7.8 ± 1.7 kJ/mol upon transition from the T-state to the R-state.

Hsp70s are probably the most characterized ATP-dependent chaperones [140]. They seem to use ATP to gain ultra affinity to their substrates through a none-equilibrium binding process. Two conformations may be considered for Hsp70s: one with an open substrate-binding domain, stabilized by ATP, and the other with a closed substrate-binding domain, stabilized by ADP. Substrates have almost a similar affinity to the both states, while they bind faster to the ATP-state and unbind slower from the ADP-state. The chaperone transitions from one conformation to the other by thermally driven nucleotide exchange (equilibrium processes) or by ATP-hydrolysis (non-equilibrium processes). Substrate binding in the ATP-bound state accelerates ATP hydrolysis and hence, shifts the chaperone to the ADP-bound state, where the dissociation constant is lower by one order of magnitude. This makes an effective dissociation constant for substrate-Hsp70 complex that is noticeably higher than ATP- and ADP-states at cellular ATP and ADP concentrations [41].

Hsp90s are highly flexible conserved chaperones that are abundant in unstressed cells. HtpG, the prokaryotic Hsp90 is the simplest member of this family and it seems to resemble a theoretical Brownian ratchet (Box 1). HtpG is a homodimer that

has the characteristic V-shape of Hsp90s and similarly sample many conformational states, ranging from fully-open to fully-closed states [111, 177, 183]. Single molecule FRET experiments show ATP binds only to the closed state and hence, HtpG has to convert into this state before ATP binding can take place [163]. In other words, the closure of HtpG is driven by thermal fluctuation and ATP acts as a ratchet that binds to direct the biochemical cycle of HtpG. Eukaryotic Hsp90s are more complex systems that own up to 20 co-chaperones [100]. The directionality of these multicomponent machines are under the control of co-chaperones and nucleotides [163], that allow them to organize broader conformational states and possibly to accomplish a multitude of functions.

Hsp100s are among AAA+ (ATPases associated with various cellular activities) family of proteins that carry out important mechanical tasks in the cells [75]. Structurally, these chaperones have one or two AAA+ domains arranged in a hexameric ring with a central pore (Fig.1.2) that is often connected to a barrel-like peptidase. According to the current experimental observations, the AAA+ domain(s) grips an unstructured part of protein substrates and undergoes ATP-driven conformational changes to pull them through the central pore. The force applied on the substrates, mechanically unfolds them and feed them through the proteolytic chambers. This scenario suggests a power stroke machine that hydrolyzes ATP to generate force and hence, perform mechanical work. Single molecule investigations have estimated the performed work by different Hsp100s containing either double [154] or single AAA+ rings [7, 127], almost equals to 5 kBT per hydrolyzed ATP.

1.3.4 Chaperones: the core of the protein quality management system

Protein biogenesis represents a central part of the cellular ‘factory’, and involves many organelles, machineries, processes and products. It allocates 45% of total cellular energy recourses to itself [160] and produces 40-55% of total cellular contents (dry mass) [143, 151, 207]. From an economic (as well as functional) point of view, proteins are the main commodities within a cell. Preserving the cellular capital (and viability), a quality management system has been evolutionarily implemented in the protein factory.

The cellular protein quality management system (pQM) is a combination of two types of strategies, one preventing defects (Quality Assurance: QA) and the other identifying and repairing failures (Quality Control: QC). Quality here could be defined simply as the native-like state of protein structures that is the only criterion meeting all the customers’ needs. pQM is obsessed with quality and commits the protein factory to a “zero defects” philosophy (good enough is not enough) [67].

The protein factory is responsible for the synthesis, folding, and transportation of proteins (Fig.1.4). In eukaryotic cells, which have a high degree of compartmentalization, synthesis mostly takes place in (or at the border of) the cytosol while folding occurs in the cytosol, endoplasmic reticulum (ER) and mitochondria. The condition and personnel of each compartment has been optimized for specific necessities [5, 21]. Many efforts have aimed to identify the molecular staffs, their responsibilities, the processes and the principles underlying the performance of each compartment

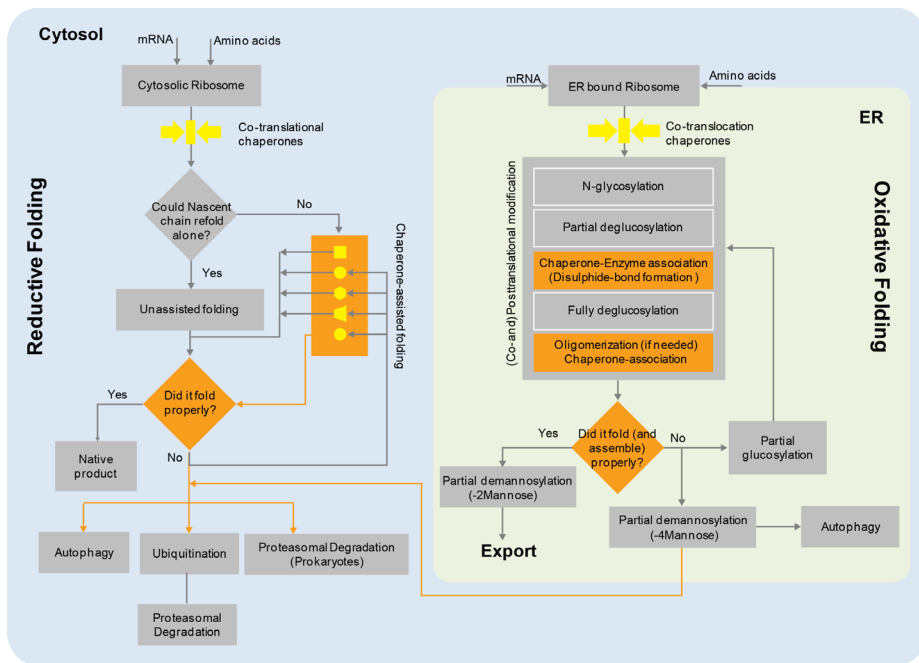


Figure 1.4: Diagram representation of work flows in the protein factory, including the cytosol and the ER. Yellow objects schematically represent molecular chaperones from different families. Orange-marked parts show chaperone-assisted processes.

[176]. Here we review the general cellular strategies to maintain the protein quality and compare the tactics of different compartments to accomplish strategic objectives, stressing the role of chaperones.

pQM strategies are specific and cell-dependent [29]. The common strategies of pQM may be classified as follows: 1) The protein factory is under control at three levels: input, output and processes. 2) Different folding environments have been provided to address the needs of different folding processes. 3) Each and every protein would be conducted to fold in a milieu topologically equivalent to its final work destination. 4) Misfolded structures should not form. 5) Possibly misfolded structures are immediately detected and prioritized to be repaired (in a short timescale). 6) Damaged irreparable proteins are instantly degraded. 7) Environmental and intrinsic risk factors (threatening proteins quality) are monitored to maximize the sustainability of the proteome.

To achieve the strategic objectives of pQM, folding compartments have different tactics (or action plans) (1.1). The cytosol, where synthesis, folding and degradation take place, offers a reducing milieu with high ionic strength to favor reduced thiol groups and disfavor covalent aggregation. The system of quality control in cytosol seems to be chaperone-based (Fig.1.4-Orange pathways). Chaperones might be the most common elements of the quality tool box used by cytosol to prevent, detect and correct failures. Chaperones function may be divided to four types: constraints

Table 1.1: Cellular pQM strategies and the action plans of different compartments

pQM strategies	
Controlling the inputs, outputs and processes of the protein factory	
Providing diverse folding environments to address different needs	
Performing folding in a milieu topologically equivalent to the protein final destination	
Preventing the deployment of misfolded structures	
Repairing salvageable aberrant proteins	
Eliminating the finally damaged proteins that could trigger cell-wide aggregation and proteotoxicity	
Prioritizing repairing to eliminating	
Monitoring the risk factors threading proteins quality to manage changes	
Cytosolic actions	ER actions
Hosting protein synthesis, folding and degradation	Hosting protein folding
	Offering an oxidizing environment to favor disulfide isomerization
Offering a reducing milieu with high ionic strength to favor reduced Thiol groups and disfavor covalent aggregation	Modulating the chaperones roles by adjusting the concentration of free luminal Ca^{++}
Chaperone-based failure-prevention, failure-detection and failure-correction approach	Using co-&post-translational covalent modification to promote proper folding and stabilize folded structure
Retaining non-native proteins along chaperone pathway (rather than being freely diffusive)	Utilizing chaperones, folding catalysts, sugar-modifying enzymes and lectins for failure managing (prevention, detection and correction)
Dynamic adjustment of chaperones (and proteases) levels to cope the changes	Retaining precursor proteins in a location appropriate for their maturation
	Favoring proper assembly by rising subunit concentration
Controlling the environmental stresses by monitoring proteins stability	Applying substrate-dependent extra necessary checkpoints
	Limiting exportation to completely native proteins
Implementing a (feedforward and) feedback control loop to respond to stress (HSR)	Outsourcing the degradation of irreparable proteins
	Implementing a feedback control loop to monitor the folding efficiency (UPR)

(to limit possible interactions and energy pathways), gage blocks (to measure how accurate the protein is folded), disassemblers (to unfold misfolded structures and afford chance of proper re-folding) and tags (to signify misfolded structures for degradation process). Each chaperone family may function as one or more than one type of quality tools (Fig.1.2).

A significant part of the cytosol action plan focuses on stress management. Cytosol, as a system that exchanges mass and energy with the surrounding environment, is affected by environmental conditions. Alteration in the environment state (i.e., temperature or composition) could trigger quality issues. To assure protein quality during stressful conditions, feedforward (in prokaryotic cells) and feedbackward (in prokaryotic and eukaryotic cells) control loops have been implemented in the cytosol (Fig.1.5) [50]. The feedforward loop uses a temperature sensor (mRNA encoding HSF/ $\sigma 32$) to quickly sense environmental alteration [147, 208]. The sensor signal is transduced to the concentration of $\sigma 32$, which the controller unit (heat shock

transcription/translation machinery) can detect. The controller unit, based on the cell type, produces different molecular signals to actuate the process (reductive folding) [165]. The “chaperone signal” is the strongest and most common response of the controller that actuates proper folding and suppresses misfolding and aggregation. The feedbackward loop senses the internal state rather than the external state. In the feedback pathway chaperones play the sensor role, sense the cytosol folding state and based on that transfer the converted signal ($\sigma 32$ /HSF concentration) to the controller. Mechanistically Hsp70-Hsp40 cytosolic chaperones form a complex with $\sigma 32$, so under stressful conditions when chaperones are recruited to act on destabilized proteins, the concentration of (free) $\sigma 32$ increases. When the stress is over (or at normal condition), chaperones sequester extra $\sigma 32$ and also mediate their transfer to the degradation pathway. Quantitative analysis suggests the feedforward mechanism implements a quick and efficient response, while the feedbackward mechanism makes the response economical and robust [50].

ER is the second important section of the protein factory in eukaryotic cells that has a specific action plan (1.1)[4, 51]. Unlike the cytosol, the ER only hosts the folding process, and outsources (synthesis and) degradation. The most differentiating feature of ER is the oxidative lumen, making it similar to the extracellular space and qualifies the ER to promote oxidative folding of secretory proteins (pQM strategies, no. 3). Oxidative folding usually is accompanied with covalent modifications (i.e., glycosylation and disulfide bond formation), so it produces more thermodynamically stable products. It also faces with a stricter failure risk, namely covalently formed aggregates. Compare to cytosol, pQM implements a more severe quality control in ER. It's equipped with a wider range of molecular tools (chaperones, folding catalysts, N-glycan enzymes and lectins) for control checks and only allows fully approved products to go for packaging and secretion. Rejected products (i.e. misfolded proteins) are retained in ER, passing frequent correction cycles until reaching the desired shape (retention-based system) or being transferred to the degradation system. In certain cases, protein products pass extra checkpoints after exiting the ER. If a misfolded protein randomly leaves ER in early secretion stages, it again would be retrieved to ER, otherwise it would be sent to the waste disposal system of secretory pathway (lysosomes).

Similar to the cytosol, pQM designed a stress management system for the ER. Being a retention-based system, using a severe quality control system and lacking an in-house degradation pathway threaten the ER to be overloaded with misfolded products. ER is equipped with a feedbackward control loop, named the UPR (unfolded protein response) that adjusts the folding capacity (Fig.1.5) [171, 198]. The residential chaperones (mostly BiP) in complex with certain transmembrane receptors (IRE1 plus PERK and ATF6 in higher eukaryotes) play the sensor role. Two mechanisms have been suggested for the generation of the sensor signal: by direct binding of misfolded proteins to the receptors (true-positive signal) or by unbinding of receptors from molecular chaperones that already sequestered by misfolded proteins (true-negative signal) [171, 198]. The sensor signal goes to the controller unit (transcription/translation machinery), where three types of actions could be triggered. Similar to the cytosol, the first action is to increase the protein folding capacity by over expressing (ER residential) chaperones. Decreasing the load of system by

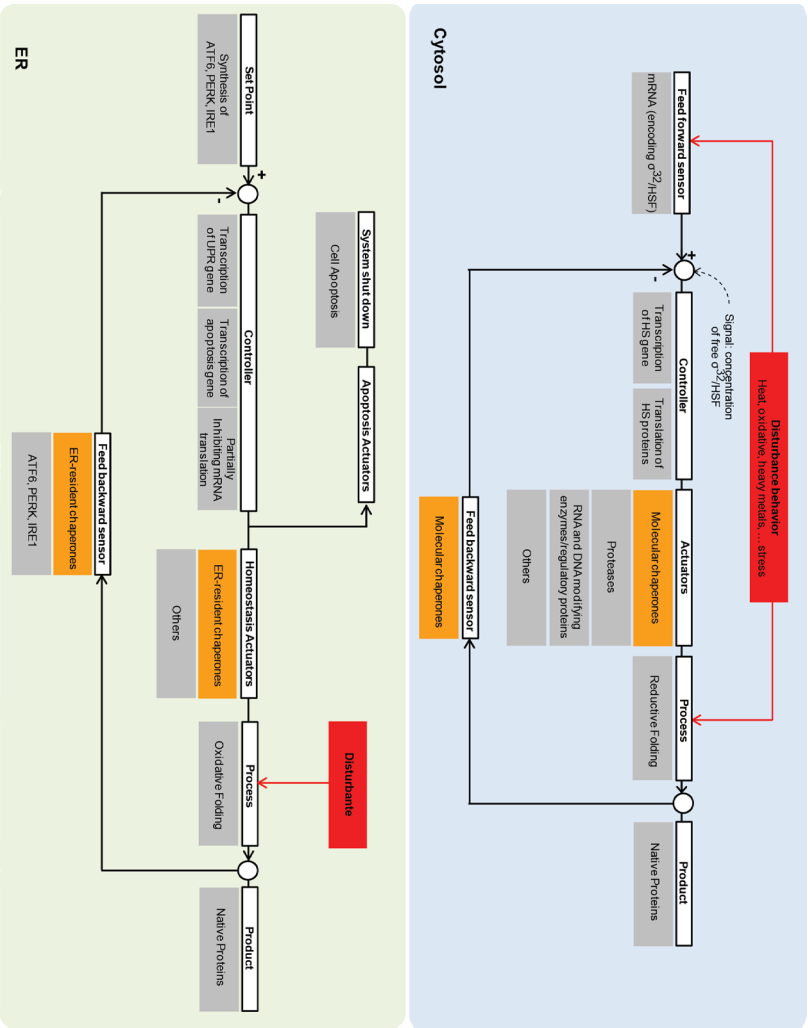


Figure 1.5: Hypothetical design models for the cytosolic and ER stress response. The functional modules, such as the sensors, controller, actuator, and processes consist of various molecular species and their interactions. (a) In the cytosol, a closed loop with feedforward control may consider to protect the proteome, whereas in ER (b), a closed loop may mitigate ER stress.

suppressing protein translation is the second action that controls the feed rate. The first two control actions are homeostatic and attempt to reestablish the ER activity during stressful conditions, but when ER stress cannot be mitigated, the third action, i.e. apoptosis is performed. The commitment of the cell to death is a critical and expensive decision that needs a complex cost-benefit analysis that is not well understood. Although apoptosis could be a tactic to satisfy higher order strategies that take care of organism homeostasis.

1.4 Outline of this thesis

The main goal of this thesis is to probe the protein-chaperone interactions at the single molecule level using force spectroscopy. Single molecule force spectroscopy methods are powerful techniques to study protein folding and the physical principles underlying it. These techniques are capable of observing the formation of folding intermediates, probing their strength and significance, and monitoring the transition between them. This competency makes them promising tools to overcome the difficulty of understanding heterogeneous substrate-chaperone complexes. In chapter 2, we introduce our method by describing a new technical improvement in the single-molecule optical tweezing. This chapter explains the establishment of a new linkage strategy that increases the mechanical stability of protein-DNA tethers and hence, practically improves the efficiency of the experiment.

In chapter 3 and 4, we investigate two different members of the sHsp family from different species. Chapter 3 addresses the molecular basis for the functioning of Hsp42, the general sHsp in the cytosol of *S. cerevisiae* using a protein substrate tends to form amorphous aggregates. Our result reveals Hsp42 suppresses tight intra-domain misfolding and at the same time promotes folding. This chaperone binds to the folded structures and preserves the individual domains in a near-native state. Chapter 4 looks at the action of a human sHsp, HspB6, and an aggregation-prone protein, α -synuclein that forms highly ordered aggregates. We found HspB6, similar to Hsp42, binds to folded structures, although the binding of HspB6 structurally has dissimilar consequences. While binding to Hsp42 destabilizes the protein structures, interacting with HspB6 molecules make stable complexes that withstand high forces.

In chapter 5, we investigate a redox-regulated bacterial chaperone Hsp33. Similar to sHsps, Hsp33 is an ATP-independent chaperone which is known as a holdase binding unfolded polypeptide chains. Using force sensing on single substrate proteins, we showed Hsp33 alters tertiary structure and stability against unfolding. Probing the interaction of repeated protein constructs and Hsp33 molecules, we found Hsp33 promotes native folding over aggregation between repeats. A novel statistical thermodynamics model further helped us to show how this ensemble phenomenon can be predicted from independent data on single-molecule events. Overall, our results in chapter 3-5 represent a new characteristic feature of ATP-independent chaperones that are currently known as holdases. We suggest to consider holdases as chaperones that not only bind and stabilize the unfolded state, but also can essentially do the opposite: to bind tertiary structures and to promote their formation.

In chapter 6, we study the folding of proteins aided by an ATP-dependent

chaperone, namely Hsp90. The Hsp90 family is involved in a wide array of cellular functions, ranging from protection against heat stress to signal transduction and protein trafficking. However, it remains poorly understood how substrate conformation is affected by Hsp90 binding. We addressed this question by measuring conformational states of single protein substrates, Luciferase and Maltose Binding Protein monomers, in the presence of HtpG, the prokaryotic homologue of Hsp90. The results showed HtpG, in an ATP-dependent and step-wise manner, can promote chain structures that are stable in time and against force. Moreover, HtpG action suppresses the formation of Luciferase misfolded states and aggregation between Maltose Binding Protein monomers. This finding is relevant to the many physiological roles of Hsp90.

In chapter 7, as the final chapter, we give a brief conclusion of the represent results in this thesis.

CHAPTER 2

A polypeptide-DNA hybrid
with selective linking
capability applied to single
molecule nano-mechanical
measurements using optical
tweezers

Abstract

Many applications in biosensing, biomaterial engineering and single molecule biophysics require multiple non-covalent linkages between DNA, protein molecules, and surfaces that are specific yet strong. Here, we present a novel method to join proteins and dsDNA molecule at their ends, in an efficient, rapid and specific manner, based on the recently developed linkage between the protein StrepTactin (STN) and the peptide StrepTag II (ST). We introduce a two-step approach, in which we first construct a hybrid between DNA and a tandem of two STs peptides (tST). In a second step, this hybrid is linked to polystyrene bead surfaces and Maltose Binding Protein (MBP) using STN. Furthermore, we show the STN-tST linkage is more stable against forces applied by optical tweezers than the commonly used biotin-Streptavidin (STV) linkage. It can be used in conjunction with Neutravidin (NTV)-biotin linkages to form DNA tethers that can sustain applied forces above 65 pN for tens of minutes in a quarter of the cases. The method is general and can be applied to construct other surface-DNA and protein-DNA hybrids. The reversibility, high mechanical stability and specificity provided by this linking procedure make it highly suitable for single molecule mechanical studies, as well as biosensing and lab on chip applications.

2.1 Introduction

Many experiments involving the manipulation of nucleic acids and proteins require multiple strong linkages that can be established *in-situ*, and can be used together and thus must be specific. For certain applications the molecules involved are immobilized on surfaces, either because the experimental setup requires fixing and controlling the position of the molecular ends or because the molecular phenomenon is measured using surface sensitive techniques [12, 206]. An example of an experiment demanding such supramolecular structures at surfaces includes the binding of liposome-ssDNA hybrids to surface immobilized-DNA in order to detect single nucleotide polymorphism using total internal reflection fluorescence (TIRF) microscopy [74]. Another example is the large-scale positioning of self-assembled functional DNA nanoarrays on surfaces [121], which have been used to construct arrays of quantum dots, proteins, and DNA targets. Supramolecular constructs that link micron-sized beads have been used to engineer molecular wires and to guide the assembly of nano and microstructures [101, 119, 137]. Metal wires have been fabricated by depositing metals on multi-protein and DNA constructs connecting the surfaces of two electrodes [18, 158].

Single molecule techniques such as optical tweezers have enabled the kinetic and thermodynamic characterization of DNA and protein molecules, as well as their interaction [15, 19, 26, 128]. In these methods, two ends of the molecule of interest typically are manipulated by linking them to surfaces, either directly or via molecular handles. Here molecular linkages are preferably established *in-situ* while still being able to sustain large forces over long timescales. Different classes of linkages have been used: Antibody-antigen linkages [15], the family of Streptavidin (STV)-biotin linkages [15, 26, 31], covalent disulfide linkages [26] and covalent binding proteins (HaloTag [7] or SNAP-tag [112]). Each has its own strength and drawbacks. Antibody-antigen interactions are specific and diverse but affinities are affected by buffer condition, pH and temperature, and thus limit the experimental conditions that can be explored. Examples are Myc-AntiMyc and Dig-AntiDig. Moreover, many commercially available antibodies are polyclonal, causing variability in the force that the linkage can sustain. The Dig-AntiDig connection can be stable mechanically, and has therefore been used extensively to link DNA to surfaces [15, 26]. However, this system is less suitable for interfacing to proteins, while as a steroid compound [30] Digoxigenin is also prone to oxidation and thus can deteriorate over time [71]. Disulfide bonds are very strong but involve long preparation times (e.g. 24-48 hr for DNA-protein coupling [25]) and the molecules of interest must be resistant to redox reactions, which limits its applicability.

The biotin-STV interaction is one of the most broadly used, as it is strong and efficiently established. STV is one of the most stable proteins showing high resistance to temperature, urea, guanidine, and proteases [88]. This is in contrast to linkages such as HaloTag or SNAP-tag that unfold, aggregate and encourage nonspecific binding under these harsh conditions [31]. In the presence of SDS, Streptavidin begins to break up into monomers only at temperatures above 60 °C [199]. Because of the usefulness of biotin-STV interactions, efforts have been made to engineer variants and further optimize this system. Avidin is a glycosylated and positively charged protein (at neutral pH) which usually appears as a tetrameric biotin-binding molecule.

Neutravidin (NTV) is a deglycosylated form of Avidin which is developed to decrease non-specific interactions [131]. It has recently been reported that Traptavidin, a mutant of STV, dissociates biotin more than tenfold slower, has increased mechanical strength and improved thermostability [31].

StrepTactin (STN) is another, recently engineered version of STV which has high affinity to biotin and in particular to its peptide ligand ($K_d \approx 1\mu\text{M}$), named StrepTag II (ST), which is 8 amino acids long (WSHPQFEK) [167]. STN has a tetrameric structure that provides four binding sites for ST. Additionally the binding can be reversed by adding Desthiobiotin which can in turn be removed by washing or dialysis. This feature has made the system popular for the purification and detection of proteins by affinity chromatography [167]. Interestingly, STN does have affinity for biotin [167] and ST can bind STV ($K_d \approx 72\mu\text{M}$) at the same surface pocket where biotin is complexed [169] while ST cannot bind Avidin (AV) [168, 169]. Because the biotin binding pockets in NTV and AV have similar surface structures, one may expect that NTV, like AV, is unable to bind ST. It has been reported that the binding affinity of ST to STV can be further increased to nanomolar levels when using multiple tandem STs [23]. It is also shown that in protein purification, having multiple tandem STs improves the binding affinity to STN [167]. ST can be cleaved enzymatically, and the ST-STN interaction is resistant to reducing agents (DTT and mercaptoethanol), denaturing agents (urea 1M), chelating agents (EDTA 50 mM) and detergents (SDS 0.1% and Triton X100 2%). ST is proteolytically stable, biologically inert and does not interfere with membrane translocation or protein folding [167]. The strength of the STN-ST linkage has been recently studied by Atomic Force Microscopy [104, 186], in which one single ST was fused to a protein and STN was anchored to a surface via PEG-based [186] or long protein-based [104] handles. The linkage showed an average dissociation force of 40 and 60 pN at pulling rates of 337 and 200 nm/s, respectively [104, 186]. It is unclear what the dissociation force is for STN that is immobilized directly on the surface, and for multiple ST binding to a single STN.

The properties of the ST-STN linkage show promise for use in optical tweezers experiments and biomaterial engineering. These applications typically require multiple linkages that are specific and strong, which ST-STN can potentially deliver. One challenge is to construct polypeptide-DNA hybrids, which would be required for such an approach. Oligonucleotides (6-16mers) conjugated to a tripeptide have been used for PCR amplification to successfully construct hybrids of DNA with short polypeptides [1]. The feasibility of synthesizing oligonucleotides conjugated to long polypeptides, and using them to amplify DNA segments, remains unclear. We present a straightforward method to efficiently construct end-joined molecular hybrids in a manner that is mechanically stable and specific. To increase the stability [23, 167], our method uses a tandem two STs (tST)-STN linkage to couple two molecules A and B, where both A and B can potentially be either DNA or protein of arbitrary size. Here we demonstrate the coupling of Maltose Binding Protein to a 920 nm long dsDNA. We find that DNA molecules can be coupled well to the surface via tST-STN linkage. The linkage is more stable against applied force than the biotin-STV linkage and can be used in conjunction with biotin-NTV to stably tether DNA and to construct protein-DNA hybrids.

2.2 Materials and Methods

2.2.1 Design and synthesis of the oligo-peptides

A tandem arrangement of two STs (tST: WSHPQFEKWSHPQFEK) was chemically synthesized and was linked to the primer (5'GTC TCG CGC GTT TCG GTG ATG ACG GTG 3') from its 5' end via a linker (-Cys-SMCC-C6) (BioSynthesis Inc.). The product was purified by HPLC and characterized by mass spectrometry (Applied Biosystems Voyager System 2051).

2.2.2 Synthesis of dsDNA-tST

The 2553 bps DNA handles were generated by PCR using Taq DNA polymerase and pUC19 plasmid DNA (New England BioLabs) as template. 500 ng of handles were generated at a time using 50 μ l of PCR reaction. The two types of handles (with and without biotin) were generated using the above oligo-peptide as a forward primer together with the primer 5'TA6GTA6CCGCTCATGAGAC 3' as a reverse (6 is biotin-dT for biotinylated DNA and is "T" for non-biotinylated DNA). Polymerase chain reaction reagents for each 50 microliter reaction volume included: 1 unit of Taq polymerase (New England BioLabs), 5 μ l of 10x PCR buffer (New England BioLabs), 10 pmol of the forward primer and 10 pmol of reverse primer, 5 μ l of 2mM dNTPs (Fermentas), and 50 ng of the plasmid DNA. The PCR profile was as follows: 1 min at 94°C, 30 cycles of 30 s at 94°C, 60 s at 52°C and 3 min at 72°C, finally followed by 10 min at 72°C and a 4°C soak.

2.2.3 Expression and purification of Maltose Binding Protein (MBP)

Two repeats of the sequence encoding the ST (tST) were introduced with PCR at the C-terminus of MBP sequence using plasmid pNN226 as a template. The inserts were ligated with HindIII/NdeI restriction sites to the pET3 vector to generate the expression plasmid. The correctness of the newly made vector was confirmed by double-strand DNA sequencing. *Escherichia coli* strain BL21.1 was used to express the MBP construct. The cells were grown at 37 °C in LB medium containing 100 μ g/ml ampicillin to OD600 0.6-0.7. After induction with 0.5 mM IPTG the cells were further incubated O/N at room temperature and harvested by centrifugation at 5000 rpm, 4 °C for 30 min. The cells were resuspended in cold MBP buffer (20mM Tris-HCl (pH 7.4), 200mM NaCl, 1mM EDTA, 10mM DTT) with 1x protease inhibitor. Lysozyme (Sigma Aldrich) was added to a final concentration of 1 mg/ml and the mixture was kept on ice for 20 min. The cells were lysed by tandem freezing (in liquid nitrogen until fully frozen) and thawing (at 37°C). A little-spatula tip of DNAase I was added to lysate and the mixture was kept on ice for 20 min. Freezing and thawing were repeated until the cloudy suspension became translucent. The extract was clarified by centrifugation (at 15000 rpm, 4 °C for 20 min). The tST-MBP hybrid was purified from the crude cell extract using amylose resin affinity chromatography (New England BioLabs). The clarified extract (10 ml) was transferred to fresh amylose

resin column (1 ml bead volume) and rocked gently at 4 °C for 2 hr. Unbound material then were removed by centrifugation (at 2000 rpm, 4 °C for 1 min). The resin was washed 3x with cold MBP buffer. The protein was eluted from resin by 2.5 ml elution buffer (MBP buffer, 10mM matose).

2.2.4 Gel analysis

DNA samples were analyzed by gel electrophoresis (Figure 1b, 1e and 1f) in non-denaturing 1% agarose gels in 0.5xTBE buffer at 80 V/cm. Agarose gels were stained with ethidium bromide (EtBr). Protein samples were applied on an 8% SDS-PAGE gel in 1x running buffer (190 mM Glycine, 25 mM Tris-base and 0.1% SDS) at 180 V/cm. SDS-PAGE gels were stained with Coomassie InstantBlue (Expedeon Ltd.)

2.2.5 Bead preparation

Carboxylated polystyrene beads (Polysciences Inc.) were covalently linked to protein (STN, NTV, STV and AntiDig) via Carbodiimide reaction (PolyLink Protein Coupling Kit, Polysciences Inc.). Briefly, 25 μ l of 1% (w/v) 1.87 μ m diameter carboxylated polystyrene microspheres were washed twice by pelleting at 13.2 rpm (for 10 min) in a microcentrifuge tube and resuspending in coupling buffer (400 μ l in first wash and 170 μ l in second washing) (PolyLink Protein Coupling Kit, Polysciences Inc.). Then 20 μ l of the freshly prepared EDCA solution (20 mg/ml; prepared by dissolving 1 mg EDCA in 50 μ l coupling buffer) was added to the microparticle suspension and mixed gently end-over-end. After that 20 μ g of desired protein (STN, NTV, STV and AntiDig) was added and mixture was incubated for 1 hr at room temperature with gentle mixing. The mixture then washed two times in 400 μ l storage buffer. Protein-coated beads were stored in 400 μ l storage buffer at 4 °C until use.

DNA-coated microspheres were made by mixing \sim 70 ng of dsDNA molecules and 1 μ l protein-coated beads in 10 μ l HMK (50 mM Hepes, pH 7.6, 100 mM KCl, 5 mM MgCl₂) buffer. After 30 minutes incubation on a rotary mixer (4 °C), the beads were diluted in 400 μ l HMK buffer for use in optical tweezers experiments.

2.2.6 Optical tweezers experiments

The optical tweezers setup has been described elsewhere [15, 133]. Detection of forces on the trapped bead was performed using back focal plane interferometry. Forces were recorded at 50 Hz. Trap stiffness and sensitivity were determined to be 169 ± 24 pN μ m⁻¹ and 2.74 ± 0.24 V μ m⁻¹ respectively. A piezo-nanopositioning stage (Physik Instrumente) was used to move the sample cell and micropipette at a speed of 50 nm s⁻¹. The beads were trapped in a flow chamber consisting of three parallel streams in laminar flow: one containing STN-coated beads; one containing NTV-coated beads with the DNA construct and a central buffer channel in which the measurements were conducted. Structure of the resulting molecular tether is schematically depicted in Figure 2.3a.

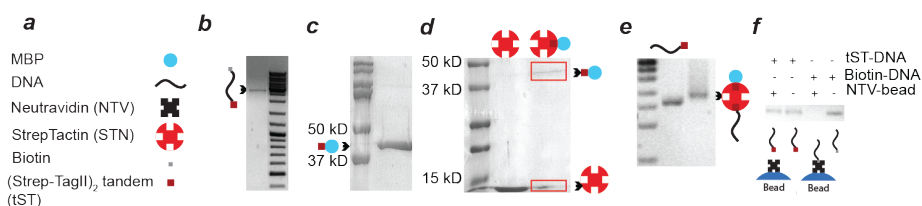


Figure 2.1: Hierarchical synthesis of protein-DNA hybrids. (a) Schematic drawing of the building blocks (b) 1% agarose gel demonstrating construction of tST-DNA-biotin hybrid at 2553 bps (c) SDS-PAGE analysis illustrating production of tST-MBP in E. coli BL21.1 (d) SDS-PAGE characterization of STN-tST-MBP hybrid after amylose column purification. STN decomposes into monomers upon boiling. The schematic represents the expected dominant stoichiometry of the complex but does not exclude the possibility of minor amounts of complexes with other stoichiometries. (e) 1% agarose gel confirming the formation of multi protein-DNA hybrid (f) 1% agarose gel showing the presence and absence of DNA strand in the supernatant of incubated NTV beads by tST-DNA and biotin-DNA respectively. Biotinylated DNA easily binds to NTV, tST labelled DNA does not and remains in the supernatant.

2.3 Results and Discussion

2.3.1 Polypeptide-DNA hybrids

To construct DNA molecules linked to polypeptide (tST-DNA), we used a primer covalently linked to the polypeptide. The PCR conditions were optimized to efficiently amplify the DNA from the template plasmid. By using gradient PCR, and testing several polymerases (Taq Polymerase and Phusion) and different PCR conditions, we found that comparatively long annealing and extension time (1 and 3 min per cycle respectively) allowed efficient amplification, resulting in a final yield of about 500 ng. The resulting construct was then characterized by agarose gel electrophoresis (Fig. 2.1 b) and later tested with an optical tweezers assay (Fig. 2.3a).

2.3.2 Polypeptide-protein hybrids

To synthesize a protein-polypeptide hybrid, we chose Maltose Binding Protein (MBP) as our model protein. MBP is a protein with a variety of applications in biotechnology and biological research, widely used to prototype a variety of biosensing platforms [142]. It is also a model protein for folding and export studies and is commonly used as fusion partner in protein biochemistry [15, 204]. The tST-MBP hybrid was constructed as described before. The hybrid was then tested with SDS-PAGE (Fig. 2.1c), which showed a molecular weight between 37-50 kDa that corresponds well to the molecular weight of tST-MBP (~ 42.5 kDa).

2.3.3 Protein-DNA hybrids

Here we aimed to optimize the specific formation of a hybrid between MBP and DNA using ST-STN linkages (MBP-tST-STN-tST-DNA). Tetrameric structure of STN provides four binding sites for STs which in principle could allow for the formation of

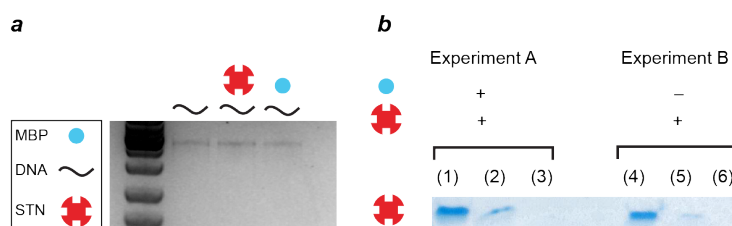


Figure 2.2: Specificity of tST-STN interactions. (a) 1% Agarose gel showing protein-DNA hybrid (shown in Figure 1e) does not form in the absence of ST. Unlabeled DNA (25 ng) was mixed with a large excess of unlabeled MBP (3 μ g) and STN (1 μ g). The mixtures were incubated for 1 hour in 4 $^{\circ}$ C and then loaded in to the 1% agarose gel. In contrast to tST-DNA, unlabeled DNA does not bind STN. In lane 2, the band appears exactly where DNA band appears in lane 1, indicating that DNA and STN do not form a complex. A gel analysis on the mixture of tST-MBP and DNA also results in a band at the same location as DNA alone. This experiment confirms that for the formation of the hybrid shown in Figure 1e, specific tST-STN interactions are required. (b) SDS-PAGE analysis illustrates that STN does not bind to MBP in the absence of ST (Experiment A) and cannot be eluted from amylose resin by maltose (Experiment B). Unlabeled MBP (0.15 mgr) was added to the STN (0.25 mgr) and the mixture was incubated for 1 hour in 4 $^{\circ}$ C (Experiment A). The complex was then combined with amylose resin (for 2 hour in 4 $^{\circ}$ C) and the resin subsequently was washed with maltose. SDS-PAGE showed STN band in master mixture (MBP+STN) (1) and supernatant sample (2), but no band was detected for eluted sample at the same location (3). This confirms that MBP-STN complex does not form specifically, in the absence of ST linkage. This process was repeated with the pure STN solution (Experiment B). The result shows that STN molecules which bind the column nonspecifically cannot be eluted by maltose. Overall, these control experiments indicate that the eluted STN molecules in Figure 1d, were linked via tST to MBP and confirm the chemical structure of the synthesized MBP-tST-STN complex.

MBP-DNA complexes with different stoichiometries. It has been shown that for STV family, a 1:1 stoichiometry can be successfully achieved by using excess amounts of ligand (e.g. biotin) or receptor (e.g. STV or AV) [90, 114].

To make this construct we first mixed STN (1 mg/ml) and tST-MBP (3 mg/ml) in 10:1 ratio. Unbound STN was removed by amylose column purification. tST-MBP bound to amylose column was then eluted with maltose. SDS-PAGE (Fig. 2.1d) showed two bands for eluted sample, with one corresponding to tST-MBP and one to STN only, thus showing that STN had successfully been bound to MBP. The previously constructed tST-DNA was then mixed with a large excess of the MBP-tST-STN hybrid (> 30-fold molar excess) in order to favour binding of a single DNA molecule to each MBP. Agarose gel analysis showed a band distinctly above from tST-DNA, consistent with the formation of a MBP-tST-STN-tST-DNA hybrid (Fig. 2.1e). As expected, MBP-tST-STN-tST-DNA hybrid shows a significantly reduced mobility as compared to tST-DNA due to its larger size and higher molecular weight. The successful formation of the complex hybrid also confirms the chemical structure of the constituting hybrids synthesized in the previous steps and the specificity of the linkages involved (Fig. 2.1e and Fig. 2.2a).

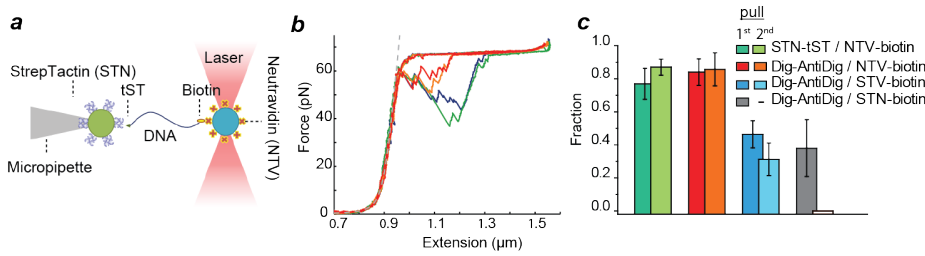


Figure 2.3: Mechanical stability analysis. (a) Optical tweezers setup (b) Force-extension curve of dsDNA showing overstretching at 65 pN, as well as the characteristic step-wise relaxation. The measured DNA stretching curves did not display additional steps that might have arisen from STN unfolding or its detachment from the surface. (c) Fraction of tethers that resisted 60 pN in first and second pull, compared between several commonly used linkage strategies and our proposed linkage strategies based on STN. For the (STN)biotin-DNA-Dig(AntiDig) system, almost all tethers broke at the first pull, and hence the subsequent pulls are not indicated.

2.3.4 Binding specificity

In many experiments, different specific linkages are typically required. For instance, when molecules are tethered between two beads in optical tweezers, each end is often attached with a different linkage. If the binding in these linkages would not be specific, both ends would bind to the same bead. Here we consider the two linkages tST-STN and biotin-NTV. To test whether NTV binds specifically to biotin and not to tST, NTV-coated beads were incubated either with tST-DNA or with biotin-DNA. After 30 min, beads were removed by centrifuging and supernatants were loaded onto an agarose gel (Fig. 2.1f). The results showed that biotinylated DNA bound the beads efficiently, as no DNA could be detected in the supernatant. In contrast, all of the input tST-DNA remained in supernatant, showing no affinity to the beads. These results indicate that NTV binds selectively to biotin and not to tST, which is a central requirement for instance for efficiently tethering tST-DNA-biotin constructs between STN- and NTV-coated beads.

2.3.5 Mechanical stability

To measure the mechanical stability of the linkage between tST and surface-bound STN, we pulled on a single synthesized DNA-tST-STN hybrid using optical tweezers. First, we immobilized tST-DNA-biotin constructs on NTV-coated beads by incubation for biotin-NTV linkage while keeping the tST-end free (Fig. 2.3a). The NTV beads were titrated with varying amount of tST-DNA-biotin so that only few DNA constructs were linked to one bead. Next, the tST-STN linkage to beads coated with STN was established *in-situ*. Pulling curves showed overstretching at 65 pN, which indicated the presence of a single tether, and showed the tST-STN linkage was able to sustain such forces without breaking (Fig. 2.3b). The measured DNA stretching curves did not display additional steps that might have arisen from STN unfolding or its detachment from surface.

Next, we performed a quantitative comparison of the mechanical stability of the

tST-DNA-biotin and the biotin-DNA-Dig constructs. The latter is often used in optical tweezers studies in conjunction with STV- and AntiDig-coated beads [25, 26]. Note that in general, NTV-coated beads have advantages compared to STV-coated beads, given the higher affinity of NTV for biotin [131]. To compare the STN and Dig linkages, we performed pulling experiments on (NTV)biotin-DNA-Dig(Antidig) and (STN)tST-DNA-biotin(NTV) constructs, where the brackets indicate the two beads.

We considered a tether was established when the connections could sustain 20pN. Connections that broke below 20pN were disregarded (a maximum of 20% of tethers broke below 20pN). The constructs were then stretched and relaxed multiple times with a displacement speed of 50 nm/sec to just beyond the DNA overstretching regime at about 65pN, until the connection broke ($N=111$ for the tST construct, $N=230$ for the Dig constructs). We monitored the fraction of tethers able to sustain DNA overstretching, and distinguished first and subsequent pulls. Overall, we found quite similar results for the two constructs, with about 80% of the tethers able to sustain overstretching (Fig. 2.3c). These data suggest that the tST-STN linkage has similar stability against applied force as incubated Dig-AntiDig in the first pull.

The stretching experiments indicated a number of additional points. For instance, for the tST-STN construct, subsequent pulls show a slight increase in the fraction of times the tether survives overstretching (Fig. 2.3c, from 77% to 87%). A possible explanation for this increase could be the proposed bimodality of the ST-STN interaction [104]. The origin of this bimodality is believed to lie in the interaction of a single ST with a single or multiple sites on STN, where the latter is supposed to be somewhat less stable. Next, we performed additional experiments on (STV)biotin-DNA-Dig(AntiDig). These constructs showed an ability to sustain overstretching only in 40% of the cases, about half of what was found when using NTV and AntiDig beads. Thus, the biotin-STV linkage was significantly less stable than the biotin-NTV linkage, consistent with the significantly lower equilibrium binding constant for biotin-NTV [131].

When comparing all three bead-tether-bead constructs, additional observations can be made. First, the biotin-STV linkage makes the third of these constructs weaker than the first two. Thus, the biotin-STV linkage is less stable against applied force than the tST-STN linkage. The comparison also suggests that the biotin-STV linkage is less stable than the Dig-AntiDig linkage, as the latter contributes to the second construct that is very stable. This finding may be surprising, as biotin-STV is considered to be among the most stable linkages. To address this issue we hypothesised that the way in which the linkage is established could be important to stability in these experiments. Linkages can either form by incubation in bulk, during which there is a lot of time (order hour) and the molecules have many degrees of freedom. Linkages can also be formed *in-situ* within the tweezers apparatus by bringing the beads together, during which there is less time and fewer degrees of freedom. The former could yield more stable linkages than the latter.

To test this, we performed experiments where the Dig-AntiDig connection was formed *in-situ*, and contrasted this with earlier results where this connection was formed by bulk incubation. In this experiment, Dig-DNA-biotin molecules were incubated with NTV-coated beads, and the Dig-AntiDig connection was formed

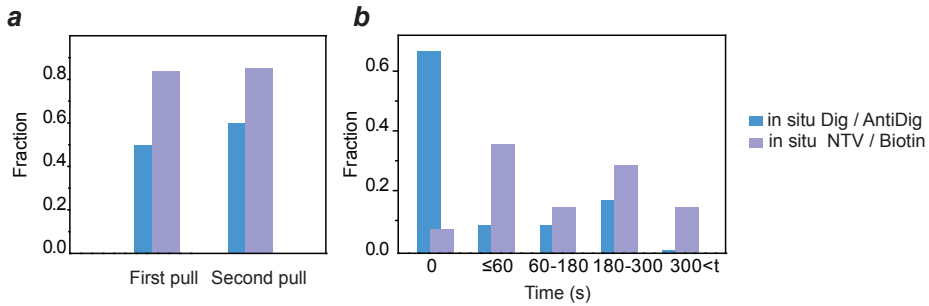


Figure 2.4: Dig-AntiDig establishment method controls the stability of linkage. (a) Fraction of (NTV)biotin-DNA-Dig(AntiDig) tethers that resisted 60 pN in first and second pull, compared between different methods of Dig-AntiDig establishment. Connections can either form by incubation in bulk or *in-situ* within the tweezers apparatus by bringing the beads together. In blue bars, Dig-DNA-biotin molecules were incubated with NTV-coated beads, and the Dig-AntiDig connection was formed *in-situ*. In purple bars, Dig-DNA-biotin molecules were incubated with AntiDig-coated beads, and the biotin-NTV connection was formed *in-situ*. The statistics show a reduction in the fraction of survived tethers (both in the first and second pull) when Dig-AntiDig linkage formed *in-situ*. (b) Histogram of unbinding time of a tethered (NTV)biotin-DNA-Dig(AntiDig) held at overstretching, compared between different methods of Dig-AntiDig establishment. Linkages can either form by incubation in bulk or *in-situ* within the tweezers. In blue bars, Dig-DNA-biotin molecules were incubated with NTV-coated beads, and the Dig-AntiDig connection was formed *in-situ* within the tweezers. In purple bars, Dig-DNA-biotin molecules were incubated with AntiDig-coated beads, and the biotin-NTV connection was formed *in-situ*. The statistics show most of the *in-situ* formed Dig-AntiDig connections broke immediately (blue bars), while a few number of Dig-AntiDig linkages which formed by incubation (purple bars), broke within that time.

in-situ within the tweezers. Compared to the bulk-incubated Dig connection, the results indeed showed a significant reduction in the fraction of tethers that survived overstretching: a 34% reduction in the first pull and a 25% reduction in the second pull (Fig. 2.4a). To further investigate this issue we measured the time at which the tethers broke during sustained overstretching. For incubated Dig-AntiDig linkages, 7% of tethers broke in less than a second, while for *in-situ* established Dig-AntiDig linkages, 67% of tethers broke within that time (Figure 2.4b). The same unbinding time has reported for fishing Dig-AntiDig connection where DNA molecules were bound to the STV-coated beads [59]. Thus, the Dig-AntiDig connection is significantly weaker when established *in-situ*. The type of AntiDig antibodies used may also affect stability. Polyclonal AntiDig antibodies are often used in single molecule pulling experiments [25], which could well bring significant variability in stability. The rupture force for a monoclonal AntiDig antibody was reported to be less than 20 pN for the pulling rate used in our study [152]. By incubation there may be a bias towards stronger Dig-AntiDig junctions. Importantly, in the experiments on the (STN)tST-DNA-biotin(NTV)construct (Fig. 2.3C), the tST-STN linkage was formed *in-situ*, showing that this linkage is not only stable but can also be formed rapidly.

Finally, a construct consisting of (STN)biotin-DNA-Dig(AntiDig) was able to sustain overstretching also in about 40% of the cases in the first pull. In these experiments, none of the tethers could sustain 65 pN in the second pull. The

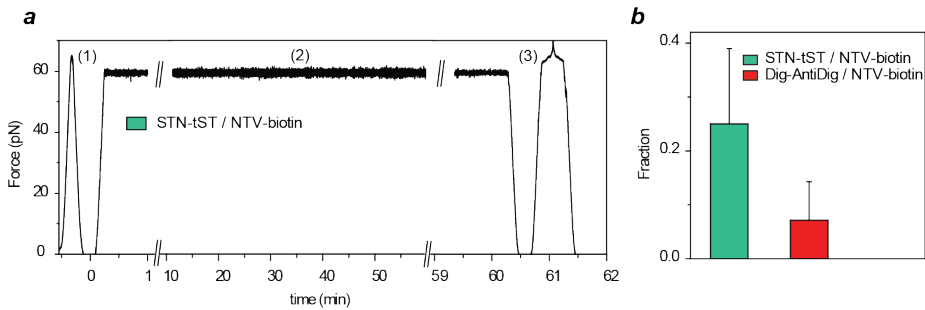


Figure 2.5: Mechanical stability analysis at constant force. (a) An example of stretched tether kept under a constant force of 60 pN in the second pulling cycle (2) by means of a force feedback for more than one hour. Stretching and relaxation cycles in the beginning (1) and at the end of the experiment (3) display a typical behaviour of dsDNA. (b) Fraction of the tethers resisting more than 10 min at 60 pN.

observed binding of STN to biotin does also illustrate the limitations of the specificity in this system: ST shows stable binding specifically to STN and not to NTV, but biotin binds stably both to STN and NTV, though more so to the latter. However, our protocol shows that these limitations can typically be overcome in practice, by first establishing the connection to biotin, which is less specific, and only then form the connection to tST which is specific.

In order to probe the difference in stability between biotin-DNA-Dig and tST-DNA-biotin tethers more exhaustively, we tested for the ability to sustain high forces for long periods of time. In this experiment, tethers were first stretched to 65 pN and those that survived the first pull were kept under constant force of 60 pN until they broke. Figure 3a illustrates a case of (STN)tST-DNA-biotin(NTV) handle that could survive this load for an hour. In the second pull, the handle was stretched to 60 pN (in less than 1 min) and kept under force feedback for 60 min without breaking. Next, it was relaxed (Fig. 2.5a, in between 60:00 and 60:30 min:sec) and showed a characteristic cycle of DNA overstretching (Figure 3a, in between 60:30 and 61:30 min:sec). The tether broke after additional 22 pulling cycles. Importantly, the fraction of strong tethers resisting more than 10 min at 60 pN in the second pull was found to be significantly higher with tST-STN as compared to Dig-AntiDig (Fig. 2.5b). Thus, the tST-DNA-biotin handle is able to withstand high forces for longer than the biotin-DNA-Dig handle.

2.4 CONCLUSIONS

We have presented a simple procedure to specifically attach a protein to a DNA molecule, using STN-tST linkages. The method is rapid and straightforward, and can be established *in-situ* within biologically relevant buffers. Binding of the DNA-tST construct to surface immobilized STN shows high mechanical stability, and can readily tolerate forces as high as 65 pN for tens of minutes. The engineered linkage

can be used as a reliable linker for optical tweezers studies of proteins and nucleic acids, both in constant pulling rate and force modes [48, 72, 122].

The motivation to use STN to end-join two molecules was based on reported high rupture forces (40 pN and 60 pN) [104]. We found that the average rupture force was beyond the overstretching transition of 65 pN for the ST-STN linkage studied here, which may be due to the dual ST repeats or other experimental differences. The specificity, stability, and rapid *in-situ* formation of the STN-tST complex allows it to be used in combination with other well-used linkages that can also be stably formed *in-situ*, such as NTV-biotin. Dig-AntiDig linkages of similar stability can be formed, but they require bulk incubation. Thus, choice of linkage depends on the precise application and formation possibilities. We find that tST-STN is more stable against applied force than the commonly used biotin-STV linkage. Moreover, we show that tST-STN can be used for surface attachments as well as for linkage between DNA and protein molecules, which has not been achieved for Dig-AntiDig linkages. Because of the high stability of STN, this complex could potentially also be used in a broad thermal range and harsh conditions.

We have shown that constructing tST-DNA hybrids is straightforward using PCR amplification, making our method suitable for broad applications. For single molecule studies, the presented approach could be applied in combination with other peptide-DNA hybrids. For example, halo tags-DNA hybrid could be constructed as a handle and be linked covalently to halogenase-coated beads. Similarly, a peptide substrate to ubiquitin ligase could be used to generate peptide-DNA hybrid and then be linked to the protein ligase-coated bead. The reversibility of the ST-STN reaction, using Desthiobiotin [167], will make the ST-STN linkage also highly suitable for biologically inspired soft matter systems, where reversibility could open up new possibilities.

CHAPTER 3

Yeast small heat shock
protein Hsp42 preserve
aggregating proteins in
native-like conformation

Abstract

*Small heat shock proteins (sHsp) act at the front line of cellular defense mechanisms against protein misfolding stress. sHsps are chaperones with reported holdase activity, that coaggregate with denatured proteins thereby sequestering potentially harmful proteins and facilitating their subsequent refolding by the Hsp70-Hsp100 bichaperone machinery. We investigated the molecular basis for this activity at single molecule level by probing the interaction between a multidomain aggregation prone substrate (4MBP) and Hsp42, a sHsp chaperone from *S. cerevisiae* cytosol. Single molecule optical tweezers analysis reveals Hsp42 prevents tight inter-domain and promotes native-like re-folding via interaction with the folded state. Investigating the folding of single domain MBP, consistently suggests the binding of Hsp42 to the folded state, as we detected destabilized refolded structures in the presence of chaperone. A similar destabilization was observed for refolded domains in the 4MBP construct. We expect these findings to be of general importance in understanding chaperoning function of broadly conserved sHsps.*

This chapter reports on a part of a research project that investigates the function of yeast sHsps using different methods. Here we report force spectroscopy results.

3.1 Introduction

A broad spectrum of stress conditions and disbalanced physiological states perturb cellular protein homeostasis (proteostasis) by promoting the misfolding of proteins. Misfolded proteins are characterized by surface exposed hydrophobic patches, which target them to the cellular quality control machinery for refolding or degradation, but due to their stickiness they are also prone to aggregation. At first approximation, the fate of a misfolded protein is determined by the kinetic partitioning between refolding, degradation and aggregation pathways. Accordingly, aggregation increases under severe stress conditions when the concentration of misfolded proteins is high and exceeds the capacity of the folding and degradation machineries.

The aggregation of proteins is linked to ageing and pathophysiological states including neurodegeneration, and may be causative to these states since aggregates can have cytotoxic effects [86]. Aggregation may however also be beneficial to cells since this process sequesters potentially toxic protein species. In support of a protective role, aggregation emerges as an organized process *in vivo*, involving dedicated machineries, rather than a stochastic process solely driven by the intrinsic physicochemical properties and concentrations of the misfolding proteins [144, 192]. For *S. cerevisiae* it has been shown that aggregases are key cellular components governing aggregation of misfolded proteins during heat stress (Fig. 3.1a). In the cytosol, the small heat shock protein (sHsp) Hsp42 drives formation, and is integral part, of microscopically visible aggregates termed CytoQ or Q-bodies [52, 144, 178]. At severe heat stress conditions, the sHsp Hsp26 undergoes thermal activation allowing it to interact with aggregating proteins and integrate into CytoQ aggregates, along with Hsp42 [79, 178].

hsp42 Δ mutants show decreased fitness at elevated temperatures [52] and hsp26 Δ mutants exhibit defects in the reactivation of aggregated proteins [24, 78], indicating that protein aggregation is indeed cytoprotective with sHsps having a key role. Consistent with this role, sHsps prevent apoptotic death of mammalian cells under various stress conditions [63] and sHsp mutations are causative to human diseases including cataracts [33].

sHsps constitute a highly diverse family of molecular chaperones sharing the α -crystallin domain (ACD) as unifying structural element [77]. The ACD is flanked by N- and C-terminal extensions (NTE and CTE, respectively) of variable length and sequence, providing the basis for sHsp diversity (Fig. 3.1b). sHsps form dimeric building blocks, which form oligomeric assemblies of varying size and stability. sHsps can be subdivided into constitutively active and stress activatable sHsps, with yeast Hsp42 and Hsp26 representing members of the respective classes [79, 81]. sHsps exhibit ATP-independent holdase activity *in vitro*, preventing the formation of large, insoluble aggregates of misfolded protein species if present at stoichiometric amounts relative to the substrate [14, 80]. It remains unclear why *in vivo*, the activity of sHsps such as Hsp42 is seemingly opposite, as Hsp42 promotes formation of large, microscopically visible aggregates. Possibly additional cellular factors are involved, and/or within the crowded environment of the cell, excluded volume effects lead to association of small sHsp-substrate complexes to larger entities. Even with this unsolved discrepancy, a large body of *in vivo* and *in vitro* evidence indicates sHsps

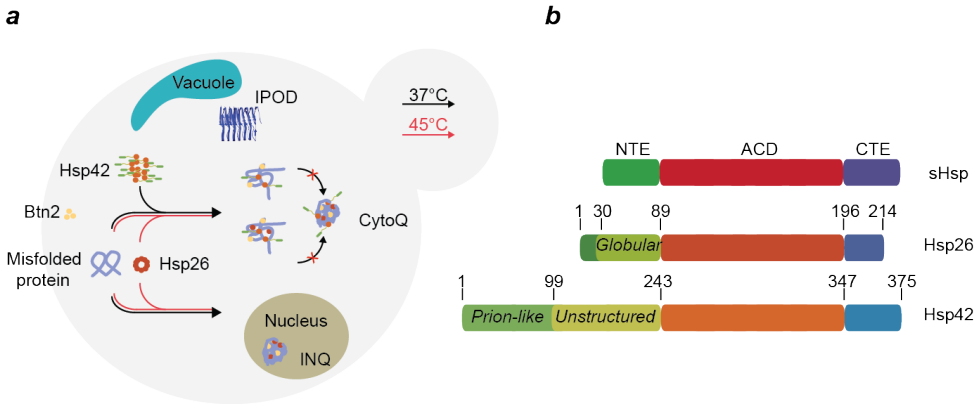


Figure 3.1: Function and structure of yeast cytosolic sHsps (a) A model to explain the role of cytosolic Hsp42 and Hsp26, in organizing misfolded proteins in *S. cerevisiae*. Yeast cells are equipped with three compartments to sequester and deposit protein aggregates, namely CytoQ (cytosolic quality control compartment), INQ (intracellular quality control compartment), and IPOD (insoluble protein deposit). During physiological folding stress (37°C), Hsp42 (and Btn2) co-aggregates with misfolded proteins, stimulating the formation of CytoQ. In stress condition, the misfolded proteins could also be bound by Hsp26 that is active at high temperatures. The (Btn2- and) Hsp26-associated aggregates usually end up in CytoQ and INQ. IPOD, usually is accumulated by amyloidogenic proteins. (b) Domain Layout of sHsps, including Hsp26 and Hsp42. sHsps consist of an N-terminal extension (NTE), a conserved alpha-crystallin domain, and a C-terminal extension. They mostly oligomerize through the crystallin domain (CTE), whereas their NTE seems to be functionally important. For example, Hsp26 uses its NTE to sense the temperature and to stabilize the oligomeric structure [58]. Similarly, the long NTE of Hsp42 has a prion-like domain that is vital for its function [193].

from various organisms form complexes with aggregation prone proteins in which several dimers of sHsps and substrate molecules assemble in unknown configuration. sHsp-substrate complexes are usually stable, requiring downstream processing by ATP-dependent Hsp70 and Hsp100 chaperones for substrate release [49, 78, 118, 145, 196]. Reactivation of substrates from sHsp complexes by Hsp70/Hsp100 occurs with higher efficiency and faster kinetics as compared to substrates aggregated in the absence of sHsps. This effect of sHsps extends to amyloids, for which sHsps can potentiate dissolution by Hsp70/Hsp100 chaperones [47].

Despite this progress we are still missing key information regarding the molecular features of stress-induced, amorphous aggregates of misfolded proteins, and the effects of sHsps on the conformation of aggregating proteins. This is critical for understanding why sequestration of substrates by sHsp association permits faster and more efficient protein reactivation. In this study we addressed some of these questions for aggregates of mechanically-denatured model proteins and the yeast Hsp42 at the single-molecule level. We show Hsp42 binds to the folded state of a client protein in native-like state and suppress inter-domains misfolding. These findings provide a new concept for the cellular strategy to cope with misfolding proteins, revising the conception of global protein unfolding during heat stress in vivo.

3.2 Materials and Methods

3.2.1 Expression and purification of biotinylated MBP/4MBP

N-terminally biotinylated MBP and 4MBP C-terminally fused with 4 Myc tag sequences were produced in *E. coli* as hybrid proteins consisting of an N-terminal Ulp1-cleavable N-terminal His₁₀-SUMO sequence followed by an AviTag sequence (Avidity, LCC, Aurora, Colorado, USA), facilitating in vivo biotinylation and four consecutive C-terminal Myc-tag sequences. Proteins were purified from *E. coli* BL21 cells harboring pBirAcm encoding the biotin ligase (Avidity, LCC, Aurora, Colorado, USA). For over-expression cells over-night cultures were diluted 1:100 in fresh LB medium supplemented with 20 mg/l Biotin, 20 mg/l Kanamycin, 10 mg/l Chloramphenicol, 0.2% glucose and incubated under vigorous shaking at 30°C. Expression was induced at $OD_{600} = 0.6$ by addition of 1 mM IPTG for 3 h. Cells were chilled, harvested by centrifugation, flash-frozen in liquid nitrogen and stored at -70°C. Cell pellets were resuspended in ice-cold buffer A (20 mM Tris-HCl pH 7.5, 0.2 M NaCl, 1% Triton X-100, 1 mM PMSF) and lysed using a French Pressure Cell. The lysate was cleared from cell debris by centrifugation at 35,000 g for 30 min and incubated with Ni-IDA matrix (Protino; Macherey-Nagel, Düren, Germany) for 30 min at 4°C. The matrix was washed extensively with buffer A and bound hybrid proteins were eluted in buffer A containing 250 mM imidazole. The eluate was supplemented with His₆-Ulp1 protease and dialyzed overnight at 4°C in buffer D (20 mM Tris-HCl pH 7.5, 0.2 M NaCl). Following dialysis coupled with Ulp1 digestion, His₆ - Ulp1 protease and the His₁₀ - SUMO fragment were removed by incubation with Ni-IDA matrix. The unbound MBP or 4 MBP that remained in the unbound fraction was then loaded on Amylose resin (New England Biolabs) previously equilibrated in buffer D, washed with cold buffer D and bound proteins were eluted in buffer D supplemented with 20 mM maltose. Elution fractions were dialyzed three times for 2 hours at 4°C in 100-fold excess volume of buffer S (20 mM Tris-HCl pH 7.5, 0.2 M NaCl, 1 mM EDTA). 4 MBP purifications in addition were subjected to size-exclusion chromatography using a HiLoad 16/600 Superdex prep grade column. Purified proteins were concentrated using Vivaspin centrifugal concentrators, aliquoted, flash frozen in liquid nitrogen and stored at -70 °C.

Biotinylated proteins were also produced as follows. Purification of MBP and 4MBP containing one N-terminal cysteine was performed as described [15]. For biotinylation the purified proteins were dialyzed in buffer B (20 mM Tris-HCl pH 7.5, 0.2 M NaCl, 1 mM EDTA) and incubated on ice for 15 min in buffer B containing 5 mM TCEP to reduce disulfide bonds. A ten-fold molar excess of Maleimide-PEG11-Biotin (Thermo Scientific) dissolved in DMSO was added and biotinylation was performed for 2 hours at 25 °C. Proteins were concentrated and subjected to size-exclusion chromatography using a HiLoad 16/600 Superdex prep grade column. Purified fractions were analyzed by SDS-PAGE, pooled, aliquoted, flash frozen in liquid nitrogen and stored at -70 °C.

3.2.2 Hsp42 expression and purification

The Chaperone sample was provided by the group of Prof. Bernd Bukau (ZMBH, Heidelberg, Germany). Briefly, C-terminally FLAG-tagged Hsp42 was cloned into pMal-c2E (New England BioLabs) creating a C-terminally fused Maltose binding protein (MBP)-tag. The Enterokinase cleavage site was changed to a PreScission cleavage site by site-directed mutagenesis and the vector was transformed into ArcticExpress™ (Agilent Technologies). Cells were grown at 37 °C to OD600 0.9, 0.5 mM IPTG was added and protein was expressed at 13 °C over night. Cells were resuspended in buffer C (50 mM Tris-HCl, 200 mM NaCl, 2 mM DTT, 10 % glycerol), lysed and centrifuged. The soluble extract was incubated with Amylose resin (New England Biolabs) and the manufacturer's protocol was followed. Hsp42 containing fractions were pooled and the MBP-tag was cleaved at 4 °C over night by PreScission protease (Sigma-Aldrich), followed by size exclusion using a Sephacryl S-300 HR 16/60 column (Amersham) equilibrated in buffer C. Fractions containing Hsp42 were unified and concentrated by dialysis against buffer C containing 20 % (w/v) PEG 20 000.

3.2.3 Optical tweezers assay

Anti-digoxigenin (anti-Dig) coated beads (DIGP-20-2, diameter 2.1 μm) were purchased from SpheroTech and stored at 4 °C until use. 2553 base pairs DNA handles with digoxigenin (Dig) and biotin at 50-ends of both strands and DNA-coated microspheres were made as described in chapter 2. 1 μl of Neutravidin solution (1% w/v) was further added to the DNA-coated microspheres and incubated at 4°C for 10 more minutes. Next, the unbound Neutravidin was washed away by centrifuging and the beads were dissolved in 400 μl HMK buffer for use in optical tweezers experiments.

Carboxylated polystyrene beads (CP-20-10, diameter 2.1 μm, SpheroTech) were covalently attached to anti-Myc antibody (Roche Diagnostics) via carbodiimide reaction (Poly-Link Protein Coupling Kit, Polysciences Inc.). Briefly, the beads were washed and then mixed with freshly prepared 1-ethyl-3-(3-dimethylaminopropyl) carbodiimide and the antibody, and mixture was incubated for 3 hours. MBP-coated beads were made by mixing 5 μl of 50 μM solution of either 1MBP or 4MBP and 2 μl Myc-coated beads in 10 μl HMK buffer and incubating the mixture for 30 minutes on a rotary mixer at 4°C. Subsequently, the beads were dissolved in 400 μl HMK buffer for use in optical tweezers experiments.

Stretching experiments were performed at room temperature using a custom made optical tweezers setup as described in 2. MBP-coated bead was trapped in the optical trap and then transferred to a micropipette tip, and, subsequently, DNA-coated bead was trapped. Next, two beads were brought in close contact, allowing a tether (DNA-MBP linker) between the beads to form. When the micropipette is moved away from the trap, the tether experiences a stretching force, leading to its extension and deflection of the trapped bead from the trap center. Such deflection is monitored by collecting the transmitted laser light and directing it to quadrant photodiode where it is recorded at 50 Hz. The data is filtered with 5th order Butterworth filter

at 20 Hz prior to saving. Trap stiffness and sensitivity, were measured to be 169 ± 24 pN/um and 2.74 ± 0.24 V/um correspondingly. A nanopositioning piezo stage is used to move the flow chamber and micropipette at a speed of 50 nm/s that corresponds to a pulling rate on the tethered MBP construct of ~ 5 pN/s at unfolding.

3.3 Results and Discussion

We performed single molecule optical tweezers experiments using a construct composed of four repeats of Maltose Binding Protein (4MBP, Fig. 3.2a). As shown previously [15], stretching individual 4MBP molecules for the first time resulted in a gradual unfolding transition (Fig. 3.2b/c, $F \rightarrow 4$), followed by the distinct unfolding of the four remaining core structures ($4 \rightarrow 3 \rightarrow 2 \rightarrow 1 \rightarrow U$). In these latter unfolding events, the measured tether length suddenly increased by about 92 nm, which corresponds to the peptide-length of one core structure, at a mean force of about 25 pN. In the absence of chaperone, after relaxation to low force, subsequent stretching curves (Fig. 3.2d/e) predominantly showed tightly misfolded structures that could not be unfolded, or more weakly misfolded structures that unfolded above 35 pN and/or released chain segments exceeding one core structure (92 nm). In these refolding experiments, the isolated protein chains thus predominantly form misfolded and aggregated structures involving more than one repeat.

Next, similar single molecule experiments were performed in the presence of Hsp42, which is constitutively active. We found that the stretching curves for the first 4MBP unfolding were similar in presence and absence of Hsp42 (Fig. 3.2b). This correspondence, which has also been observed for SecB [15] and Trigger Factor [135], indicates that Hsp42 chaperones do not interact with natively folded repeats, or if they do, do not significantly alter their unfolding characteristics. Upon complete unfolding and relaxation to low force, subsequent stretching curves show important differences (Fig. 3.2f/g). First, the tight misfolds between multiple repeats were now absent (Fig. 3.2g). This finding showed that Hsp42 suppressed non-native contacts between repeats. Weak misfolds were still observed (Fig. 3.2f/g), which indicates that the suppression is not perfect, possibly because client monomers have a very high effective local concentration in this assay. Second, the number of folded core structures that unfolded in native-like manner increased substantially (Fig. 3.2f/g). In these cases, the measured tether length increased by about 92 nm at forces below 35 pN. Thus, interactions with Hsp42 promoted the presence of native-like structures.

The data gave rise to further questions regarding the nature of the Hsp42-client complex. In particular, we also observed an increased frequency of unfolding events with small length increases (smaller than one core, Fig. 3.2f/g), which could either indicate complexes between Hsp42 and partially folded native-like structures, as seen previously for Trigger Factor [135], or a (partial) disruption of an aggregated state. To address this issue, we did two different experiments. First, we added Hsp40 to the chaperone buffer and repeated the stretching-relaxation experiments of 4MBP in the presence of Hsp42 and the bacterial Hsp40 (DnaJ) (Fig. 3.3). Hsp40 is known to be a strong holdase which blocks the refolding of polypeptide chains through

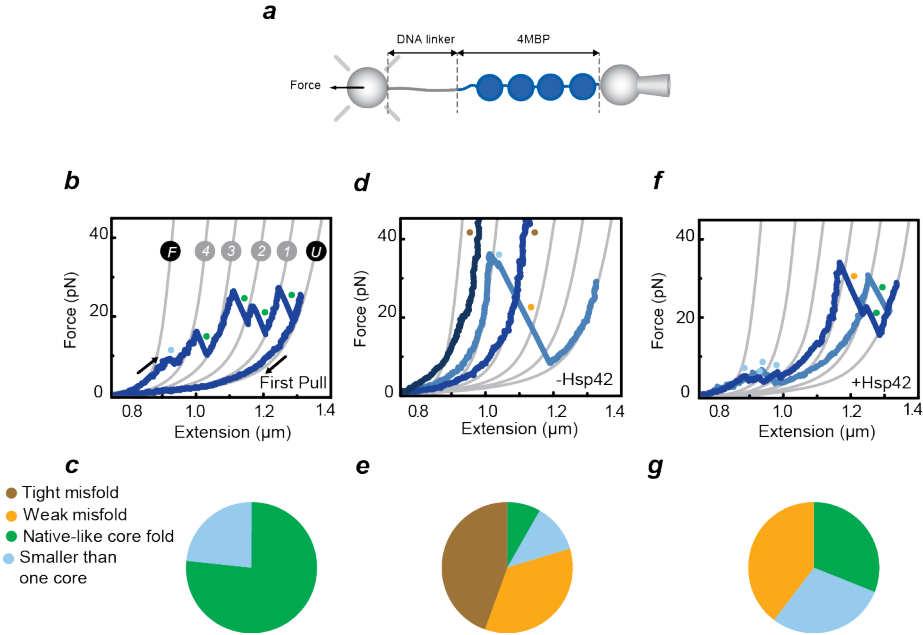


Figure 3.2: Hsp42 suppresses inter-domain misfolding (a) Schematic diagram of the set-up; Maltose Binding Protein constructs are tethered by means of a DNA handle between two beads: one held on a position controlled micropipette, another by an optical trap that allows force detection. (b) First stretching-relaxation curve, showing the unfolding pattern of natively-folded 4MBP. Gray lines represent the theoretical WLC characterizing the DNA-4MBP construct from fully-folded (F) to fully unfolded (U) state. After C-terminal unfolding ($F \rightarrow 4$), four core unfolding events ($4 \rightarrow 3 \rightarrow 2 \rightarrow 1 \rightarrow U$) are observed. Colored points indicate the type of observed protein structures. (c) Corresponding fractions of the types of observed structures (N=20). Fractions are normalized by the length of the amino acid chains that form the structure. (d) Second or subsequent stretching curves after relaxation and waiting at zero force for 5 s without chaperone. (e) Corresponding fractions of the types of observed structures (N=30). (f) Second or subsequent stretching curves in the presence of Hsp42 ($5\mu\text{M}$). (g) Corresponding fractions of the types of observed structures (N=30).

stabilizing the unfolded state [102]. Consistently, in our setup with Hsp40 present, the refolding of 4MBP was entirely suppressed (Fig. 3.3a), that shows high affinity and/or strong binding between an unfolded chain of 4MBP and Hsp40. In a buffer containing both Hsp40 and Hsp42, strikingly some parts of the protein chain did form folded structures (Fig. 3.3b). Within the structured part of the polypeptide chains, one third were native-like folds (Fig. 3.3c). This suggests that Hsp42 removes Hsp40 from the polypeptide chain and promotes folding.

In the second set of experiments, we focused on a single-repeat MBP protein, which can refold but cannot aggregate as there are no aggregation partners. In stretching-relaxation experiments in the absence of chaperone (Fig. 3.4a), 1MBP either refolded fully, and then unfolded in native-like manner or did not refold, and then did not show unfolding features during stretching. These data reconfirmed

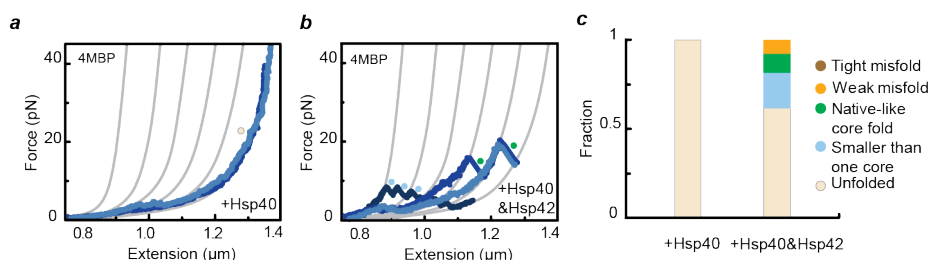


Figure 3.3: Hsp42 promotes folding (a) Second or subsequent stretching curves of 4MBP with Hsp40 (1 μM) present, which mainly show no refolding. This suggests strong interactions between Hsp40 and the unfolded protein chain. (b) In a buffer containing a mixture of Hsp42 (5 μM)-Hsp40 (1 μM), second or subsequent stretching curves show the polypeptide chain partially regains its ability to refold. Some parts of the protein chain is involved in native-like unfolding signature (green bullets). (c) Corresponding fractions of the types of observed structures (N=20).

that 1MBP refolds without the assistance of chaperones [15]. In experiments on 1MBP with Hsp42, unfolding events with length increases smaller than one core were now absent, in contrast to the 4MBP data with Hsp42 (Fig. 3.2f/g). The unfolded and relaxed chains either refolded to the core state or did not refold at all (Fig. 3.4b). This behavior is different than observed for Trigger Factor [135], and indicated that the small length changes seen for 4MBP originated from (partial) disruption of aggregated states. Interestingly, we found that the unfolding force of these refolded core states was lower than in the absence of chaperone (15 pN vs 24 pN, $p < 0.05$) (Fig. 3.4c). This finding suggested that Hsp42 bound to and destabilized the core structure, possibly by binding to small detached peptide segments at the core termini, or by interfering with the core fold in a different manner. Consistently, a similar destabilization was observed for refolded cores in the 4MBP construct (Fig. 3.4c). Note that we did not find evidence for Hsp42 binding to fully native MBP, as the first stretching curve on purified 1MBP or 4MBP in the presence of Hsp42 showed native unfolding forces. Thus, these data provided evidence that Hsp42 binds near-native folded structures.

In this study we investigated the molecular basis for the activity of sHsps to trap misfolded proteins in a state that facilitates their refolding by ATP-dependent chaperones. This activity is crucial for stress survival of cells and plays important roles in numerous diseases and the ageing process. We determined the effects of the yeast cytosolic sHsp, Hsp42, on the aggregation of a mechanically-denatured model protein and the conformational states of sHsp-bound substrates. Our single molecule measurements on 4MBP and single MBP revealed that Hsp42 binding promotes native-like MBP folds and suppresses aggregation and off-pathway interactions between misfolded protein domains. These features of Hsp42 contrast with those of other chaperones including SecB, whose binding to denatured MBP suppresses aggregation, but does not promote native-like folds [15]. The activity of sHsps resembles more that of trigger factor, which promotes both suppression of aggregation and promotion of folding of MBP [135]. Trigger factor however binds a range of folds smaller than one domain, whereas Hsp42 was observed to bind the near-native core structure of

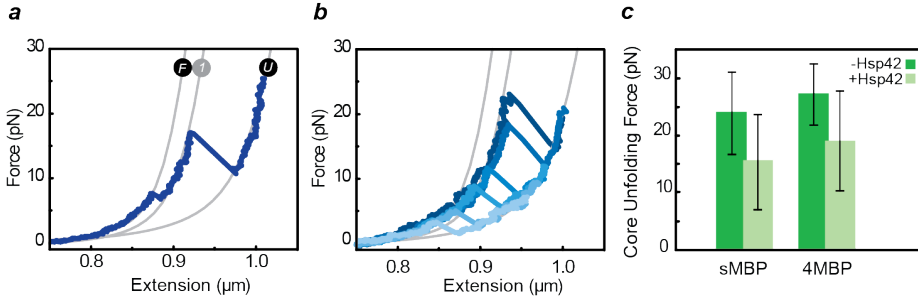


Figure 3.4: Hsp42 binds folded structures near native states (a) Stretching curves for sMBP. Gray lines represent WLC model for DNA-sMBP for the fully-folded (F), the single core (1), and fully unfolded (U) states. (b) Stretching curves in the presence of Hsp42 (5 μM). (c) Corresponding core unfolding forces ($N = 51$ and $N = 42$ for sMBP and 4MBP respectively).

MBP. We note the findings of our single molecule study were further corroborated by Amide hydrogen exchange analysis at bulk level [193].

Summarizing, we show that Hsp42 is not a simple holdase chaperone that only acts by suppressing the formation of large aggregates. It instead has an effect on the structure of aggregating proteins, preserving a native-like conformation. sHsps may thus assure the fast supply of functional protein during and after misfolding stress, enabling efficient recovery and restoration of a balanced cellular state.

CHAPTER 4

Small heat shock protein
HspB6 facilitates the
compaction of α -synuclein

Abstract

Aggregation of α -synuclein (α Syn) results in a range of neurodegenerative disease in vertebrates, including human. Structurally, the α Syn aggregates are highly ordered and are quite different with the amorphous aggregates of denatured proteins, forming usually in stress conditions. Here we study how HspB6, a human small sHsp, affects on α Syn aggregation. We found HspB6, counterintuitive to its supposed role as a holdase interacting with unfolded polypeptide chains, stimulates the formation of compact structures and stabilizes them against force unfolding. Our results suggest that interacting with the folded structures may be the generic feature of HspB6 functioning, as we observed HspB6 similarly stabilizes native-like MBP folds. We expect these findings to be of general importance in understanding the role of chaperones to inhibit the fibrillar aggregates.

4.1 Introduction

Protein aggregates are often described as amorphous chunks consisting of disordered monomers of mixed sequences, however most of the disease-associated proteins, such as tau and α -synuclein, show tendency to form highly ordered, fibrillar aggregates. These aggregates are arrangements of mostly unfolded or partially folded protein substrates that often have the same sequence. They adopt a fibrillar structure of few nanometers in diameter, and are capable of reaching to some micrometers in length. The structural core of fibrillar aggregates is hydrogen bonded beta-sheets [56], Which makes them thermodynamically super stable structures and they often exceed the stability of native proteins [8, 64]. Fibril architecture is generic for different primary protein sequences [56, 124, 201].

The fibrils are relatively well characterized [107]. At early stages of fibrillar aggregation, proteins often form oligomeric structures of various sizes that are believed to act as precursors for fibrillization. For some proteins, it has been demonstrated that they are capable of slow compaction resembling the beta-sheet formation [197]. However, the dynamic process of fibril formation remains poorly understood due to extreme heterogeneity of pre-fibrillar species. Their structural features and aggregation pathways are challenging to identify in ensemble studies. Apart from the possible key structural role in the fibril formation, oligomeric aggregates are widely suspected to have negative effect on cell viability and serve as toxic agents in the aggregation-associated diseases [37, 115]. Hence, having a thorough understanding of them is important for effective drug development.

α -synuclein (α Syn) is an amyloidogenic protein mainly expressed in the neural tissue of vertebrates, including humans [117]. All homologs of α Syn are quite small (127-140 residues) and highly charged [34]. Human α Syn has 140 amino acids and features three distinct fragments (Fig.4.1a); lysine-rich N-terminus, which regulates interaction with membranes, acidic C-terminal tail, which is involved in interaction with metals and proteins, and central highly hydrophobic non-amyloid-beta (NAC) fragment, which is essential for α Syn aggregation [116]. Monomeric α Syn can adopt a whole zoo of conformations (Fig.4.1b). In the test tube, native α Syn lacks any stable secondary or tertiary structure [194, 203]. However, upon association to the cell membrane, α Syn becomes partially alpha-helical [40]. Furthermore, a stable tetramer α Syn state resisting aggregation has been observed at physiological conditions [13, 200]; although, there are still debates over this finding [54]. In physiological state, α Syn is essential for normal development of cognitive functions in mice [108]. At the presynaptic terminal, α Syn plays an important role in the synaptic function by regulating neurotransmitter release and vesicle trafficking [116]. α Syn also has been suggested to act as a molecular chaperone assisting in folding and refolding of synaptic SNARE proteins [28].

An aggregation of α Syn results in the deposition of inclusions mainly consisting of aggregated α Syn in neuronal cell cytoplasm, which are called Lewy bodies (Fig. 4.1b). Together with degradation of dopaminergic neurons, they are markers of Lewy body diseases [141]. It still remains rather unclear how exactly protein aggregation results in disease symptoms. Lewy bodies are considered less toxic by themselves. They are assumed to reflect a part of protective mechanism, where toxic species are

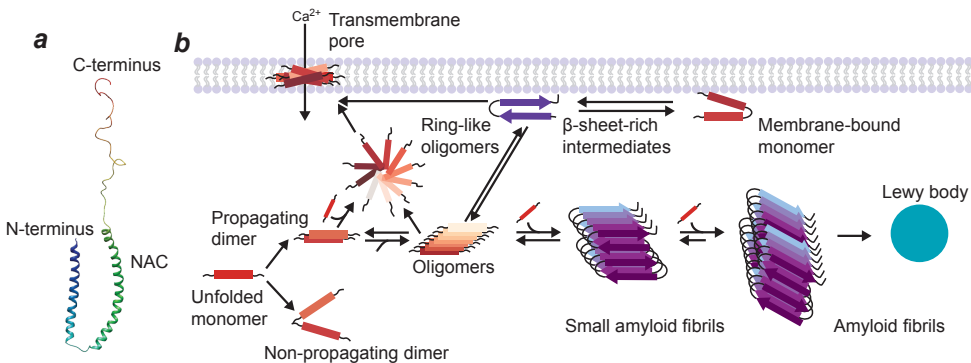


Figure 4.1: α Syn structure, propagation and accumulation (a) Structure of micelle-bound α Syn monomer (Protein Data Bank ID: 1XQ8). The N-terminal region, the NAC region, and the C-terminal region are shown in blue, orange and red color, respectively. Numbers refer to amino acids flanking corresponding regions. (b) Schematic representation of interplay between different α Syn structures, suggested by Lashuel et. al [116]. Briefly, α Syn monomers can aggregate in conjugation with the cellular membrane or in the cytosol. The cytoplasmic aggregation takes place via the interaction of unfolded monomers that initially form unstable dimers. The dimers further oligomerize to make bigger structures of different morphologies, such as spherical and ring-like oligomers, that finally assemble to amyloid fibrils. The fibrils can then accumulate and make intracellular inclusions, named as Lewy bodies. Membrane-associated α Syn monomers mainly represent an α -helical confirmation, but can adopt α -sheet-rich structures through oligomerization at high concentrations. These structures can incorporate into the formation of either membrane-bound (e.g. trans-membrane amyloid pores) or cytosolic amyloid fibrils.

sequestered, inactivated and deposited in a less toxic state [116]. Instead of fibrils, α Syn oligomeric aggregates are widely suspected as toxic agent in the Lewy body diseases. Both in vivo and in vitro, α Syn can form various oligomeric structures [89] that are possibly involved in amyloid fibril formation. They exist in equilibrium with monomeric α Syn and can slowly convert to fibrils [89]. Furthermore, round pore-like α Syn oligomers have toxic effects on the cells, since they can cause membrane leakage [60]. Hence, a thorough understanding of the relationship between different oligomeric states and the kinetics of their interconversions is essential to potentially develop the drugs against neurodegenerative diseases.

SHsps have been suggested to regulate α Syn folding and aggregation [20]. In humans, sHsps family, also named as HspB family, features 10 members. For all HspBs, some extent of chaperone activity was detected in vitro, but it remains unclear how physiologically relevant this activity is. In vivo evidence exists for an ability of HspBs to interact with and modulate the structure and stability of the cytoskeleton [46]. Due to the fact that they exist as large and dynamic oligomer assemblies that constantly interconvert in the cell depending on their posttranslational state, little is known about how exactly they interact with client proteins. Apart from the holdase activity, it has been suggested that HspBs can use transient low-affinity interactions to redirect unfolded-like protein intermediates back on the folding pathway to allow their spontaneous refolding [113]. Moreover, it has also been demonstrated that HspBs are capable of collaboration with other chaperones, such as Hsp70 system

together with Hsp110, to promote depolymerization of preformed α Syn fibrils [47].

HspB6 is a ubiquitous chaperone with the highest level of expression in muscles [39, 92]. This heat shock protein which is named also as Hsp20 has rather small molecular weight and features C-terminal alpha-crystalline domain. The expression of this chaperone is not heat-inducible and it has shown to be active at physiological temperature (37°C). HspB6 molecules do not assemble in big oligomers, but forms only dimers (Fig. 4.2) [202]. HspB6 can inhibit the formation of amorphous aggregation [202], as well as mature α Syn fibrils [20]. However, the mechanisms underlying the chaperone-protein interaction remain elusive.

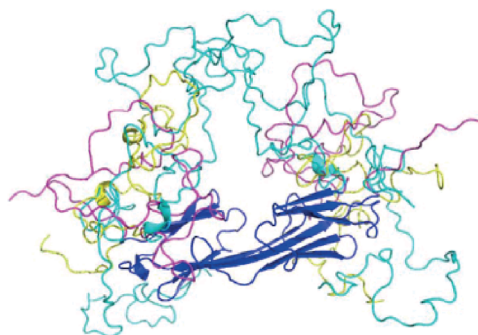


Figure 4.2: Cartoon representation of the functional HspB6 dimeric structure. Ensemble of the structures made by Weeks et al. [202] is represented. Crystallographic core is colored in blue, modeled extensions are colored in magenta, cyan, and yellow. Reprinted with permission

Here we study the effect of HspB chaperones on the formation of fibrillar aggregates by probing the aggregation of small α Syn oligomers in the presence of HspB6 at the single molecule and bulk levels. Using optical tweezers, we found HspB6 stimulates the formation of compact structures within α Syn oligomers and stabilizes them against force unfolding. The complexation of HspB6 molecules and mature α Syn fibrils was further confirmed by scanning transmission electron microscopy in bulk. Our results show interacting with the folded structures is probably the generic feature of HspB6 functioning, as we observed HspB6 similarly stabilizes MBP (Maltose Binding Protein) folds with the known tertiary structure. To pinpoint the role of sHsps during amyloid formation, these findings suggest sHsps, rather than inhibiting the fibrillization via binding to the unfolded polypeptide chains in the early stages, act later upon the formation of structured precursors. This can be seen as a part of cell strategy to maintain the protein hemostasis through sequential chaperone-mediated checkpoints.

4.2 Materials and Methods

4.2.1 Expression and purification of α yn-DNA chimera

A construct of tetrameric α Syn protein and two DNA handles was made by the group of Prof. Michael Woodside (University of Alberta, Edmonton, Canada) as described before [153]. Briefly, the tetrameric α Syn protein was engineered to contain four copies of the 140-amino-acid sequence of human α Syn as a tandem repeat separated by 3-amino-acid peptide linkers: GSG, GTG, and GSG. The protein construct also contained a cleavable N-terminal His-tag for purification, as well as N- and C-terminal cysteines for attaching DNA handles. The tetramer gene was synthesized and cloned into the bacterial expression vector pJexpress 406 (DNA2.0, Menlo Park CA), and expressed in *Escherichia coli* C41(DE3) cells (Lucigen). The resulting 61-kDa protein was purified by nickel affinity chromatography. The purity of the protein construct was assessed by SDS-PAGE, and the identity of the protein was verified by Western blotting (6xHis mAb/HRP conjugate (Clontech) and α Syn mAb/HRP conjugate (Millipore)). The tandem-repeat oligomers formed amyloid fibrils in bulk when subjected to the same conditions that induce amyloid fibril formation by monomeric α Syn. DNA handles produced by PCR were attached to the protein as described previously [26]. One of the handles was 2113 bp long, labeled with digoxigenin, and the other was 798 bp long, labeled with biotin.

4.2.2 Beads preparation

We used commercially available polystyrene beads covalently coated with antidigoxigenin (Anti-Dig) antibody (DIGP-20-2), and beads coated with Neutravidin (NVP-20-5) from SpheroTech Inc. The protein-DNA chimeras were incubated at ~ 100 pM with ~ 250 pM Anti-Dig-coated beads for 30 min. The beads were diluted to ~ 500 fM in 50 mM MOPS, pH 7.0, with 200 mM KCl and oxygen scavenging system (8 mU/ μ L glucose oxidase, 20 mU/ μ L catalase, 0.01% w/v D-glucose), before insertion into a sample cell for the optical trap. The tethers were formed later in the trap (Fig. 4.3) by approaching the Anti-Dig-coated beads -coated beads, with the protein-DNA chimeras immobilized on the surface, and the Neutravidin-coated beads. Stretching experiments were performed at room temperature using a custom made optical tweezers setup as described in 2.

4.2.3 HspB6 expression and purification

The Chaperone sample was provided by the group of Professor Rachel Klevit (University of Washington, Washington, United States) as explained before [42]. Briefly, HSPB6 in *Escherichia coli* BL21(DE3) cultured in Luria-Bertaini medium containing 100 μ g/mL ampicillin. Protein expression was induced with the addition of isopropyl thio- β -d-thiogalactoside to a final concentration of 0.5 mM at 22 $^{\circ}$ C for 16 h. The protein was purified later by an ammonium sulfate precipitation, followed by anion exchange chromatography and size exclusion chromatography in 25 mM sodium phosphate and 150 mM sodium chloride (pH 7.5) (PBS 7.5).

4.2.4 STEM imaging

α Syn was expressed in *Escherichia coli* strain BL21(DE3) using the pT7-7 expression plasmid and purified in the presence of 1 mM DTT as previously reported [162]. To prepare amyloid fibrils, 100 mM of α Syn monomer was placed in PBS buffer in eppendorf tubes and kept under constant shaking at 37°C at 1000 rpm in a Thermomixer. Subsequently, the resulting mature fibrils were filtered to remove non-aggregated monomers and diluted with MilliQ water to a final concentration of 10 mM. α Syn fibrils were allowed to interact with 1:1 ratio of HspB6 for 1 hour and then imaged using scanning transmission electron microscopy (STEM). 5 μ l of 20 μ M α Syn fibrils (in the presence and in the absence of HspB6) were adsorbed on 300 mesh formvar coated copper grids for 5 minutes and then washed 5 times with water. The grid was dried at 37°C and then transferred under vacuum into the STEM setup. Prior to acquiring the images, condenser stigmators were carefully adjusted to give a circular beam profile when the beam was viewed on the grids, and the beam was carefully centered and spread to produce uniform illumination over the field of view. The images were acquired using a FEI Verios 460 microscope operating at 20 kV electron beam energy.

4.3 Results and Discussion

We performed single molecule optical tweezers experiments using a construct composed of four repeats of α Syn (4 α Syn, Fig. 4.3a). Although α Syn monomer is mostly unstructured, but stretching 4 α Syn molecules results in a wide range of compacted structures, as shown previously (Fig. 4.3b) [153]. After the protein was completely stretched out and relaxed for 5 s, some compaction was observed in 59% of cases ($N = 32$). Most of these structures did not sustain subsequent stretching (77% of all compaction events, $N = 26$). However, a minor fraction (23%) of compact protein structures were stable over multiple stretching-relaxation cycles and sustained forces over 60 pN (Fig. 4.3c), indicating the formation of stable misfolded states. In order to estimate the protein length involved in the compaction, we measured the anticipated contour length change of α Syn upon unfolding by fitting the force-extension data to the WLCs with different α Syn folded fractions. In most of the compaction events (62%, $N = 26$), the involved protein length did not exceed the length of α Syn monomer, indicating the prevalence of short-range interactions (Fig. 4.3d).

Next, we performed stretching-relaxation experiments on 4 α Syn in the presence of 5 μ M of HspB6 in the experimental buffer (Fig. 4.4a). With the chaperone present, the force-extension data changed significantly, indicating the interaction between the chaperone and the protein (Fig. 4.4b). Tight compacted structures formed more often (47% of compaction events, $N = 36$), however, the total fraction of curves that became compacted did not change (Fig. 4.4c). In the presence of HspB6, partially compacted α Syn is more resistant to applied force than in the isolation (Fig. 4.5a). Apparently, HspB6 is capable of binding α Syn and stabilizing its partially compact states against forced unfolding. Shorter protein lengths are more populated in the presence of HspB6, indicating that the chaperone favors the compaction of α Syn (Fig.

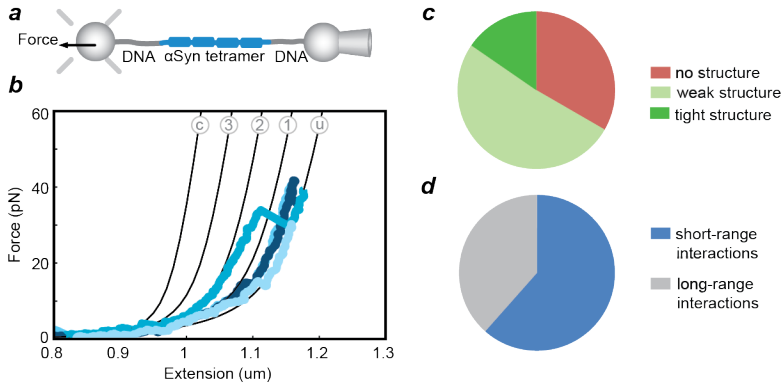


Figure 4.3: Diverse structures form by small oligomers of α Syn. (a) Schematic drawing of the experimental assay. (b) Force-extension data of α Syn tetramer. Subsequent stretching curves are shown in blue. Grey lines: theoretical compliance of DNA-protein construct in the states from compact (c) to fully unfolded (u). (c) Events fraction during subsequent α Syn stretching. (d) Fractions of short-range (within one α Syn domain, 55 nm) and long-range interactions in all compaction events during α Syn stretching.

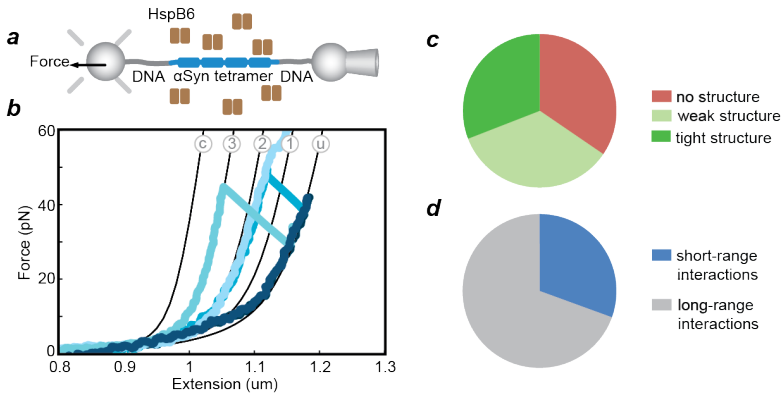


Figure 4.4: HspB6 promotes and stabilizes long-range interactions within α Syn oligomeric structures (a) Schematic drawing of the experimental assay. (b) Force-extension data of α Syn tetramer. Subsequent stretching curves are shown in blue; they indicate increased compaction in the presence of HspB6. (c) Events fraction during subsequent α Syn stretching. (d) Fractions of short-range and long-range interactions in all compaction events during α Syn stretching.

4.5c). Moreover, longer fragments of α Syn are involved in the structure formation in the presence of HspB6 (Fig. 4.5b). The fraction of unfolding events smaller than α Syn monomer decreased to only 31% (Fig. 4.4d). It suggests that HspB6 stimulates α Syn compaction by promoting long-range interactions in the protein client.

We further compared the mechanical stability of all unfolding events in a scatter plot (Fig. 4.5d). Most of the short-range interactions (smaller than α Syn monomer, blue-shaded area) disrupted at forces lower than 45 pN and were slightly stabilized by the chaperone (Fig. 4.5e). However, the stability of long-range interactions in α Syn

depends more significantly on the presence of HspB6. In the absence of the chaperone, they sustain much lower forces, than with HspB6 (Fig. 4.5e). They are also more frequent, when HspB6 is present (Fig. 3d, 4d). These results indicate that HspB6 favors long-range interactions in α Syn and can stabilize them against applied force. However, they do not reveal the mechanism of HspB6- α Syn interactions underlying the unexpected effect of α Syn compaction.

To get more insight in the nature of HspB6-substrate complex, we did two further set of experiments. First, we tested the preference of HspB6 to structured or unstructured protein fragments using single MBP (Fig. 4.6a). As shown before, a tethered unfolded MBP molecule can refold after relaxation without the assistance of chaperones (Fig. 4.6d). Native-like MBP molecules, consisting of a stable core and a c-terminal α helix, unfold via two transitions. The C-terminal α helix unfolds first, around 10 pN, and results in a step of 28 nm. Upon increasing the force to ~ 25 pN (mean = 24.68 ± 6.8 pN), subsequently the core unfolds in a step of 92 nm (Fig. 4.6b). With HspB6 present, we observed the formation of stable structures (Fig. 4.6c) that either unfolded at significantly higher forces (>35 pN) or did not unfold (up to 65 pN). In terms of length, the stable structures were typically as compact as native or as core structures, while stable intermediate lengths were rarely observed. This suggests HspB6 interacts with tertiary folded structures. However, the total refolding probability was reduced from $\sim 75\%$ (no chaperone) to $\sim 60\%$ (chaperone present), consistent with HspB6 interacting with the unfolded state (Fig. 4.6d).

To test if we could extend our single molecule findings to the bulk level, we performed a complementary experiment using pre-formed α Syn fibrils. The α Syn fibrils, first were pre-formed in the absence of chaperon and then were isolated from non-aggregated α Syn monomer and incubated with HspB6 molecules for 60 min. Using scanning transmission electron microscopy (STEM), we found complexes of fibrils and HspB6. In the absence of α Syn, the pure solution of HspB6, showed dot-like structures (Fig. 4.7a). The fibrils by themselves, looked like smooth filaments and did not feature any irregularity without chaperone (Fig. 4.7b). Interestingly, the fibrils after incubation with HspB6 molecules resulted in filaments that were decorated with dot-like structures (Fig. 4.7c). The images demonstrate that the chaperones are able to interact with the mature α Syn fibrils along its length. This is consistent with our single molecule observations, and overall, the findings suggest HspB6 binds directly to structured fragments of the protein client.

The ability of HspB6 to bind folded structures is similar to what we found for Hsp42 (chapter 3). This data suggests sHsps, rather than binding with the unfolded polypeptide chains [22, 202], interact with tertiary folded structures. Whereas binding to Hsp42 destabilized protein structures, interacting with HspB6 stabilizes the protein folds. This could be related to the diversity of N-terminal domains of sHsps and hence, their different (monomeric and oligomeric) structures.

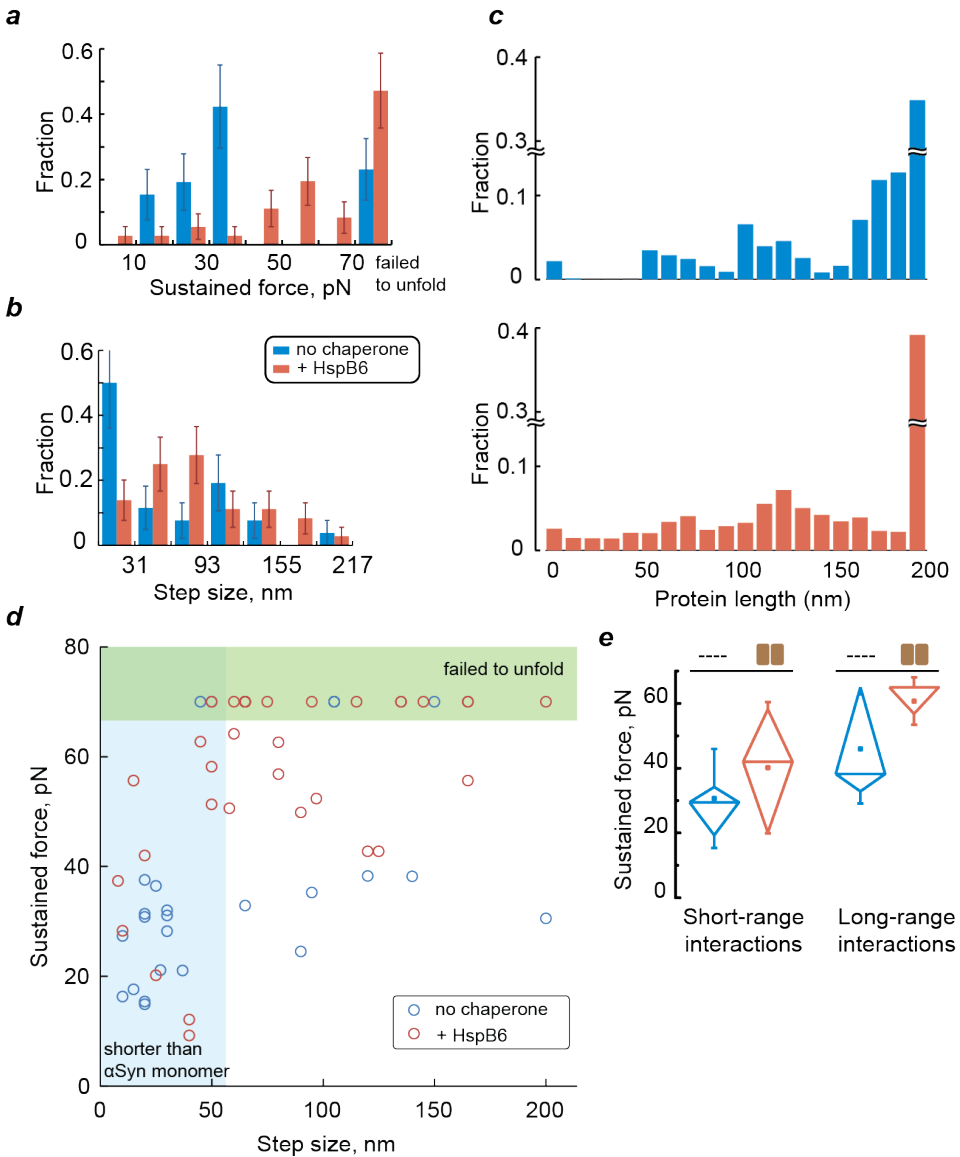


Figure 4.5: Effect of HspB6 on α Syn folding pathways. (a) Force sustained by compacted α Syn structures distribution affected by HspB6. (b) Step sizes statistics in the presence and in the absence of the chaperone. (c) Absolute protein length histograms. Shorter protein lengths are favored by HspB6. (d) Scatter force-step size plot of structures observed in the isolation and with HspB6. (e) Box-and-whisker plot of forces sustained by short-range and long-range interactions. Long-range interactions are more stabilized by HspB6.

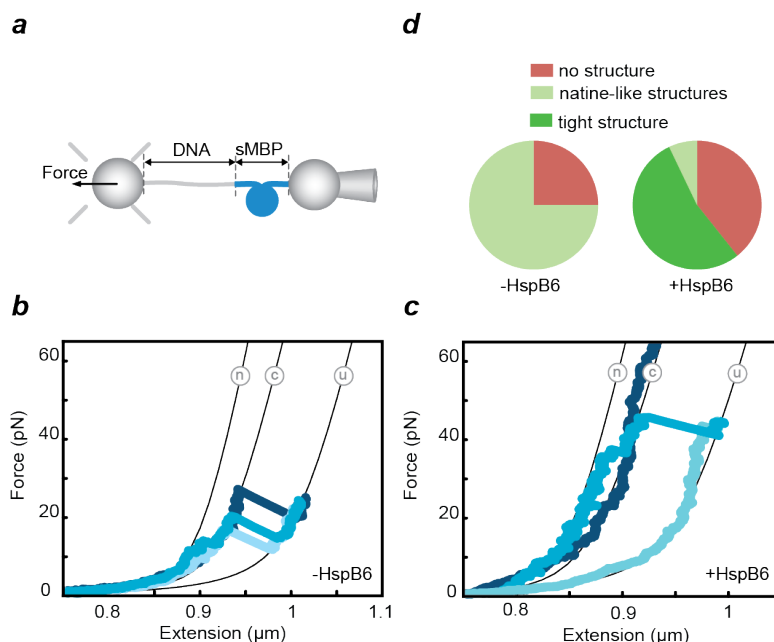


Figure 4.6: HspB6 binds and stabilizes MBP folds. (a) Schematic drawing of the experimental assay. Force-extension data of single MBP, (c) with (N=32) and (b) without (N=40) HspB6. Subsequent stretching curves are shown in blue. Grey lines: theoretical compliance of DNA-protein construct in the states from native (n) to (core (c) to fully unfolded (u). (d) Events fraction during subsequent single MBP stretching.

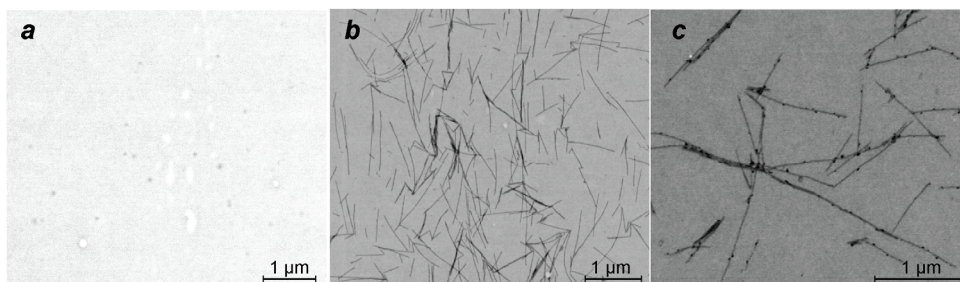


Figure 4.7: STEM imaging of the interaction between HspB6 and mature α Syn fibrils. Under the microscope, (a) HspB6 molecules represent dot-like structures in solution, probably pointing out their oligomeric conformation. In parallel, (b) mature α Syn fibrils look like smooth filaments that do not feature any irregularity. (c) After incubating the fibrils and HspB6 molecules, the smooth filaments were substituted with rough fibrillar structures, showing the capability of dot-like HspB6 structures to decorate the α Syn fibrils along their length.

CHAPTER 5

Aggregation suppression by the chaperone Hsp33 at the single molecule level

Abstract

The suppression of protein aggregation by holdase chaperones is central to cellular stress defenses and neurodegeneration, and has been studied extensively using structural and bulk assays. However, the causal protein chain conformational transitions and interactions at the molecular level are difficult to detect using these approaches. Here we study how the Escherichia coli holdase Hsp33 affects aggregation between Maltose Binding Proteins at the single-molecule level, using optical tweezers and head-to-tail repeat protein constructs. We find Hsp33 stabilizes the protein chains in the unfolded and non-aggregated state, but also promotes partial refolding within monomers over aggregation between monomers. Moreover, force spectroscopy on refolded monomers indicates Hsp33 binds and deforms an intermediate refolded state, weakening it against unfolding and blocking transition to the native state. A statistical mechanics model allows us to dissect the competition between folding, aggregation, and binding transitions using, and to predict how Hsp33 affects the state of interacting MBP monomers without additional fitting. The study shows that Hsp33 can act late in folding by affecting tertiary structure, and provides a first step to a bottom-up understanding of the suppression of protein aggregation.

5.1 Introduction

Molecular chaperones are key to controlling the state of proteins within cells [21]. Two chaperone classes can be distinguished: foldases that can guide the conformational search for the native state during *de novo* folding, and holdases that can for instance suppress aggregation during episodes of protein denaturing stress. ATP-dependent chaperones like members of the Hsp70 and GroEL families are examples of the former, and assist in the folding of substrate proteins using an ATP-controlled binding and release cycle. ATP-independent chaperones like small heat shock proteins [78] and Hsp33 [87] are examples of the latter. Hsp33 is a holdase chaperone that is activated upon oxidative stress. In the presence of reactive oxygen species, it undergoes extensive conformational rearrangements that generate regions of intrinsic disorder and triggers stable binding to unfolding polypeptide chains of substrate proteins [94].

While significant progress has been made in understanding the structure, activation, and conformational changes of holdases, we have limited molecular-level insight into their effect on the conformational changes of substrate proteins, which are central to aggregation. At the molecular level, many types of interactions underlie the suppression of aggregation: aggregation interactions between substrates, folding interactions within substrates, as well as binding interactions between chaperones and substrates in various stages of folding and aggregation. These diverse states and transitions are difficult to detect and disentangle using existing bulk methods. It has been shown that ATP-independent holdases including Hsp33 stably bind unfolding polypeptide chains, which can protect them against aggregation, and, by the same token, block folding [95]. Refolding into functional proteins with tertiary structure is thought to require transfer to foldase chaperones such as the Hsp70 system [87]. At the same time, recent experiments have shown that Hsp33 exploits its intrinsically disordered regions to bind alpha-helical structures [164]. These findings raise key questions about the range of substrate structural states that holdases interact with [78, 190], and underscore the importance of obtaining a molecular view of aggregation-suppression.

Here we aimed to address these questions using mechanical manipulation and force sensing on single protein constructs using optical tweezers, in combination with a model of aggregation suppression. This approach allowed us to classify and disentangle folding, aggregation, and binding at the level of molecular events. By contrasting transitions for a single substrate protein (Maltose Binding Protein or MBP) with a repeated protein construct composed of four MBP monomers, we could determine the effect of Hsp33 in the absence and presence of aggregation. Surprisingly, we found that Hsp33 promoted folding over aggregation, while suppressing chain-to-chain contacts overall. Analysis of unfolding forces and distances showed Hsp33 binds not only unfolded peptide chains but also nearly fully folded substrates with tertiary structure. A statistical mechanics model was able to quantitatively predict the outcome of the competitive interplay between aggregation, folding, and chaperone interactions.

5.2 Material and Methods

5.2.1 Expression and purification of Hsp33

Expression and purification of the constitutively active Hsp33-Y12E mutant has been done by the group of Prof. Ursula Jakob (University of Michigan, Ann Arbor) as previously described [38]. Briefly, the Hsp33-Y12E mutant was generated by introducing a single site mutation into the wild-type Hsp33 gene (*hslO*) using pUJ30 (pET11a-*hslO*) as a template. The plasmid was transformed into JH13 (BL21, Δ *hslO*), generating the expression strain CC4 (JH13, pET11a-*hslO*-Y12E). To overexpress large amounts of soluble Hsp33-Y12E protein, cells were grown to an A_{600} of 0.6–0.8 at 37 °C and then shifted to 18 °C. Once the temperature was reached, Hsp33-Y12E expression was induced with 1 mM isopropyl-1-thio- β -D-galactopyranoside (IPTG) for 24 h. Afterwards, the standard protocol for the Hsp33 purification was followed [95]. The protein was stored in 40 mM potassium phosphate buffer (KH_2PO_4) (pH 7.5) at -20 °C.

5.2.2 Design, expression and purification of MBP constructs

Expression and purification of MBP and 4MBP constructs, DNA linker and beads preparation, and the characteristics of the optical tweezers have been described previously (see section 3.2.3 and 3.2.1).

5.3 Results

5.3.1 Hsp33 suppresses the formation of compact protein structures

To study aggregation at the molecular level, we tethered individual protein constructs composed of four Maltose Binding Protein monomers (4MBP) between trapped beads by means of a DNA handle (Fig. 5.1a and 5.2a). Stretching this construct first produced a gradual unfolding of external α -helices followed by distinct length increases of 92 nm at 25 pN that reflect the unfolding of the four MBP core structures (Fig. 5.1b and 5.1f) [15, 135]. In the absence of Hsp33, and after relaxation and waiting for 5 s. at 0 pN, subsequent stretching curves showed distinct length increases larger than that of one MBP core as well as a lack of complete unfolding up to 65 pN (Fig. 5.1c). The curves did sometimes show distinct length increases corresponding to one core, which indicated the proper refolding of one of the cores, but these cases were rare (Fig. 5.1f). These experiments confirmed our previous observations that MBP monomers in unfolded and relaxed 4MBP have a large probability to form stable aggregated structures with other monomers within the repeated construct [15, 135].

Next we investigated how Hsp33 affected this aggregation process. The chaperone function of Hsp33 is tightly controlled by the folding status of a linker region. When four cysteines within Hsp33 are oxidized, the linker region becomes unfolded and Hsp33 active. The Hsp33 mutant Y12E has a constitutively unfolded linker,

and indeed its activity is constitutive and indistinguishable from oxidized wild-type Hsp33 [38]. We performed 4MBP stretching and relaxation cycles in the presence of constitutively active Hsp33 (0.5 μ M and 5 μ M), as oxidative conditions are not compatible with the single-molecule tethering. For increasing amounts of Hsp33, the average fraction of the 4MBP chain that was compact and hence had adopted a folded or aggregated structure after relaxing unfolded 4MBP chains was found to decrease (from 0.46 to 0.11), while the fraction that remained unfolded, or unfolded gradually below 10 pN increased (from 0.54 to 0.89, see Fig. 5.1f). Note that the latter category not only corresponds to fully unfolded chain segments, but also to alpha-helices that do not yield distinct unfolding events, as well as marginally stable higher-order structures. Overall, these data are consistent with models in which Hsp33 limits the formation of stable compact structures by binding chain segments that lack tertiary structure or are fully unfolded [87, 95].

5.3.2 Hsp33 promotes folding over aggregation

The data allowed us to focus on the structured part of the chain, and identify the contributions of aggregated and folded structures within it (Fig. 5.1b). We found that with increasing Hsp33, the relative fraction of aggregated structures decreased while the relative folded fraction increased (Fig. 5.1f). Thus, whereas the absolute fraction of the chain that formed stable structures decreased (from 0.46 to 0.11) with increasing Hsp33; within these stable structures, the relative fraction of native-like folded core structures increased (from 0.28 to 0.52). Note that in absolute terms, the fraction of the chain engaged in folded core structures remained approximately constant, while the absolute aggregated fraction decreased (Fig. 5.1f). These results thus suggested Hsp33 promoted the formation of folded over aggregated contacts, in addition to suppressing chain-to-chain contacts overall, which is remarkable for a holdase chaperone. However, how Hsp33 achieved control over the competition between aggregation and folding remained unclear. The data did not allow deduction of how Hsp33 affected MBP repeats when they were not interacting with other MBP repeats, or whether Hsp33 acted by interacting only with unfolded segments or also with structured parts, as the latter are highly diverse and we did not identify unique changes mediated by Hsp33.

5.3.3 Hsp33 suppresses folding in single isolated substrates

To isolate the effects of Hsp33 on a single MBP monomer (sMBP), we tethered the latter between two beads in similar fashion as for 4MBP (Fig 1.2a). In the absence of Hsp33, stretching sMBP typically yielded an unfolding pattern consistent with the 4MBP data: a small transition around 10 pN representing the unfolding of the external α -helices, and a larger step of 92 nm at 25 pN, reflecting the unfolding of the core structure (Fig 1.2b). When sMBP was relaxed to low force and allowed to refold for 5 s, we found that sMBP refolded in 70% of the time (Fig 1.2b-1.2e), consistent with previous studies [15, 135]. As observed for 4MBP, we did not detect any changes in the first stretching curve when Hsp33 was present, consistent with a lack of interactions between Hsp33 and native MBP. However, refolding of the

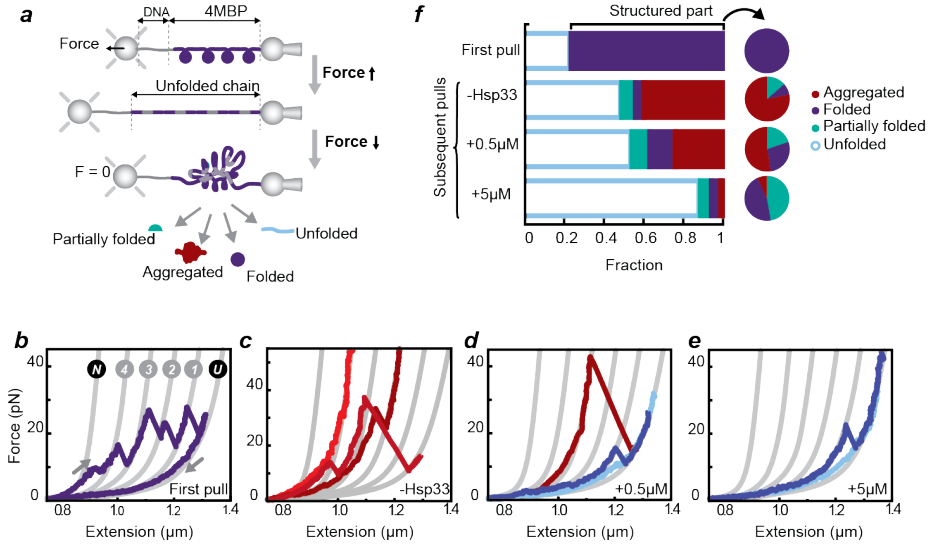


Figure 5.1: Hsp33 suppresses misfolding between domains and promotes native-like folds. (a) Schematic diagram of the experimental set-up. A construct of four connected Maltose Binding Protein molecules (4MBP) is tethered between two beads using a DNA handle. One bead is connected to a position controlled micropipette while the other bead is held by an optical trap that allows force detection. The DNA-protein tether is stretched by displacement of the pipette bead, resulting in protein unfolding. By moving the beads back together, the applied force decreases and the polypeptide chain relaxes. Upon keeping the construct at zero force for 5 sec, the chain can either refold, misfold or remain unfolded. (b) Stretching - relaxation curves are used to monitor the unfolding pattern of 4MBP. Gray lines represent the theoretical WLC characterizing the DNA-protein construct from natively-folded (N) to the unfolded (U) state. After the initial C-terminal unfolding event ($N \rightarrow 4$) as indicated by the upward arrow, four native-like core unfolding events ($4 \rightarrow 3 \rightarrow 2 \rightarrow 1 \rightarrow U$) are observed in the absence of Hsp33. After subsequent relaxation (downward arrow) and maintenance of the construct at zero force for 5 s, (c) second or subsequent stretching curves did not reveal any additional unfolding (left lines), suggestive of tight misfolding interactions between domains ($N=39$). Some misfolded structures are weaker and open under force (right line). (d) In the presence of 0.5 μM Hsp33, second or subsequent stretching curves ($N=43$) show characteristics of native (purple line) or weak non-native interactions (red line). Some MBP constructs appear fully unfolded (blue line). (e) In the presence of 5 μM Hsp33, the stretching - relaxation curves ($N=36$) do not represent misfolded structures and the MBP polypeptide chains either stay fully unfolded (blue line) or show characteristics of native interactions (purple line). (f) Statistics of unfolded chains, native-like folds, structures smaller than one domain and misfolded structures. Indicated fractions in bar charts, are the average length fraction of the protein chain that is involved in one of the four states. Pie charts represent relative fractions of different folded structures within folded part.

unfolded sMBP polypeptide chain was suppressed in subsequent pulls (Fig 1.2c-1.2d). This suppression depended on Hsp33 concentration: the refolded fraction decreased from 0.7 in the absence of Hsp33, to 0.5 in the presence of 0.5 μM Hsp33 and about 0.1 in the presence of 5 μM Hsp33 (Fig 1.2e). These findings indicated that Hsp33 suppressed native refolding in MBP monomers, and suggested that Hsp33 had not increased the relative folded fraction within 4MBP (Fig. 5.1f) by directly promoting refolding within monomers. The results are thus consistent with Hsp33

binding to 4MBP polypeptide chains (Fig. 5.1f). At the same time, the stretching curves displayed additional features that could not be explained by interactions with extended polypeptide segments or secondary structure only, which we probe further in the next section.

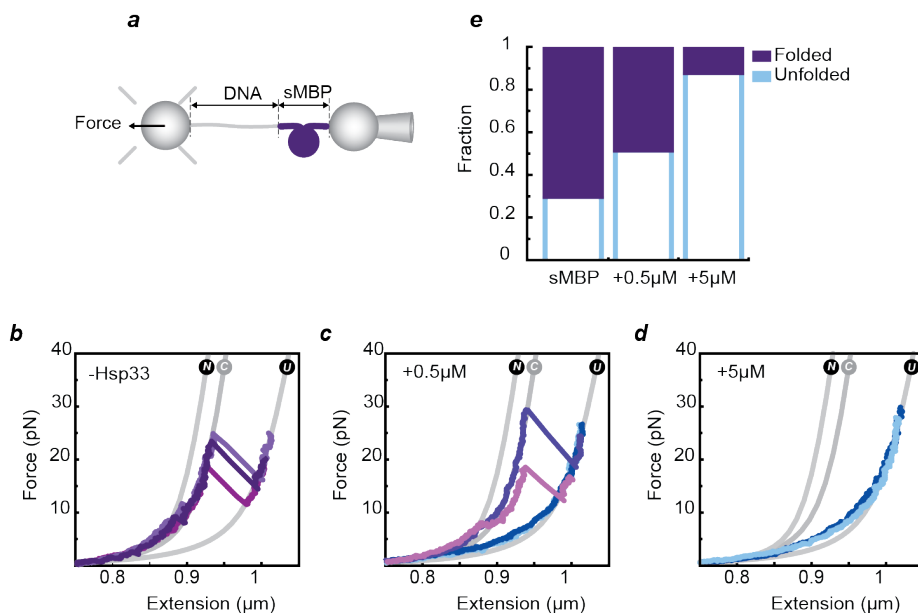


Figure 5.2: Hsp33 prevents folding (a) Schematic diagram of a single MBP (sMBP) construct tethered between two beads. (b) Stretching-relaxation curves ($N=70$) in the absence of Hsp33 show a frequently native-like refolding of sMBP. The native-like structure unfolds via two transitions, corresponding to C-terminal unfolding ($N \rightarrow C$) and core unfolding ($C \rightarrow U$) respectively. (c) In the presence of Hsp33 ($0.5 \mu\text{M}$), stretching-relaxation curves ($N=60$) indicate the refolding of sMBP is partially prevented. However, by increasing the concentration of Hsp33 (5M) refolding could be almost prohibited ($N=69$) (e) Statistics of refolding probabilities in the absence and presence of Hsp33.

5.3.4 Hsp33 also binds structured protein chains

At first glance, sMBP molecules folded in the presence of $0.5 \mu\text{M}$ Hsp33 seemed to be native-like (Fig. 5.1c). Upon stretching, they appeared as compact as folded single MBP below 5 pN, and typically unfolded via one small and one large transition. However, upon closer inspection several differences were apparent. In particular, after the first transition, the data often followed a WLC curve to the right of the core WLC curve (Fig. 5.3a, dashed line), thus indicating a structure that is smaller than a typical core. Consistently, these structures unfolded with a smaller step-size (Fig. 5.3a). The distribution of measured protein lengths for these core structures was indeed broader than in the absence of Hsp33 (Fig. 5.3b). We distinguished ‘typical’ cores with unfolding step-sizes similar to native MBP (protein length from 20 to 40

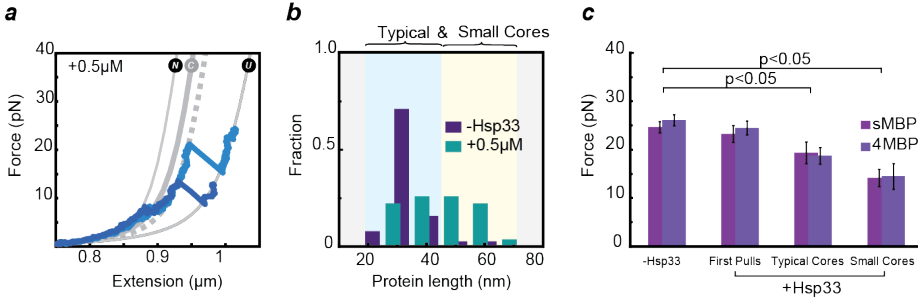


Figure 5.3: Hsp33 binds and destabilizes folded structures (a) The force-extension data suggests some of the structures that formed in the presence of Hsp33 have a smaller core-size (dashed line), as compared to the native MBP core (C line). This could be a consequence of interaction between the folded structure and Hsp33 (b) Protein length distribution of cores formed with (green) and without (purple) Hsp33, as derived from the force-extension data. Lengths are determined by fitting to the worm-like chain model (text S3). The number of times a certain protein length is visited is indicated as a fraction of the total number of visits to all lengths. Without Hsp33, there is a clear sharp pick at ~ 30 nm (corresponds to the MBP native core, theoretical length=28 nm) (N=42) that with Hsp33 (0.5 μ M) significantly becomes shorter and wider (N=31). (c) Core unfolding forces of sMBP (dark purple) and 4MBP (light purple) constructs. In the presence of Hsp33, while in the first pulls cores withstand the same type of force (N=40), they become less stable in the subsequent pulls and get unfolded at lower forces, as compared to no chaperone condition. This is statistically significant ($p < 0.05$) for both typical (protein length: 20-40 nm, N=48) and small (protein length: 50-70 nm, N=26) cores. Error bars, ± 1 se.

nm) and ‘small’ cores with protein length from 50 to 70 nm. These data suggested that Hsp33 had mediated small changes in the core structure, and was potentially still bound. Indeed, MBP proteins fold at timescales (~ 1 sec [15]) shorter than the lifetime of the modified core states (over 5 sec), which suggests Hsp33 maintains the MBP state by binding it. We also found that the C-terminal external α -helices typically docked onto the core structure appeared to unfold more gradually (Fig. 5.2c and 5.3a) than in the absence of Hsp33 (Fig. 5.2a), consistent with a modified core structure bound by Hsp33.

The data showed that Hsp33 promoted the occurrence of a modified core structure, and thus stabilized it against entry into the native state during the waiting time at 0 pN. At the same time, we found that with Hsp33, typical and small core structures unfolded at a lower average force ($p < 0.05$, Fig. 5.3c). The reduction in unfolding force was larger for small cores (-10 pN) than for typical cores though (-5 pN). This reduced resistance against forced unfolding supported the notion that Hsp33 interfered with MBP core structure. Modified cores should then be observable in the 4MBP data as well. Indeed, small cores were found for 4MBP and they displayed an unfolding force similar to those observed for 1MBP ($p < 0.05$, Fig. 5.3c). In contrast, the first stretching curve on single MBP and 4MBP molecules was similar with or without Hsp33 (Fig. 5.3c), and hence we found no evidence of Hsp33 interaction with fully natively folded proteins.

5.3.5 Statistical mechanics of aggregation suppression

The effect of Hsp33 on 4MBP involves multiple protein molecules, as well as folding, aggregation and binding events between them. To understand aggregation suppression in terms of these underlying events, we developed a statistical mechanics model (section 5.4). Similar approaches have described helix-to-coil transitions [43, 120, 159, 209, 210], folding-unfolding thermodynamics [66, 82, 150], and aggregation without chaperones [170]. In our model, each MBP monomer within fully unfolded and relaxed 4MBP molecules can bind Hsp33 with probability η , and then remain unfolded and non-aggregated (Fig. 4a). Importantly, the MBP monomers within 4MBP can be bound in a number of patterns, which are essential to their fate because they determine the presence of aggregation partners (Fig. 4b). Unbound monomers can fold, remain unfolded, or aggregate if another unbound monomer is present, with probabilities β , γ , and α respectively (Fig. 4a). Changes in the Hsp33 concentration c affect $\eta(c)$ as a first order reaction (Eq. S.2), which in turn affects $\alpha(c)$, $\beta(c)$, and $\gamma(c)$, because the sum of the probabilities equals 1 (Eq. S.7).

We determined model parameters using 4MBP data without Hsp33 (no Hsp33 binding), and sMBP data with and without Hsp33 (no aggregation), and then used the model to predict the behavior for 4MBP and Hsp33 (Hsp33 binding and aggregation, section 5.4). Briefly, the 4MBP molecules showing no aggregation yielded $\alpha(0)$ (Fig. S.1c and equations S.3), while sMBP refolding then gave $\beta(0)$ and $\gamma(0)$ (Eq. S.6). sMBP refolding with 0.5 and 5 μM Hsp33 gave $\eta(c)$, and in turn also $\alpha(c)$, $\beta(c)$, and $\gamma(c)$ for these Hsp33 concentrations (Eq. S.7). The model then predicted the probability to form 0, 1, 2, 3, or 4 aggregated ($P_a^i(c)$, Eq. S5), unfolded ($P_u^i(c)$, Eq. S.9), and folded ($P_f^i(c)$, Eq. S.10) monomers. These predictions were remarkably similar to the measured data, and displayed the same trends (Fig. 5.4c-5.4e). For instance, P_u first increased and then decreases for increasing i in the case of 0.5 μM Hsp33, whereas it increased monotonically for 5 μM (Fig. 5.4c).

The close correspondence indicated the model reproduced key features of the data. Deviations were also apparent. For instance, the P_u^i distribution of the model was shifted to somewhat higher number of unfolded monomers i compared to the data (Fig. 5.4c), and correspondingly, to lower numbers of folded monomers (Fig. 5.4e). These differences could result from the assumption that Hsp33 affects unfolded monomers only. To relax the model constraints, we fitted the complete dataset to one set of equations (equation S.11), which indeed resulted in a closer agreement (Fig. S.2). A key difference was that the probability to refold $\beta(c)$ could now vary for different c values, and was indeed found to increase for increasing c . This finding could be linked to the observed ability of Hsp33 to bind folded structures, as this could promote their formation, and hence explain an increased refolding probability. However, other mechanisms cannot be excluded.

5.4 Discussion

ATP-independent holdase chaperones including Hsp33 are known to bind unfolded protein chains with or without secondary structure [78, 164], which can protect them from aggregation, and by the same token, suppress refolding into tertiary structure

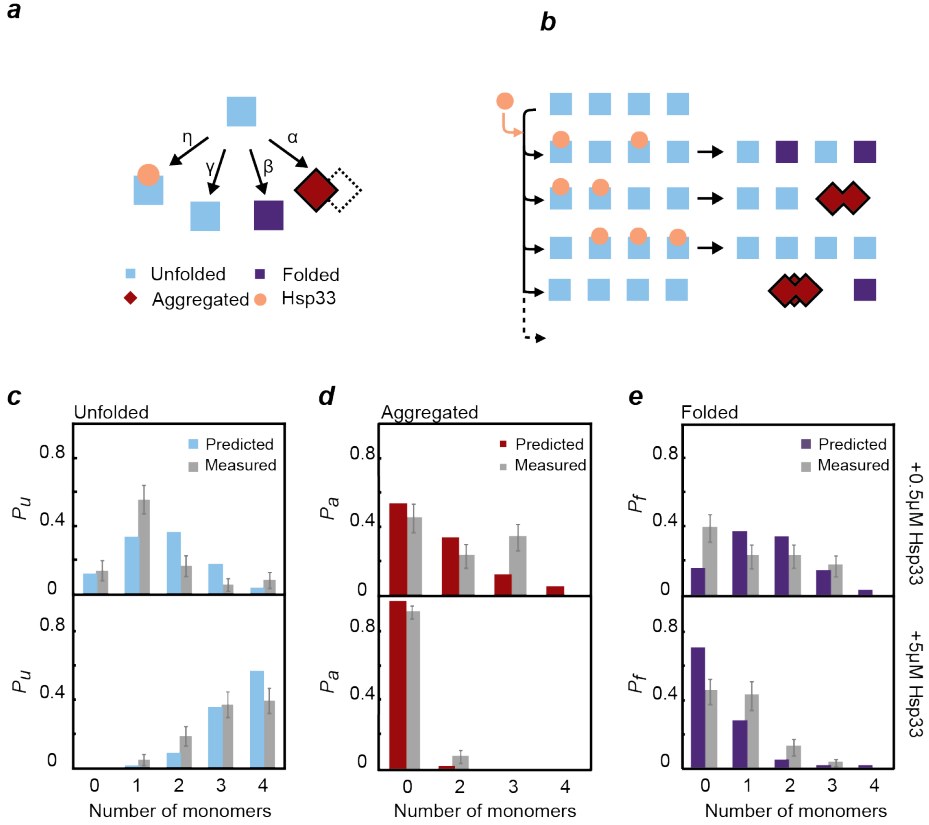


Figure 5.4: A model to predict the 4MBP refolding in the presence of Hsp33 (a) Within a fully unfolded and relaxed 4MBP molecules, the model assumes each MBP monomer can adopt either an aggregated, folded, or unfolded state, with the probability of α , β , and γ respectively. Binding to Hsp33 molecules, blocks the monomer in the unfolded state (η). (b) The chaperones can bind four unfolded MBP monomers in a number of combinatorial patterns. Monomers bound by Hsp33 remain unfolded, whereas unbound monomers can fold, aggregate, or remain unfolded. Predicted versus measured probability for an unfolded and relaxed 4MBP molecule to form i number of unfolded (c), aggregated (d) and folded (e) core structures. Error bars show 95% confidence intervals estimated by bootstrapping.

until removal by Hsp70 and end to episodes of stress [164]. Consistent with this notion, we found that Hsp33 promotes the unfolded state in MBP amino acid chains (on average 90% of both sMBP and 4MBP chains for 5 mM Hsp33). Notably however, the data indicated that Hsp33 bound and induced small changes in the partially folded MBP core state, indicating that Hsp33 function goes beyond binding secondary structure and unfolded chains [164]. The direct binding to (partially) folded tertiary structures is difficult to detect using bulk methods, but has been observed for the chaperone Trigger Factor using optical tweezers [135]. In contrast however, Trigger Factor bound partial folds of various sizes and increased their resistance against unfolding, whereas for Hsp33 the affected structures were within a narrow size-range,

and resulted in decreased resistance against forced unfolding. One may speculate a structural origin for these differences. Trigger Factor can stabilize diverse substrate structures by encapsulating them with its arm domains [175], while the flexibility of the intrinsically disordered domains of Hsp33 could allow it to bind less accessible substrate residues, and hence perturb its structure and stability. Consistently, we observe a negative correlation between Hsp33-mediated structure size and unfolding force (Fig. 5.3c). Note that the similarity between Hsp33-mediated and native MBP states, in terms of size, unfolding forces, and two-transition unfolding pattern, suggests the underlying substrate structure is close to the MBP core state and bound by Hsp33.

Hsp33 was also found to increase the relative fraction of native-like folded structures, and hence promote folding over aggregation - a function that is typically not attributed to holdases but rather to foldases [76]. At the same time, the promoted structures were not fully natively folded, and hence would not be detected by bulk refolding assays that measure function [134]. In order to understand the ingredients that could explain these observations, we developed a statistical mechanics model that includes a minimal set of interactions. Without fitting, key features of the numbers of unfolded, folded, and aggregated MBP monomers in 4MBP with Hsp33 were reproduced by a model that accounts for the combinatorial pattern of Hsp33 binding to unfolded MBP monomers. The model provides an explanation for promotion of folding over aggregation by Hsp33, as it shows that aggregation is more sensitive to the Hsp33 binding probability η than folding. Indeed, the former is suppressed when either the monomer itself or its aggregation partner is bound (scaling is η^{10} vs η^4 respectively). The binding of Hsp33 to folded structures may also contribute to suppressing aggregation and promoting folding, and indeed can contribute to a better agreement between model and data. Hsp33 may remain loosely bound to the chain as it explores conformation towards the folded state [96], or be detached during the conformational search.

The functional role of holdases has been discussed extensively. Holdases can act early by binding polypeptide chains and suppressing their aggregation, with foldases like Hsp70 required for disassembly and refolding. The presented data and analysis shows the Hsp33 holdase can act later, promote folding over aggregation, bind folded tertiary structure, and hence affect the protein conformational search. The holding of proteins in a near-functional state may benefit cells after episodes of stress. Finally, the bottom-up single-molecule approach in probing the statistical mechanics of aggregation suppression can be applied to other systems, such as the effect of small Hsp's on the aggregation between amyloid-beta and alpha synuclein monomers.

Supplementary information

S.1 determining protein lengths

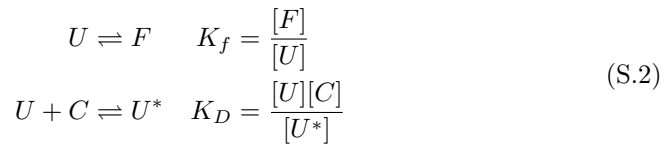
To determine protein lengths, we fitted measured force-extension data to a worm-like chain model [6] of a DNA-Polypeptide construct, with the polypeptide-contour length (L_p) as the fitting parameter (Eq. S1). D and p indexes indicate DNA and protein, respectively.

$$\begin{aligned} F_{WLC,D}(x) &= \frac{k_B T}{p_D} \left(\frac{1}{4} \left(1 - \frac{x_D}{L_D} + \frac{F}{K} \right)^{-2} - \frac{1}{4} + \frac{x_D}{L_p} - \frac{F}{K} \right) \\ F_{WLC,p}(x) &= \frac{k_B T}{p_p} \left(\frac{1}{4} \left(1 - \frac{x_p}{L_p} \right)^{-2} - \frac{1}{4} + \frac{x_p}{L_p} \right) \end{aligned} \quad (\text{S.1})$$

Within the equations S1, F is the force, x is the extension, L is the contour length, p is the persistence length, K is the stretch modulus, k_B is the Boltzmann constant, and T is absolute temperature. The force-extension data was fitted assuming the DNA linker and the polypeptide as two springs in series, i.e. $F = F_{WLC,D} = F_{WLC,p}$; $x_{Total} = x_D + x_p$. We note the protein length is assumed to be equal to the contour length of the unfolded part of the protein chain, given the comparatively small contribution of folded structures to the measured length.

S.2 Hsp33-MBP affinity

To calculate the MBP-Hsp33 complex dissociation constant, we modeled the system as two first-order reactions (Eq. S2). We assumed the chaperone (C) only interacts with the unfolded state (U) and make a complex that stabilizes the protein in the unfolded state (U^*). When an unfolded polypeptide chain is not in complex with chaperone, it could either fold (F) or stay unfolded. Assuming the fraction of bound chaperones was equilibrated at zero force, the folding (K_f) and dissociation constants (K_D) could be calculated as follows:



We used the experimentally obtained refolding probability of MBP in the presence of different concentrations of Hsp33 to compute the equilibrium constants (Eq. S3).

$$p_f = \frac{[F]}{[F] + [U] + [U^*]} = \frac{K_f}{K_f + 1 + \frac{[C]}{K_D}} \quad (\text{S.3})$$

$$1 - p_f = \frac{1 + \frac{[C]}{K_D}}{K_f + 1 + \frac{[C]}{K_D}}$$

Using no chaperone experiments, the K_f value is computed to equal to 2.34 and accordingly the K_D values for 0.5 μM and 5 μM are computed to be 0.43 μM and 0.31 μM , respectively. These values are obviously similar in magnitude and are consistent with the range of values observed previously [7]. The equilibrium constants can be further used to estimate the fraction of proteins in complex with the chaperone, i.e. $[U^*]$, at any given chaperone concentration (Eq. S4).

$$\eta(C) = \frac{[U^*]}{[U^*] + [U] + [F]} = \frac{\frac{[C]}{K_D}}{K_f + 1 + \frac{[C]}{K_D}} \quad (\text{S.4})$$

S.3 A prediction-based model

Here we aim to predict the refolding behavior of 4MBP in the presence of chaperones, using the experimental data of sMBP refolding in the absence and presence of chaperone, and of 4MBP refolding in the absence of chaperone. In this model, a fully unfolded 4MBP is a linear chain of four tandem MBP monomers, where each monomer can adopt three different states; "aggregated", "folded", and "unfolded" with the probability of α , β and $(\eta + \gamma)$, respectively (Fig. 4a). The monomers adopted the unfolded state are either bound to the chaperone (with the probability of η) or unbound (with a probability of γ). We note individual monomers can independently transition to the folded or unfolded states, whereas they need at least one aggregating partner, i.e. another unfolded monomer to aggregate (Fig. 4a).

S.3.1 Aggregated state

Here we describe the aggregation probability within 4MBP in the presence of Hsp33. We defined aggregation as an interaction between two unbound unfolded monomers (Fig. S1b), whereas the monomers bound by Hsp33 do not aggregate (Fig. 4b). The adjacent and non-adjacent monomers are considered to have the same probability to form an aggregate. The equations S5 are used to determine the probability P_a^i of having i aggregated monomers ($i = 0, 2, 3, \text{ or } 4$).

$$\begin{aligned} P_a^0 &= f_4 \times (1 - \alpha)^6 + f_3 \times (1 - \alpha)^3 + f_2 \times (1 - \alpha) + f_1 + f_0 \\ P_a^2 &= f_4 \times 6(1 - \alpha)^5 \alpha + f_3 \times 3(1 - \alpha)^2 \alpha + f_2 \times \alpha \\ P_a^3 &= f_4 \times (4(1 - \alpha)^3 \alpha^3 + 12(1 - \alpha)^4 \alpha^2) + f_3 \times (\alpha^3 + 3\alpha^2(1 - \alpha)) \\ P_a^4 &= f_4 \times (\alpha^6 + 6(1 - \alpha)\alpha^5 + 15(1 - \alpha)^2 \alpha^4 + 16(1 - \alpha)^3 \alpha^3 + 3(1 - \alpha)^4 \alpha^2) \end{aligned} \quad (\text{S.5})$$

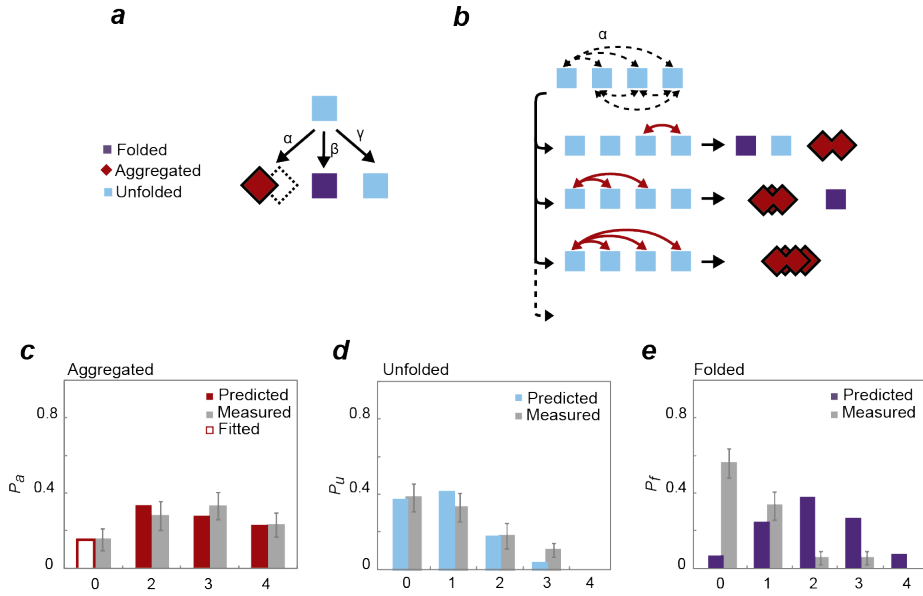


Figure S.1: The predictive model computes the 4MBP refolding in the absence of chaperone (a) Within an unfolded and relaxed 4MBP molecule, the monomers can adopt three different states; "aggregated", "folded", and "unfolded" with the probability of α , β and γ , respectively. (b) Aggregation has defined as a pair-wise interaction between monomers with the probability of α . There are six possible pair-wise interactions between four monomers that could form in a number of combinatorial patterns. (c) Using the experimentally measured value of $P_a = 0$, we computed α and accordingly predicted the probability of forming 2, 3, 4 aggregated monomers. The model also predicts the probability of having i unfolded (d) and folded (e) monomers, where $i = 0, 1, 2, 3$, and 4. Error bars show 95% confidence intervals estimated by bootstrapping.

f_i represents the fraction of protein chains with i number of unbound monomers, and so $\sigma f_i = 1$. In the absence of chaperone, all monomers are unbound and so we have a homogeneous ensemble of protein chains with 4 monomers capable of adopting the aggregated states (Table S1). Thus, $f_4 = 1$ and $f_3 = f_2 = f_1 = f_0 = 0$. We use the experimentally measured frequency of 4MBP chains that do not show aggregation (Fig. S1c) in conjunction with P_a^0 (Eq. S5) to determine the alpha value ($\alpha(0)$). We find that using this alpha value, the other S5 equations predict the experimental data for $i = 2, 3$, and 4 aggregated monomers quite well (Fig. S1c). Note that $P_a^1 = 0$ because a single monomer cannot aggregate.

In the presence of chaperone, we have a heterogeneous ensemble of 4MBP chains with different numbers of bound Hsp33 and different binding patterns (Table S2). To obtain the f_i values, we need to know the probability of a monomer to bind the chaperone ($\eta(c)$), that already has been computed in the previous section (Eq. S4). Using the $\eta(c)$ values, the equations S6 are then used to determine the probability P_{bi} of having i bound monomers ($i = 0, 1, 2, 3$, or 4). Afterward, the f_i values can be computed as $f_i = P_b^4 - i$.

$$\begin{aligned}
P_b^4 &= \eta^4 \\
P_b^3 &= 4\eta^3(1 - \eta) \\
P_b^2 &= 6\eta^2(1 - \eta)^2 \\
P_b^1 &= 4\eta(1 - \eta)^3 \\
P_b^0 &= (1 - \eta)^4
\end{aligned} \tag{S.6}$$

Alteration in the number of unbound monomers, also changes the availability of aggregation partners and so, the probability of a monomer to aggregate ($\alpha(c) \neq \alpha(0)$). To compute $\alpha(c)$ at any given chaperone concentration, we assumed a linear effect that lowers the probabilities among the unbound states (α , β , and γ) proportionately (Eq. S7). Using the η values and $\alpha(c)$, equation S5 predicts the probability to observe i aggregated monomers in the presence of Hsp33 (Fig. 4d).

$$\begin{aligned}
\alpha(c) &= \alpha(0) \times (1 - \eta) \\
\beta(c) &= \beta(0) \times (1 - \eta) \\
\gamma(c) &= \gamma(0) \times (1 - \eta)
\end{aligned} \tag{S.7}$$

S.3.2 Unfolded states

Here we describe the probability of a monomer to remain unfolded within 4MBP chain. In the absence of chaperone, a non-aggregated monomer has two possibilities: i) to remain unfolded with a probability of γ ii) to adopt a folded state with a probability of β (Fig. 1Sa). We assumed that among the non-aggregated monomers the competition between folding and remaining unfolded is similar to sMBP that lacks the aggregated state. So the $\beta(0)$ and $\gamma(0)$ values can be estimated using the experimentally measured probabilities of sMBP to fold (p_f) or remain unfolded (p_u) (Eq. S8).

$$\begin{aligned}
\gamma(0) &= p_u \times (1 - \alpha(0)) \\
\beta(0) &= p_f \times (1 - \alpha(0))
\end{aligned} \tag{S.8}$$

In the presence of chaperone, 4MBP can be bound by Hsp33 in different combinatorial patterns, and have $i = 0, 1, 2, 3$, or 4 unfolded monomers (Table S3). However, the unbound monomers can also adopt the unfolded state with the probability of $\gamma(c)$ (Eq. S7). The equations S9 give the overall probabilities P_u^i of having i unfolded monomers ($i = 0, 1, 2, 3$, or 4) using the fraction of bound ($\eta(c)$) and unbound ($\gamma(c)$) unfolded monomers.

$$\begin{aligned}
P_u^4 &= (\eta(c) + \gamma(c))^4 \\
P_u^3 &= 4(\eta(c) + \gamma(c))^3(1 - \eta(c) - \gamma(c)) \\
P_u^2 &= 6(\eta(c) + \gamma(c))^2(1 - \eta(c) - \gamma(c))^2 \\
P_u^1 &= 4(\eta(c) + \gamma(c))(1 - \eta(c) - \gamma(c))^3 \\
P_u^0 &= (1 - \eta(c) - \gamma(c))^4
\end{aligned} \tag{S.9}$$

The equations S9 evidently can predict the P_u^i values in the absence of chaperone, using $\gamma(0)$ (Fig. 1Sd).

S.3.3 Folded state

Here we describe the refolding of monomers within 4MBP in the presence of chaperone. Table S4 indicates all the 4MBP states, in which each monomer can be in one of three states (unfolded, folded, aggregated), but 4MBP cannot have a single aggregated monomer. Based on these 4MBP states and using the probability of a monomer to fold ($\beta(c)$), equation S8 indicates the probability P_f^i of having i folded monomers ($i = 0, 1, 2, 3, \text{ or } 4$).

$$\begin{aligned} P_f^4 &= \beta(c)^4 \\ P_f^3 &= 4\beta(c)^3(1 - \beta(c)) \\ P_f^2 &= 6\beta(c)^2(1 - \beta(c))^2 \\ P_f^1 &= 4\beta(c)(1 - \beta(c))^3 \\ P_f^0 &= (1 - \beta(c))^4 \end{aligned} \tag{S.10}$$

Note for no chaperone condition, the P_f^i values also can be determined, using the equations S8 and $\beta(0)$ value (Fig. 1Se).

S.4 Fitting the complete data set

Here, we aim to fit the complete data set and relax some of the assumptions in the previous predictions. For this purpose, we assign x as the statistical weight of a monomer to be unfolded, and y to account for the aggregation between two monomers. These weights are relative to the folded monomer, hence its statistical weight can be assumed to be unity without any loss of generality. These statistical weights (x ; y) are related to Boltzmann weights, implicitly accounting for chain entropy, enthalpy and temperature. These factors are not probabilities but can be used to compute probabilities of different states as outlined below. Based on this, we construct the statistical weight of 11 distinct micro-states (Table S5). These states are labeled as $(n_u; n_a; n_f)$ where n_u is the number of unfolded monomers, n_a is the number of aggregated monomers and n_f is the number of folded monomers, such

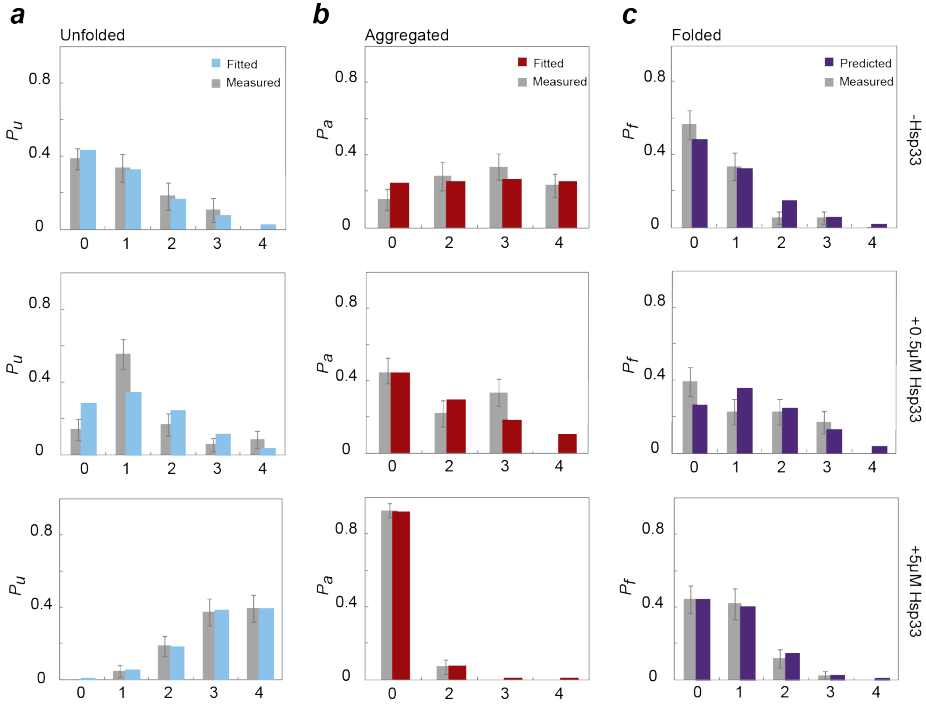


Figure S.2: Fitting the data set to describe the refolding of 4MBP, using Boltzmann weights. The fitting model assigns different statistical weights for monomers in different states, i.e. folded, unfolded and aggregated. At any given chaperone concentration (0, 0.5μM and 5μM), the experimentally measured probabilities for the formation of aggregated (a) and unfolded (b) monomers were fitted by the model to predict the formation of folded monomers (c). The plots represent the probabilities versus number of monomers. Error bars show 95% confidence intervals estimated by bootstrapping.

that $n_u + n_a + n_f = 4$. The equations S11 show the statistical weights of these states.

$$\begin{aligned}
 w_{400} &= x^4 \\
 w_{301} &= 4x^3 \\
 w_{202} &= 6x^2 \\
 w_{220} &= 6x^2y \\
 w_{130} &= 4x(3y^2 + y^3) \\
 w_{121} &= 12xy \\
 w_{103} &= 4x \\
 w_{040} &= y^6 + 6y^5 + 15y^4 + 16y^3 + 3y^2 \\
 w_{031} &= 4(3y^2 + y^3) \\
 w_{022} &= 6y \\
 w_{004} &= 1
 \end{aligned} \tag{S.11}$$

Different powers of x accounts for the number of monomers that are in the unfolded configuration, additional contributions from the polynomials in y represent combinations of pair-wise interactions between individual monomers that lead to aggregation (Table S5). Following usual statistical mechanical procedure, the partition sum Q is defined as the sum of the weights (S12), and can be used to obtain probabilities from weights [8].

$$Q = w_{400} + w_{301} + w_{202} + w_{130} + w_{121} + w_{103} + w_{040} + w_{031} + w_{022} + w_{004} \quad (\text{S.12})$$

The probability distributions of unfolded, folded and aggregated monomers are computed using equations (S13), (S14) and (S15), respectively.

$$\begin{aligned} P_u^4 &= \frac{w_{400}}{Q} & P_u^3 &= \frac{w_{301}}{Q} \\ P_u^2 &= \frac{w_{220} + w_{202}}{Q} & P_u^1 &= \frac{w_{130} + w_{121} + w_{103}}{Q} \\ P_u^0 &= \frac{w_{040} + w_{031} + w_{022} + w_{004}}{Q} \end{aligned} \quad (\text{S.13})$$

$$\begin{aligned} P_f^4 &= \frac{w_{004}}{Q} & P_f^3 &= \frac{w_{103}}{Q} \\ P_f^2 &= \frac{w_{202} + w_{022}}{Q} & P_f^1 &= \frac{w_{031} + w_{121} + w_{301}}{Q} \\ P_f^0 &= \frac{w_{400} + w_{220} + w_{130} + w_{040}}{Q} \end{aligned} \quad (\text{S.14})$$

$$\begin{aligned} P_a^4 &= \frac{w_{040}}{Q} & P_a^3 &= \frac{w_{130} + w_{031}}{Q} \\ P_a^2 &= \frac{w_{220} + w_{022} + w_{121}}{Q} & P_a^1 &= 0 \\ P_a^0 &= \frac{w_{400} + w_{301} + w_{202} + w_{004} + w_{103}}{Q} \end{aligned} \quad (\text{S.15})$$

We now use this formalism to fit the experimentally observed probability distribution of unfolding and aggregation simultaneously and determine the best fit values of x and y (Fig. S2). The fitted values of x ; y under different chaperone conditions are reported in Table S6.

Table S.1: Schematic distribution of aggregated monomers in the absence of chaperone. The red boxes represent aggregated monomers, whereas the hatched boxes represent monomers in the non-aggregated state, i.e. unfolded or folded states.










Micro-states	Schematics	Probability
$a=0$		$(1-\alpha)^6$
$a=2$		$6(1-\alpha)^5\alpha$
$a=3$		$12(1-\alpha)^4\alpha^2$
		$4(1-\alpha)^3\alpha^3$
$a=4$		$3(1-\alpha)^4\alpha^2$
		$15(1-\alpha)^2\alpha^4$
		$16(1-\alpha)^3\alpha^3$
		$6(1-\alpha)\alpha^5$
		α^6

Table S.2: Schematic distribution of aggregated monomers in the presence of chaperone. The red, blue, and purple boxes represent aggregated, unfolded, and folded monomers, respectively.










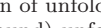

Micro-states	Schematics	Probability
$a=0$		f_0
		f_1
		$f_2 \times (1-\alpha)$
		$f_3 \times (1-\alpha)^3$
		$f_4 \times (1-\alpha)^6$
$a=2$		$f_4 \times 6(1-\alpha)^5\alpha$
		$f_3 \times 3(1-\alpha)^2\alpha$
		$f_2 \times \alpha$
$a=3$		$f_4 \times \{4(1-\alpha)^3\alpha^3 + 12(1-\alpha)^4\alpha^2\}$
$a=4$		$f_3 \times \{a^3 + 3a^2(1-\alpha)\}$
		$f_4 \times \{a^6 + 6(1-\alpha)a^5 + 15(1-\alpha)^2a^4 + 16(1-\alpha)^3a^3 + 3(1-\alpha)^4a^2\}$

Table S.3: Schematic distribution of unfolded monomers in the presence of chaperone. The blue boxes represent (bound and unbound) unfolded monomers, whereas the dotted boxes represent monomers in the structured state, i.e folded or aggregated.






Micro-states	Schematics	Probability
$u=0$		$(1-(\eta+\gamma))^4$
$u=1$		$4(\eta+\gamma)(1-(\eta+\gamma))^3$
$u=2$		$6(\eta+\gamma)^2(1-(\eta+\gamma))^2$
$u=3$		$4(\eta+\gamma)^3(1-(\eta+\gamma))$
$u=4$		$(\eta+\gamma)^4$

Table S.4: Schematic distribution of folded monomers in the presence of chaperone. The purple, blue and red boxes represent folded, unfolded and aggregated monomers, respectively.
















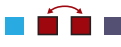



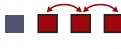








Micro-states	Schematics	Probability
f=0		$(1-\beta)^4$
		
		
		
f=1		$4 \beta (1-\beta)^3$
		
		
f=2		$6 \beta^2 (1-\beta)^2$
		
f=3		$4 \beta^3 (1-\beta)$
f=4		β^4

Table S.5: Schematics of 11 different micro-states in the fitting model. Blue represents an unfolded monomer (statistical weight of x), red denotes an aggregated monomer and purple denotes a folded monomer. Solid black lines connecting two aggregated monomers denote pair-wise interactions (statistical weight of y). Degeneracy of different micro-states due to combinatorics is given by g , and w is the overall weightage

Micro-states	Schematics	Weightage	Degeneracy
400		x^4	1
301		$4x^3$	4
202		$6x^2$	6
220		$6x^2y$	6
121		$12xy$	12
022		$6y$	6
130		$4x(3y^2)$	12
		$4xy^3$	4
031		$4(3y^2)$	12
		$4y^3$	4
040		$3y^2$	3
		y^6	1
		$6y^5$	6
		$15y^4$	15
		$16y^3$	16
103		$4x$	4
004		1	1

CHAPTER **6**

**Direct observation of
Hsp90-induced
conformational changes in a
protein chain**

Abstract

Heat shock protein 90 (HSP90) is an essential molecular chaperone that interacts with a wide range of client proteins in higher eukaryotes. A number of Hsp90 clients are oncogenic or otherwise required for cell proliferation, however the molecular mechanism of this interaction has been elusive. Here, we investigate the principals underlying the chaperone function of HtpG, the prokaryotic homologue of Hsp90 using optical tweezers at the single molecule level. We directly observe HtpG influences the unfolding and refolding pathways of Luciferase in real time. Our results show HtpG, in an ATP-dependent and step-wise manner, can promote chain structures that are stable in time and against force. Moreover, HtpG action suppresses the intra- and inter-domain misfoldings. This finding seems to be relevant to the many physiological roles of Hsp90.

6.1 Introduction

Heat shock protein 90 (Hsp90) is a chaperone that is essential in eukaryotic cells and highly conserved from bacteria to mammals. Hsp90 is involved in a wide array of cellular functions, ranging from protection against heat stress to signal transduction and protein trafficking [185]. Many of its functions are coordinated by the Hsp70 chaperone system [65, 105]. Hsp90 also interacts with more than 20 co-chaperones in Eukaryotes [138], while no co-chaperone has been identified for the *Escherichia coli* Hsp90, which is also termed HtpG (high temperature protein G). Two Hsp90 monomers, each consisting of a nucleotide binding, linker, and dimerization domain, form a V-shaped structure that undergoes large conformational changes driven by the ATP cycle (Fig. 6.1a). The Hsp90 dimer populates distinct conformations, ranging from a fully extended state to a compact state, which can coexist in an equilibrium that depends on nucleotide, pH, and osmolyte conditions [111, 173, 181].

Hsp90 and its substrates display a complex interplay. The intrinsically disordered Tau protein was found to bind Hsp90 in an open conformation in an ATP-independent manner, while ATP did affect Hsp90 conformation of pre-formed Tau-Hsp90 complexes [103]. The intrinsically disordered ribosomal protein L2 accelerates ATP hydrolysis by Hsp90, suggesting that L2 binding can stimulate Hsp90 closure [149]. The bacterial Hsp90 has been found to bind a locally structured region of the partially folded model protein $\Delta 131\Delta$ [182]. Hsp90 has been reported to bind the glucocorticoid receptor ligand-binding domain both in open and closed conformations, though more efficiently in the former [123]. In contrast to $\Delta 131\Delta$ and L2 however, binding here slowed down Hsp90 closure decelerated ATP hydrolysis. Overall, these findings indicate that substrate binding affects and depends on Hsp90 conformation.

In contrast, it remains poorly understood how substrate conformation is affected by Hsp90 binding. Bacterial Hsp90 can stimulate reactivation of misfolded Luciferase in collaboration with the Hsp70 system [65]. Eukaryotic Hsp90 has been shown to reactivate Luciferase together with co-chaperone Hop/Sti1 [99], and modulate the activity of steroid receptors in conjunction with the Hsp70 system and different co-chaperones [146]. Hsp90 is also known to facilitate de novo folding in the cellular context [188]. Whether Hsp90 can alter the conformational state of its substrates directly is incompletely understood [182]. Addressing this issue is challenging, for instance because of the involvement of other chaperone systems and co-chaperones, and because proteins are inherently dynamic and hence change conformation independently of chaperone interactions.

Here we study this question by measuring conformational states of single protein chains using optical tweezers. We find that HtpG can compact Luciferase protein chains in an ATP-dependent and step-wise manner. Moreover, HtpG action suppresses the formation of Luciferase misfolded states and aggregation between Maltose Binding Protein monomers.

6.2 Material and Methods

6.2.1 Design, expression and purification of Luciferase

Luciferase was expressed and purified as explained previously [132]. Briefly, Avi-luci-4myc was expressed as hybrid protein consisting of an Ulp1-cleavable N-terminal His₁₀-SUMO tag followed by an AviTag, the luciferase gene and four consecutive myc-tags at the C-terminus. Overexpression was performed in *E. coli* BL21 cells harboring pBirAcm (Avidity, LCC, Aurora, Colorado, USA) in LB medium supplemented with 20 mg/l Biotin, 20 mg/l Kanamycin, 10 mg/l Chloramphenicol, 0.1 mM IPTG at 20°C for about 20 hours. Cells from 1.5 l culture volume were lysed in buffer L containing 50 mM NaPO₄, pH 8, 0.3 M NaCl, 10% glycerol, 2 mM mercaptoethanol. The lysate was cleared from cell debris by centrifugation at 35.000 g for 30 min and incubated for 1 hour with 2 g Ni-IDA matrix (Protino; Macherey-Nagel, Düren, Germany). The matrix was washed extensively with buffer L and bound protein was eluted in buffer L containing 250 mM imidazol. Eluate fractions containing the hybrid protein were pooled, His₆-Ulp1 protease was added and dialyzed over night at 4°C in buffer L. The next day, the protein mixture was subjected to a second Ni-IDA purification to remove the His-tagged protease and the His₁₀-SUMO fragment and flow-through fractions containing purified Avi-luci-4myc were concentrated using Vivaspin concentration columns (Vivaproducts, Inc. Littleton, MA).

6.2.2 Expression and purification of HtpG

The Chaperone sample was provided by the group of Prof. Bernd Bukau (ZMBH, Heidelberg, Germany). Briefly, HtpG and HtpG^{E34A} were expressed as C-terminal His₁₀-fusions in *E. coli* MC4100 $\Delta htpG::kan$, and purified by Ni-DA-chromatography (Protino, Macherey-Nagel) and anion-exchange chromatography (ResourceQ, GE Healthcare). The purified proteins were checked to be nucleotide-free by anion-exchange chromatography (ReSourceQ) and by UV detection by 254 nm.

6.2.3 other preparations

The beads preparation, the optical tweezers measurements and the expression and purification of 4MBP construction were done as described before (see section 3.2.3 and 3.2.1).

6.2.4 Calculation of unfolding and refolding energies

The unfolding energy was assumed to be equal to the mechanical work done by the trapped microsphere to unfold the protein and similarly the refolding energy was considered to be equivalent to the mechanical work performed by the tethered protein chain to move the trapped microsphere. The unfolding and refolding works were calculated as the area below a force vs. extension curve during stretching and relaxation, respectively (Mossa, de Lorenzo et al. 2009). The energy contribution of DNA handle was accounted by subtracting corresponding contribution of a WLC-model (equation S1).

6.3 Results

6.3.1 Protein chain compaction by HtpG

To assay interactions between HtpG and a single protein chain, we tethered a Luciferase molecule between two polystyrene beads via a DNA linker (Fig. 6.1b and 6.1c). In the absence of chaperone, Luciferase typically unfolded in several steps upon stretching, as evidenced by discrete increases in extension [132] (Fig. 6.1d). During subsequent lowering of the applied force, the protein chain remained unfolded (Fig. 6.1d). After complete relaxation to 0 pN and waiting for 5 s, stretching curves in subsequent stretching and relaxation cycles typically resulted in unfolding (87% of the traces, Fig. 6.1d and 6.1f), indicating the relaxed protein chain had refolded fully or partially during the waiting time at 0 pN. In the remaining 13% of the traces no unfolding features were observed. In the absence of chaperone, the protein chains thus exhibited a high probability to form folded structures (Fig. 6.1f).

In the presence of HtpG and ATP, the first stretching curves were similar as without chaperone. Thus, no interaction between HtpG and natively folded Luciferase was detected. Subsequent stretching curves after relaxation lacked unfolding features more often than in the absence of HtpG (33%, Fig. 6.1f). These data suggested that HtpG could bind unfolded protein chains, which is consistent with previous reports [103, 149].

Several other changes could be distinguished in the data (Fig. 6.1d and 6.1e). In particular, unfolding seemed to require lower applied forces during stretching, while measured forces appeared higher during relaxation. In addition, the shapes of the curves were different and appeared smoother. To quantify these diverse changes, we determined the surface area under the relaxation and stretching curves, which reflects the performed work (Fig. 6.1g and 6.1h). As our focus is on protein conformation, we subtracted the area corresponding to the DNA linker and the extended part of the protein chain, using theoretical worm-like chain curves [148]. The corresponding histograms showed that on average, interactions with HtpG increased the area under the relaxation curve (Fig. 6.1g), indicating that the protein chain was more contracted. These data suggested that HtpG could promote more compact conformations of the protein chain against applied forces.

In contrast, the area under the stretching curve decreased with HtpG (Fig. 6.1h). Thus, whereas relaxation indicated an increased stability of compact structures against forced unfolding, stretching indicated a decreased stability. These opposing trends are not in contradiction however, as folding- and HtpG-promoted conformational changes may be different, and exhibit more or less hysteresis in their formation and disruption. Consistently, the area under stretching curves was equal or larger than the area under the previous relaxation curve (Fig. 6.1i). This finding supported the notion that HtpG promoted more compact chain structures during relaxation that were disrupted during subsequent stretching.

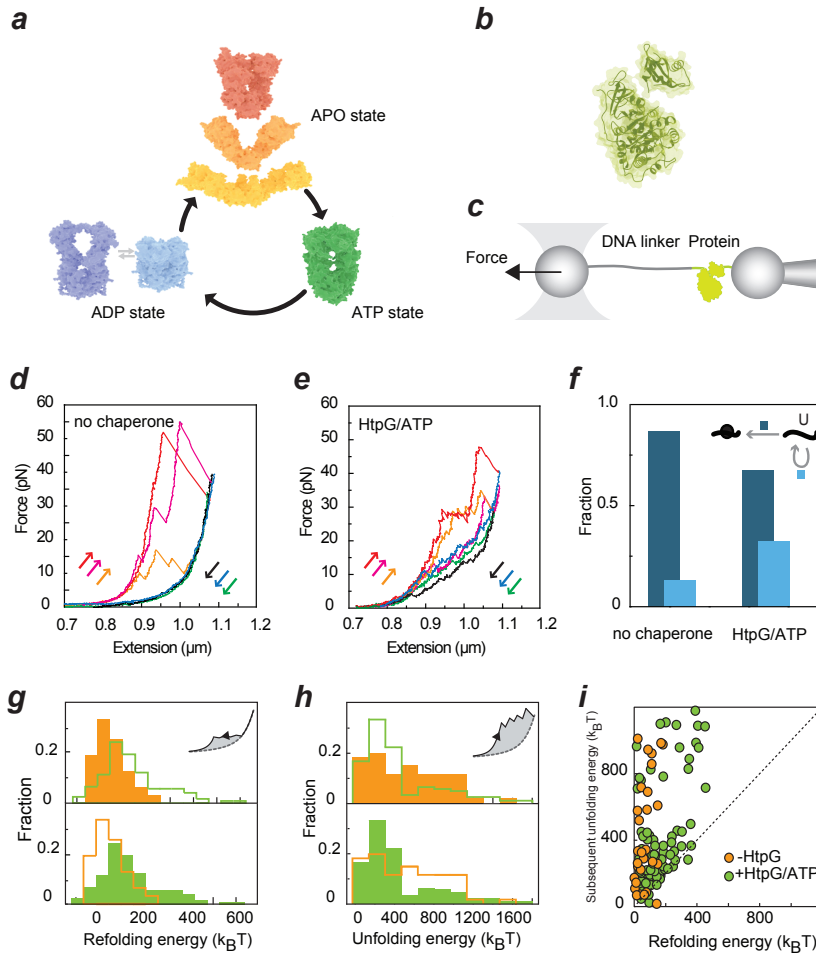


Figure 6.1: HtpG compacts protein chains (a) HtpG conformational equilibrium. At APO state, HtpG is crystallized in a V-shaped conformation (top panel-middle molecule)[173]. SAXS measurements have revealed that, in solution, more extended (top panel-upper molecule) and compact (top panel-lower molecule) conformations are mainly populated [110]. Binding to ATP, HtpG undergoes N-terminal dimerization and forms a "closed state" (right panel). The crystallized HtpG, in complex with ADP shows a compact state that probably forms after ATP hydrolysis (left panel, left molecule) [2]. EM experiments characterize another highly squeezed conformation at ADP state (left panel, right molecule) that is not easily detectable using other methods [173] (b) Structure of model protein, Firefly Luciferase (550 residues). (c) Schematic diagram of the set-up. (d) Luciferase stretching-relaxation pathways in the absence of any chaperone. The force-extension data shows the protein unfolds in single or multi big steps and after full unfolding, it stays fully extended all the way to zero force. (e) Stretching-relaxation pathways in the presence of HtpG(1 μ M)/ATP(1mM) indicating the alteration of protein structure by the chaperone. The compaction of unfolded protein, during relaxation is the most obvious difference (f) Fraction of unfolded proteins that (partially or completely) fold is also affected by the presence of HtpG/ATP complex. (g) Comparing the work done during relaxation to compact the unfolded polypeptide chain against applied force (h) Comparing the work done during stretching to unfold Luciferase with and without HtpG/ATP, the protein structure seems to be destabilized by the chaperone (i) The essential work to unfold protein structure vs the amount of energy it has gained during preceding relaxation cycle shows the compacted polypeptide chains could energetically form two types of structures; stable structures that need high energy to be disrupted and unstable structure that conserved the gained energy during preceding relaxation.

6.3.2 Step-wise HtpG-promoted compaction

Interactions with HtpG affected not only the area under the stretching and relaxation curves, but also their shape (Fig. 6.1d and 6.1e). To analyse these changes, we determined the effective length of the proteins using the worm-like chain model (Fig. 6.2a and 6.2b). This protein length is approximately equal to the contour length of the unfolded part of the protein chain, given the comparatively small contribution of folded structures to the measured length. In the absence of HtpG, the protein length typically increased in a few large steps (20-200 nm, see Fig. 6.2d) during stretching but was otherwise constant. The protein length remained approximately constant during subsequent relaxation (Fig. 6.2b), until folding occurred at 0 pN and tertiary structure was formed. The latter is not observed directly as lengths cannot be measured without applied force, but is rather evidenced from subsequent stretching and unfolding in a few discrete steps.

In the presence of HtpG and ATP, the protein length also displayed step-wise increases during stretching (Fig. 6.2b). The step-sizes were broadly distributed, lower on average, and showed a pronounced peak at about 12 nm (Fig. 6.2e and 6.2f). The relaxation traces now also displayed discrete steps (Fig. 6.2b). The step-sizes were more narrowly distributed, and peaked again at about 12 nm (Fig. 6.2e and 6.2f). We also observed gradual changes in protein length without detectable discrete steps (Fig. 6.2c). Both gradual decreases in protein length during relaxation, and gradual increases in protein length during stretching were observed.

The analysis provided further indications that HtpG can promote conformations within the protein chain that are stable both in time and against forced unfolding. Specifically, the steps with similar size distributions for relaxation and stretching (Fig. 6.2e and 6.2f), which are scarcely observed without HtpG (Fig. 6.2d), suggest HtpG can promote structures during relaxation that remain stable until disruption during stretching. The stability of these structures may rely on continued interaction with HtpG. Similarly; we observed gradual transitions promoted by HtpG during relaxation and stretching. The step-size distribution suggested a typical length scale of about 12 nm. Interestingly, HtpG extends to about 13 nm (the distance between the NTD domains) in its fully extended conformation [110], and may thus accommodate a protein chain of that order. Indeed, during relaxation we did not observe steps beyond 25 nm (Fig. 6.2f). The formation of the small structures occurred predominantly between 5 and 25 pN, and disruption between 5 and 40 pN (Fig. 6.2g). Note that energy considerations can also play a role in the length-scale for HtpG-promoted structures. As can be seen in the data (Fig. S1), step-wise protein length decreases pull the trapped bead away from the laser centre, and produce force increases. Because of the associated work, the probability of forming structures becomes smaller as the structures become larger.

6.3.3 Suppression of misfolding by HtpG

The data so far indicated that HtpG can promote gradual and small step-wise length-changes smaller than 25 nm, which reflect small chain structures that could be complexed with HtpG. At the same time, the stretching curves also displayed discrete

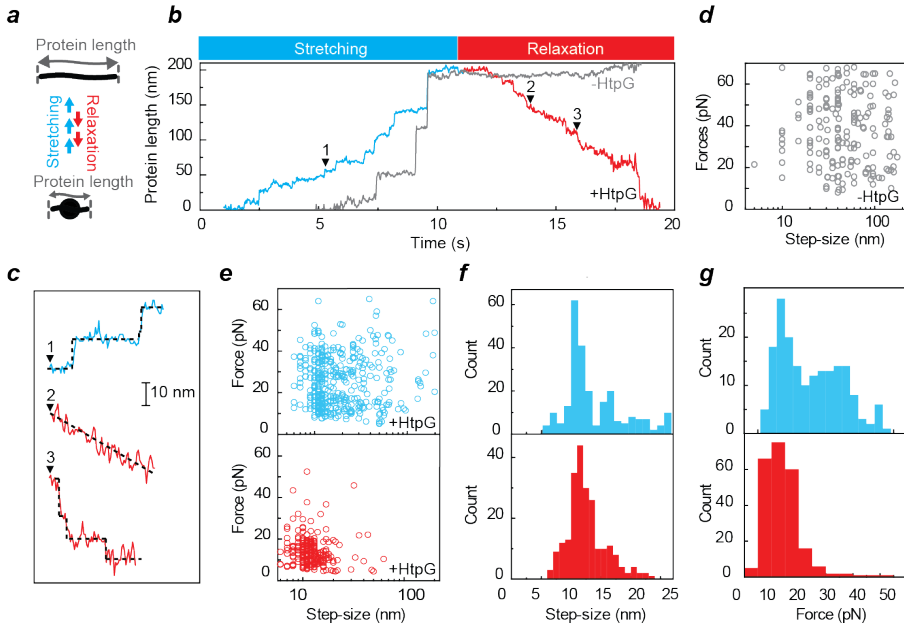


Figure 6.2: HtpG induces small steps in the protein structure, detectable during stretching and relaxation pathways. (a) When a folded protein undergoes unfolding, accordingly the protein length, i.e. the end to end distance increases. The apparent length could be quantified by fitting the force-extension data to a worm-like chain model. (b and c) Variation of protein length vs time in the presence and absence of HtpG indicates during stretching, Luciferase unfolds quickly via a few big jumps without HtpG. Whereas with HtpG Luciferase opens slowly through passing many small steps (1▼) and some big jumps. During relaxation, unfolded Luciferase stays fully extended without HtpG, while with HtpG the protein length decreases till full compaction. The compaction could be either gradually (2▼) or step-wisely (3▼). Characterizing the observed steps during stretching cycle without (d) and with (e-top panel) HtpG shows the significant number of small steps had emerged in the presence of chaperone. These steps are also detectable during relaxation cycle (e-bottom panel). (f) Histograms of step sizes, zoomed on small steps, confirm an almost same length for the peak position during stretching (upper panel) and relaxation (lower panel). (g) Histograms of forces, corresponding to the observed small steps ($L < 14\text{nm}$), represent two peaks during stretching; a narrow peak at low forces and a broad peak at high forces. The low force peak is similar to the observed peak during relaxation, while the broad peak overlaps with the unfolding force distribution of Luciferase in the absence of chaperone.

unfolding steps larger than 25 nm (Fig. 6.2e) and large curve-areas (Fig. 6.1g and 6.1i). These features were characteristic for the stretching curves in the absence of HtpG (Fig. 6.1h and 6.1i, Fig. 6.2d), and suggested the formation of larger tertiary structures that contain many cooperative intra-chain interactions, and hence unfold in discrete steps. We could also observe such unfolding steps of more than 25 nm when unfolded chains were relaxed down to 5 pN with HtpG and then stretched (Fig. S1b), which suggested that the gradual and small step-wise length changes observed during relaxation can contribute to the formation of larger structures that unfold in discrete steps. We note that these observations do not formally exclude the possibility that the large (over 25 nm) steps reflect the disruption of HtpG-Luciferase

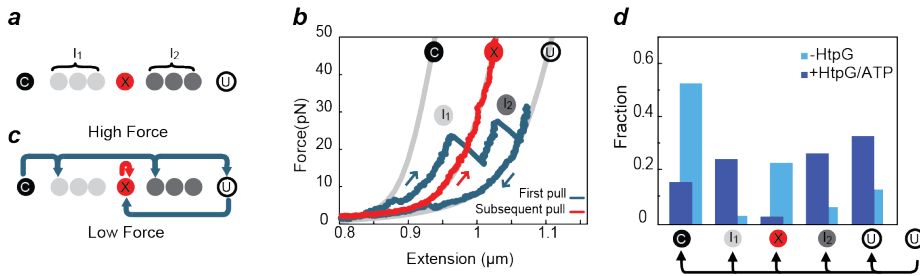


Figure 6.3: HtpG suppresses the misfolding of Luciferase (a) The mechanical unfolding of native-like Luciferase, from fully compact state (C) to fully unfolded state (U), could involve multiple transitions between partially folded structures. One of these intermediates, named as X state, is stable over several minutes and withstands high unfolding forces. The X state can be distinguished from larger (I₁) and smaller (I₂) states of intermediate length. (b and c) In the absence of chaperone, the frequent stretching and relaxation cycles of Luciferase (waiting time at zero force=5 sec) often result in the formation of X state. The gray lines represent the theoretical WLC characterizing the DNA-protein construct. (d) In the presence of HtpG(1μM)/ATP(1mM), after full unfolding in the first pulling cycle, second or subsequent stretching pulls rarely show characteristics of X state.

complexes in which the Luciferase chain does not have significant tertiary structure.

To further probe whether HtpG affects tertiary-structure formation, we studied Luciferase misfolding. Luciferase can adopt non-native states by repeated freeze-thaw, which can be rescued by HtpG [65, 99]. Luciferase has also been shown to misfold in mechanical stretching-relaxation cycles [132]. During the 5 s waiting time at 0 pN in stretching and relaxation cycles, and in the absence of chaperone, Luciferase most often (25% of the cases) formed folded structures termed the X state that are characterized by a protein length of 105 nm (Fig. 6.3b and 6.3c). These states can be distinguished from larger (I₁) and smaller (I₂) states of intermediate length, and from the fully compact (C) and fully unfolded (U) states, which are populated less frequently (Fig. 6.3a). X states have been identified as misfolded states, as they have a significantly longer lifetime (minutes) and larger unfolding force (43 pN) than other states of intermediate length (seconds and 24 pN respectively), and are infrequently populated during unfolding of fully folded proteins [132].

In the presence of HtpG and ATP, relaxed Luciferase chains formed misfolded X-state structures less frequently during the 5 s waiting time at 0 pN. Compared to the absence of chaperones, we observed an almost 10-fold reduction (from 25% to about 3% of the cases, Fig. 6.3d). The X states that did form rarely unfolded even when stretching beyond 65 pN or continued folding in a subsequent waiting time at 0 pN. Together, these data suggest that the presence of HtpG suppresses entry into the X state, without completely abolishing it. This suppression may be explained by an overall suppression in forming folded structures, caused by HtpG binding that competes with tertiary structure formation. We indeed observed an increase in the cases in which the protein chain remained unfolded (from 13% to 33% of the cases, Fig. 6.1f and 6.3d). At the same time however, protein structures larger than the X state (the C and I₁ states) together decreased by less than 2-fold (from 55% to 39% of the cases, Fig. 6.3d). Thus, the formation of X-state structures was impaired

more strongly than structures of larger size. Overall, the findings indicate that HtpG can suppress misfolding in Luciferase, and that it appears targeted specifically to misfolding.

Next, we explored the effect of HtpG on misfolding in a different protein system. We focused on a construct composed of four Maltose Binding Protein monomers arranged head-to-tail, which we refer to as 4MBP [15, 135]. Stretching this protein for the first time in the absence of HtpG results in an unfolding pattern that is characterized by four discrete events reflecting the unfolding of four MBP core structures (Fig. S2b). After relaxation and waiting at 0 pN for 5 s, stretching showed the protein chain adopted a compact structure that often could not fully unfold (Fig. S2c). The curves also showed steps larger than one MBP monomer (Fig. S2c). These data indicated misfolding and aggregation of MBP cores (Fig. S2e). In the presence of HtpG and ATP, we found that the first stretching curve was similar as without HtpG, thus mirroring the lack of interaction in the first Luciferase stretching curves. Relaxation curves were also similar as without HtpG, and hence did not show chain compaction as was observed with Luciferase. However, subsequent stretching curves now were quite different. Tight misfolds that could not be unfolded were only rarely observed (Fig. S2d and S2e). Moreover, we now observed the discrete events reflecting the unfolding of MBP core structures (Fig. S2d). The presence of HtpG led to an about 3-fold increase of such events (Fig. S2e, from 4% to 13%). Overall, these data indicated that HtpG interacted with the MBP protein chains, in a way that suppressed misfolding while still allowing the folding of MBP cores.

6.3.4 HtpG-promoted conformational changes are stimulated ATP hydrolysis

HtpG undergoes conformational changes driven by an ATP hydrolysis cycle (Fig. 6.1a), which presses the question whether the observed effects depend upon it. In experiments with HtpG but without ATP, we found that the area under Luciferase relaxation curves was on average smaller than with HtpG and ATP, but larger than without HtpG (Fig. 6.4a and 6.4c). These data suggested a non-zero but weak capacity of HtpG^{APO} to promote chain-compaction, which is stimulated by ATP hydrolysis. To further investigate this issue we aimed to perturb ATP hydrolysis. ATP hydrolysis in Hsp90 proteins occurs within a conserved ATP binding site [161]. In HtpG, a Glu to Ala mutation at residue 34 in this binding site decreases the rate of ATP hydrolysis about 10-fold [65, 69]. In the presence of HtpG^{E34A} and ATP, the majority of stretching curves (67%) showed extended chains that lacked unfolding features (Fig. 6.4b and 6.4d). This data indicated that the mutant interacted with the protein chain and suppressed its refolding, as also observed for WT HtpG (Fig. 6.1f and 6.4d). However, in the stretching curves that did show unfolding features, the gradual and small step-wise length changes seen with WT HtpG were lacking, and rather displayed large unfolding steps as seen without HtpG (Fig. S1c). In addition, the relaxation curves lacked the compaction seen for WT HtpG, and indeed followed the worm-like chain behaviour more closely than other conditions (Fig. 6.4c and 6.1g). These data indicated that ATP hydrolysis stimulates HtpG-promoted gradual and small step-wise length changes.

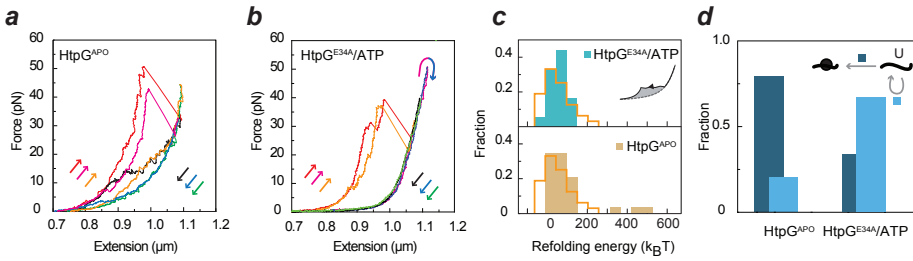


Figure 6.4: HtpG-promoted conformational changes are stimulated by ATP hydrolysis. (a) Stretching-relaxation pathways in the presence of HtpG (1μM) and absence of ATP suggest a non-zero but weak capacity of HtpG^{APO} to promote chain-compaction, (b) whereas in the presence of HtpG^{E34A}, the ATPase deficient mutant of HtpG and ATP no compaction was detected during relaxation pathways. (c) Comparing the work done to compact the unfolded polypeptide chains against applied force during relaxation in the presence of HtpG^{APO} and HtpG^{E34A}/ATP. Orange lines mirror no chaperone condition. (d) The refolding probability of Luciferase is greatly affected by HtpG^{E34A} and moderately influenced by HtpG^{APO}

6.4 Discussion

Mechanical manipulation and force sensing have enabled a direct observation of single protein chain conformations altered by the *E. coli* Hsp90. Real-time length measurements of unfolded chains tethered under low tension displayed gradual and small discrete contractions below 25 nm. These compaction features may result from Hsp90 molecules binding and stabilizing small chain structures that form spontaneously, driven by Brownian motion and intra-chain contacts. Various observations are consistent with this scenario: 1) Hsp90 suppresses the formation of large structures that unfold in large discrete steps, which suggests it binds unfolded chains or small early folding structures. The binding of Hsp90 to unstructured and partially folded chains is consistent with data on the tau [103] and Δ131Δ [181] substrates respectively. 2) The gradual and step-like features observed during relaxation are also seen during stretching, which suggests the underlying Hsp90-promoted chain structures can remain stable in between. 3) ATP hydrolysis arrest and supposed Hsp90 closure [181] abolishes compaction, indicating Hsp90-binding is specific. Interestingly, Hsp90 maintains chains in their unfolded state under these conditions, which indicates continued interaction. These data suggest that open Hsp90 is central to compaction, consistent with reported binding in the open state. 4) In the absence of Hsp90, Luciferase chains already show deviations from a non-interacting worm-like chain and hence compaction (Fig. 6.1g), which suggests that intra-chain contacts form dynamically and spontaneously during relaxation. MBP shows less spontaneous compaction than Luciferase without Hsp90, and consistently Hsp90 does not promote compaction. We note that other factors, such as differences in charge distributions, could also contribute. More generally however, the data does not exclude that conformational transitions in Hsp90 rather than in the substrate chain plays the more causal role in the observed contractions.

The data indicated that Hsp90 can suppress entry into misfolded and aggregated

states in Luciferase and MBP respectively. By binding unstructured segments of the chain, Hsp90 could neutralize them as aggregation and misfolding partners, and hence allow other (unbound) chain segments to form a tertiary structure. Previous work indicated that the chaperone trigger factor can limit MBP aggregation by suppressing interactions between different monomers while promoting local chain interactions within a single monomer [135, 175]. Such a mechanism that promotes local interactions could also underlie the suppression of misfolding observed for Hsp90. The observed Hsp90-promoted small chain structures are in line with such a scenario. By binding local structures, Hsp90 could suppress interactions between Luciferase domains that give rise to misfolding. In the open state Hsp90 has been suggested to form cradle that can accommodate a folding protein chain, as also proposed for Trigger Factor [135]. Differences are also evident. For instance, trigger factor does promote small structures MBP whereas Hsp90 does not to a detectable level.

Overall, the study provides a direct observation of Hsp90 affecting the conformation of a protein chain. We find that Hsp90 does not merely bind a chain locally, but that binding can promote chain structures that are stable in time and against force. This finding is relevant to the many physiological roles of Hsp90. It is of interest to consider whether the interaction of Hsp90 with diverse regulatory proteins involves the promotion of local structures, and how this contributes to modulating their activity.

Supplementary information

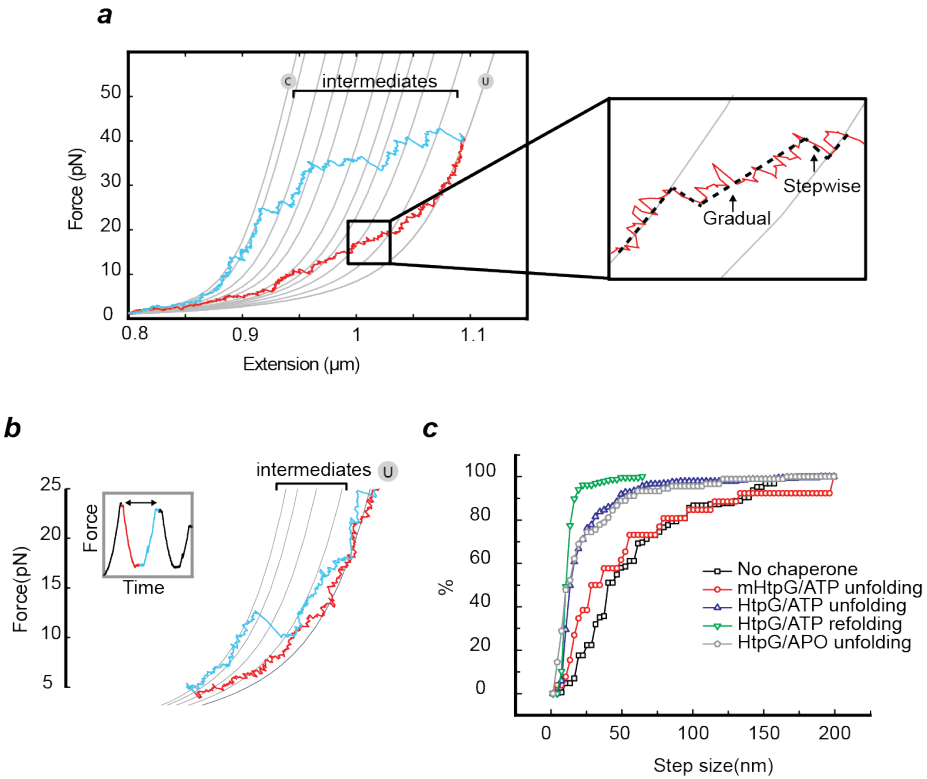


Figure S.1: Characterizing the HtpG-induced conformational change in Luciferase. (a) A representative Force-Extension curve recorded during stretching (blue) and subsequent relaxation of Luciferase in the presence of HtpG/ATP. The magnification of the region marked by the black square allows observation of deviation from WLC during relaxation. Two types of events can be distinguished that underlie the deviation: step-wise and gradual contractions. (b) These contractions can contribute to the formation of larger structures that unfold in discrete steps. (c) The length statistics of steps at different conditions.

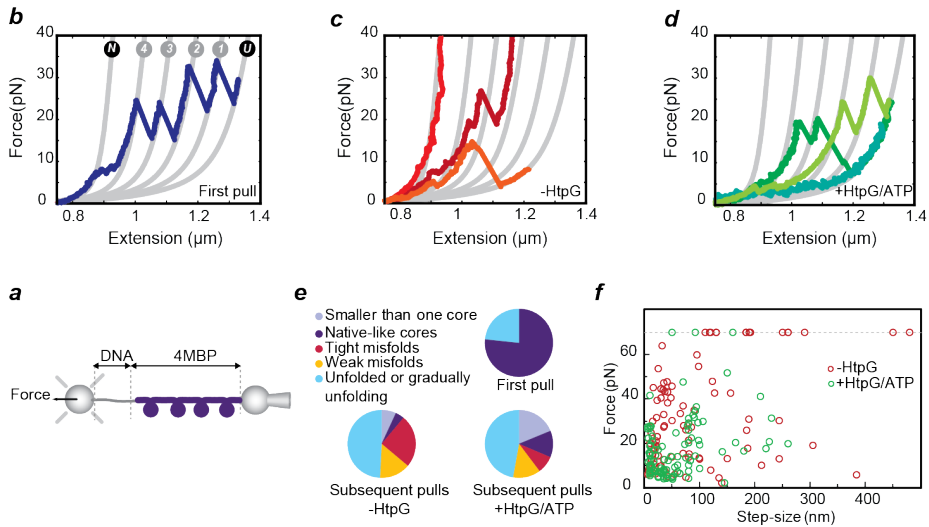


Figure S.2: HtpG suppresses inter-domain misfolding (a) Schematic representation of tethering a 4MBP molecule between two anti-body-coated beads via a DNA linker. Force-extension curves for 4MB construct, (b) showing the unfolding pattern of natively-folded 4MBP. Gray lines represent the theoretical WLC characterizing the DNA-protein construct from fully-folded (F) to fully unfolded (U) state. After C-terminal unfolding ($U \rightarrow 4$), four native-like core unfolding events ($4 \rightarrow 3 \rightarrow 2 \rightarrow 1 \rightarrow U$) are observed. In the absence of chaperone, (c) second or subsequent stretching curves mostly show either tight misfolds (that cannot unfold) or weak misfolds (that release chain segments exceeding one core structure, i.e. 92 nm). In the presence of HtpG/ATP, (d) tight misfolds are suppressed while native-like folds are promoted. (e) Corresponding event fractions ($N=xx$) and (f) scatter force-step size plot of structures observed in the isolation and with HtpG/ATP.

CHAPTER 7

conclusion

Protein folding is an assembly process that transforms an unstructured polypeptide chain of amino acids to a functionally active three-dimensional structure. The intrinsic properties of the amino acid sequence as well as the extrinsic characteristics of crowded cellular milieu influence on the folding process. However, the precise mechanism of protein folding is still one of the grand challenges of modern science [44].

The proteins that fail to fold properly, or cannot stay properly folded, are considered as the origin of a wide variety of diseases. To suppress the formation of misfolded structure, different compartments of diverse cells are equipped with molecular chaperones. Chaperones are considered as protein machines that monitor the folding process, interact with non-native conformations, and assist the transition to the native state whereas ultimately they do not incorporate into the final structure. Some chaperones are capable of rescuing the misfolded and even aggregated protein substrates. They give a new chance to damaged proteins to fold properly, and at the same time transfer terminally misfolded or irreversibly damaged proteins to the degradation pathway. Chaperone-mediated protein foldings are complex processes that need further investigations to be understood.

Many details of the functions of chaperones have been determined by bulk studies over the past decades, but several fundamental questions are still unanswered because of the transient and heterogeneous nature of chaperon-substrate interactions. For example, we do not know precisely how chaperones affect on the conformation of protein substrates, which is considered to be fundamental to the chaperones function. The conformational dynamics of different chaperone families, their relation to the dynamics of client proteins, the physical principles underlying the chaperones functions, the exact role of energy consumption for ATP-dependent chaperones are some examples of many important questions that remain to be answered. The emerging single molecule techniques provide new promising ways to adress many of these questions.

Single-molecule approaches can monitor the conformational dynamics of individual isolated protein molecules over a prolonged period of time, in the presence and absence of chaperones. This makes these techniques capable of detecting hidden folding intermediates, as well as revealing the chaperone-promoted states. Currently two types of methods are used to study protein folding at the single molecule level, namely fluorescence methods and force spectroscopy. These methods can provide complementary information and have different capabilities to detect intermediates. Fluorescence methods, such as single pair Förster Resonance Energy Transfer (FRET), Fluorescence Correlation Spectroscopy (FCS), and Photoinduced Electron Transfer (PET), study the structure, conformation, interactions, and dynamics of the substrate-chaperone system, using naturally fluorescent compounds or synthetic fluorophore labels. Force spectroscopy methods, including Atomic Force Microscope (AFM) and Optical Tweezers (OT), mechanically perturb folded proteins and monitor their unfolding and refolding pathways in real time. These methods are capable of observing the formation of folding intermediates, probing their strength and significance, and monitoring the transition between them.

In this thesis, we used a force-based assay, optical tweezers, to investigate how chaperones influence the folding of proteins, at the single molecule level. We studied the interactions between different model proteins and four chaperones from three

different families, including small Hsps (yeast Hsp42 (chapter 3), and human HspB6 (chapter 4), redox-regulated chaperones (yeast Hsp33 (chapter 5)), and Hsp90 family (bacterial HtpG (chapter 6))). Our results probe the preferable binding state of each chaperone, and in real time show how the chaperone affects the conformation of client proteins during folding and/or unfolding. In chapter 3, we studied the role of yeast small Hsp Hsp42 in preventing amorphous aggregation, using a construct of MBP repeats (4MBP) as the substrate. Our results show Hsp42 prevents tight intra-domain and promotes native-like re-folding via interacting with the folded state. To precisely probe how Hsp42 influences the folded state, we further investigated the folding of single domain MBP, which folds efficiently in isolation, in the presence of chaperone. When Hsp42 is present, the refolding of MBP is not suppressed whereas the unfolding force of refolded structures was lower than in the absence of chaperone. Consistently, a similar destabilization was observed for refolded cores in the 4MBP construct. This finding suggested that Hsp42 bound to and destabilized the folded structure, possibly by binding to small detached peptide segments.

We continued investigating the chaperone function of small Hsps, by looking into the interaction of HspB6, a human small Hsp and α -synuclein in chapter 4. α -synuclein is a well-known substrate to form highly ordered aggregates and is mainly expressed in the neural tissue of vertebrates, including humans. Using a construct of four tandem α -synuclein, we found HspB6 stimulates the formation of compact structures and stabilizes them against force unfolding. Our results suggest interaction with the folded structures is the generic feature of HspB6 functioning, as we observed that HspB6 similarly stabilizes MBP folds with the known tertiary structure. Overall, the findings of chapter 3 and 4 suggest small Hsps can interact with the folded state which is counterintuitive to the current image of small Hsps as holdases interacting with unfolded polypeptide.

In chapter 5, we explored another chaperon that is mostly known as a holdase, namely Hsp33. Consistent with the present definition of an holdase, we found Hsp33 stabilizes the protein chains in the unfolded state, but surprisingly also promotes partial refolding within monomers over aggregation between monomers. Moreover, force spectroscopy on refolded monomers indicates Hsp33 binds and deforms an intermediate refolded state, weakening it against unfolding and blocking transition to the native state. A statistical mechanics model allowed us to dissect the competition between folding, aggregation, and binding transitions, and to predict how Hsp33 affects the state of interacting MBP monomers without additional fitting.

In contrast to the previous chapters, chapter 6 is dedicated to an ATP-dependent chaperone. HtpG is the bacterial homologue of Hsp90, an essential eukaryotic chaperone known to interact with a variety client proteins (e.g. receptors, transcription factors and kinases) in their native or near-native states, however the molecular mechanism of this interaction has been elusive. We found that HtpG, in an ATP-dependent and step-wise manner, can promote chain structures in the model protein Luciferase that are stable in time and against force. Moreover, HtpG action suppresses the intra- and inter-domain misfoldings. This finding seems to be relevant to the many physiological roles of Hsp90.

In summary, our single molecules studies reveal new mechanistic information on the action of investigated chaperones and represent a broader range of chaperone

functions than previously assumed.

Bibliography

- [1] I. Afonina et al. “Efficient priming of PCR with short oligonucleotides conjugated to a minor groove binder”. In: *Nucleic Acids Res* 25.13 (1997), pp. 2657–60. ISSN: 0305-1048 (Print) 0305-1048 (Linking). URL: <http://www.ncbi.nlm.nih.gov/pubmed/9185578>.
- [2] M. M. U. Ali et al. “Crystal structure of an Hsp90-nucleotide-p23/Sba1 closed chaperone complex”. In: *Nature* 440.7087 (2006), pp. 1013–1017. ISSN: 0028-0836. DOI: 10.1038/nature04716.
- [3] M. H. Ali and B. Imperiali. “Protein oligomerization: how and why”. In: *Bioorganic & medicinal chemistry* 13.17 (2005), pp. 5013–5020.
- [4] T. Anelli and R. Sitia. “Protein quality control in the early secretory pathway”. In: *The EMBO journal* 27.2 (2008), pp. 315–327.
- [5] K. Araki and K. Nagata. “Protein folding and quality control in the ER”. In: *Cold Spring Harbor perspectives in biology* 3.11 (2011), a007526.
- [6] R. D. Astumian. “Biasing the random walk of a molecular motor”. In: *Journal of Physics: Condensed Matter* 17.47 (2005), S3753.
- [7] M. E. Aubin-Tam et al. “Single-molecule protein unfolding and translocation by an ATP-fueled proteolytic machine”. In: *Cell* 145.2 (2011), pp. 257–67. ISSN: 1097-4172 (Electronic) 0092-8674 (Linking). DOI: 10.1016/j.cell.2011.03.036. URL: <http://www.ncbi.nlm.nih.gov/pubmed/21496645>.
- [8] A. J. Baldwin et al. “Metastability of native proteins and the phenomenon of amyloid formation”. In: *J Am Chem Soc* 133.36 (2011), pp. 14160–3. ISSN: 1520-5126 (Electronic) 0002-7863 (Linking). DOI: 10.1021/ja2017703. URL: <http://www.ncbi.nlm.nih.gov/pubmed/21650202>.
- [9] B. Banecki et al. “Structure-function analysis of the zinc finger region of the DnaJ molecular chaperone”. In: *Journal of Biological Chemistry* 271.25 (1996), pp. 14840–14848.
- [10] A. Bar-Even et al. “The moderately efficient enzyme: evolutionary and physicochemical trends shaping enzyme parameters”. In: *Biochemistry* 50.21 (2011), pp. 4402–4410.

- [11] A. Barducci and P. D. L. Rios. “Non-equilibrium conformational dynamics in the function of molecular chaperones”. In: *Current Opinion in Structural Biology* 30 (2015), pp. 161–169. ISSN: 0959-440X. DOI: <http://dx.doi.org/10.1016/j.sbi.2015.02.008>. URL: <http://www.sciencedirect.com/science/article/pii/S0959440X15000172>.
- [12] A. Barhoumi et al. “Light-induced release of DNA from plasmon-resonant nanoparticles: towards light-controlled gene therapy”. In: *Chemical Physics Letters* 482.4-6 (2009), pp. 171–179. ISSN: 0009-2614. DOI: 10.1016/j.cplett.2009.09.076.
- [13] T. Bartels, J. G. Choi, and D. J. Selkoe. “Alpha-synuclein occurs physiologically as a helically folded tetramer that resists aggregation”. In: *Nature* 477.7362 (2011), pp. 107–10. ISSN: 1476-4687 (Electronic) 0028-0836 (Linking). DOI: 10.1038/nature10324. URL: <http://www.ncbi.nlm.nih.gov/pubmed/21841800>.
- [14] E. Basha, H. O’Neill, and E. Vierling. “Small heat shock proteins and alpha-crystallins: dynamic proteins with flexible functions”. In: *Trends Biochem Sci* 37.3 (2012), pp. 106–17. ISSN: 0968-0004 (Print) 0968-0004 (Linking). DOI: 10.1016/j.tibs.2011.11.005. URL: <http://www.ncbi.nlm.nih.gov/pubmed/22177323>.
- [15] P. Bechtluft et al. “Direct observation of chaperone-induced changes in a protein folding pathway”. In: *Science* 318.5855 (2007), pp. 1458–61. ISSN: 1095-9203 (Electronic) 0036-8075 (Linking). DOI: 10.1126/science.1144972. URL: <http://www.ncbi.nlm.nih.gov/pubmed/18048690>.
- [16] S. J. Benkovic, G. G. Hammes, and S. Hammes-Schiffer. “Free-energy landscape of enzyme catalysis”. In: *Biochemistry* 47.11 (2008), pp. 3317–3321.
- [17] O. Boudker, M. J. Todd, and E. Freire. “The structural stability of the co-chaperonin GroES”. In: *Journal of molecular biology* 272.5 (1997), pp. 770–779.
- [18] E. Braun et al. “DNA-templated assembly and electrode attachment of a conducting silver wire”. In: *Nature* 391.6669 (1998), pp. 775–8. ISSN: 0028-0836 (Print) 0028-0836 (Linking). DOI: 10.1038/35826. URL: <http://www.ncbi.nlm.nih.gov/pubmed/9486645>.
- [19] B. van den Broek, M. C. Noom, and G. J. L. Wuite. “DNA-tension dependence of restriction enzyme activity reveals mechanochemical properties of the reaction pathway”. In: *Nucleic Acids Research* 33.8 (2005), pp. 2676–2684. ISSN: 0305-1048. DOI: 10.1093/nar/gki565.
- [20] I. B. Bruinsma et al. “Inhibition of alpha-synuclein aggregation by small heat shock proteins”. In: *Proteins* 79.10 (2011), pp. 2956–67. ISSN: 1097-0134 (Electronic) 0887-3585 (Linking). DOI: 10.1002/prot.23152. URL: <http://www.ncbi.nlm.nih.gov/pubmed/21905118>.
- [21] A. Buchberger, B. Bukau, and T. Sommer. “Protein quality control in the cytosol and the endoplasmic reticulum: brothers in arms”. In: *Molecular Cell* 40.2 (2010), pp. 238–252. ISSN: 1097-2765. DOI: 10.1016/j.molcel.2010.10.001.

- [22] O. V. Bukach et al. "Some properties of human small heat shock protein Hsp20 (HspB6)". In: *Eur J Biochem* 271.2 (2004), pp. 291–302. ISSN: 0014-2956 (Print) 0014-2956 (Linking). URL: <http://www.ncbi.nlm.nih.gov/pubmed/14717697>.
- [23] M. Busby et al. "Optimisation of a multivalent Strep tag for protein detection". In: *Biophysical Chemistry* 152.1-3 (2010), pp. 170–177. ISSN: 0301-4622. DOI: 10.1016/j.bpc.2010.09.005.
- [24] A. G. Cashikar, M. Duennwald, and S. L. Lindquist. "A chaperone pathway in protein disaggregation. Hsp26 alters the nature of protein aggregates to facilitate reactivation by Hsp104". In: *J Biol Chem* 280.25 (2005), pp. 23869–75. ISSN: 0021-9258 (Print) 0021-9258 (Linking). DOI: 10.1074/jbc.M502854200. URL: <http://www.ncbi.nlm.nih.gov/pubmed/15845535>.
- [25] C. Cecconi et al. "DNA molecular handles for single-molecule protein-folding studies by optical tweezers". In: *Methods Mol Biol* 749 (2011), pp. 255–71. ISSN: 1940-6029 (Electronic) 1064-3745 (Linking). DOI: 10.1007/978-1-61779-142-0_18. URL: <http://www.ncbi.nlm.nih.gov/pubmed/21674378>.
- [26] C. Cecconi et al. "Protein-DNA chimeras for single molecule mechanical folding studies with the optical tweezers". In: *European Biophysics Journal with Biophysics Letters* 37.6 (2008), pp. 729–738. ISSN: 0175-7571. DOI: 10.1007/s00249-007-0247-y.
- [27] H. S. Chan and K. A. Dill. "Protein folding in the landscape perspective: Chevron plots and non-Arrhenius kinetics". In: *Proteins: Structure, Function, and Bioinformatics* 30.1 (1998), pp. 2–33.
- [28] S. Chandra et al. "Alpha-synuclein cooperates with CSP-alpha in preventing neurodegeneration". In: *Cell* 123.3 (2005), pp. 383–96. ISSN: 0092-8674 (Print) 0092-8674 (Linking). DOI: 10.1016/j.cell.2005.09.028. URL: <http://www.ncbi.nlm.nih.gov/pubmed/16269331>.
- [29] B. Chen et al. "Cellular strategies of protein quality control". In: *Cold Spring Harbor perspectives in biology* 3.8 (2011), a004374.
- [30] J. Chevalier et al. "Biotin and digoxigenin as labels for light and electron microscopy in situ hybridization probes: Where do we stand?" In: *Journal of Histochemistry & Cytochemistry* 45.4 (1997), pp. 481–491. ISSN: 0022-1554.
- [31] C. E. Chivers et al. "A streptavidin variant with slower biotin dissociation and increased mechanostability". In: *Nat Methods* 7.5 (2010), pp. 391–3. ISSN: 1548-7105 (Electronic) 1548-7091 (Linking). DOI: 10.1038/nmeth.1450. URL: <http://www.ncbi.nlm.nih.gov/pubmed/20383133>.
- [32] H. S. Chung and W. A. Eaton. "Single-molecule fluorescence probes dynamics of barrier crossing". In: *Nature* 502.7473 (2013), pp. 685–688.
- [33] A. R. Clark, N. H. Lubsen, and C. Slingsby. "sHSP in the eye lens: crystallin mutations, cataract and proteostasis". In: *Int J Biochem Cell Biol* 44.10 (2012), pp. 1687–97. ISSN: 1878-5875 (Electronic) 1357-2725 (Linking). DOI: 10.1016/j.biocel.2012.02.015. URL: <http://www.ncbi.nlm.nih.gov/pubmed/22405853>.

- [34] M. R. Cookson. “The biochemistry of Parkinson’s disease”. In: *Annu Rev Biochem* 74 (2005), pp. 29–52. ISSN: 0066-4154 (Print) 0066-4154 (Linking). DOI: 10.1146/annurev.biochem.74.082803.133400. URL: <http://www.ncbi.nlm.nih.gov/pubmed/15952880>.
- [35] A. Cooper. “Protein heat capacity: an anomaly that maybe never was”. In: *The Journal of Physical Chemistry Letters* 1.22 (2010), pp. 3298–3304.
- [36] N. C. Corsepis and G. H. Lorimer. “Measuring how much work the chaperone GroEL can do”. In: *Proceedings of the National Academy of Sciences* 110.27 (2013), E2451–E2459.
- [37] N. Cremades et al. “Direct observation of the interconversion of normal and toxic forms of alpha-synuclein”. In: *Cell* 149.5 (2012), pp. 1048–59. ISSN: 1097-4172 (Electronic) 0092-8674 (Linking). DOI: 10.1016/j.cell.2012.03.037. URL: <http://www.ncbi.nlm.nih.gov/pubmed/22632969>.
- [38] C. M. Cremers et al. “Unfolding of metastable linker region is at the core of Hsp33 activation as a redox-regulated chaperone”. In: *Journal of Biological Chemistry* 285.15 (2010), pp. 11243–11251. ISSN: 0021-9258. DOI: 10.1074/jbc.M109.084350.
- [39] B. E. Cross, H. M. O’Dea, and D. J. MacPhee. “Expression of small heat shock-related protein 20 (HSP20) in rat myometrium is markedly decreased during late pregnancy and labour”. In: *Reproduction* 133.4 (2007), pp. 807–17. ISSN: 1470-1626 (Print) 1470-1626 (Linking). DOI: 10.1530/REP-06-0291. URL: <http://www.ncbi.nlm.nih.gov/pubmed/17504924>.
- [40] W. S. Davidson et al. “Stabilization of alpha-synuclein secondary structure upon binding to synthetic membranes”. In: *J Biol Chem* 273.16 (1998), pp. 9443–9. ISSN: 0021-9258 (Print) 0021-9258 (Linking). URL: <http://www.ncbi.nlm.nih.gov/pubmed/9545270>.
- [41] P. De Los Rios and A. Barducci. “Hsp70 chaperones are non-equilibrium machines that achieve ultra-affinity by energy consumption”. In: *Elife* 3 (2014), e02218.
- [42] S. P. Delbecq, J. C. Rosenbaum, and R. E. Klevit. “A mechanism of subunit recruitment in human small heat shock protein oligomers”. In: *Biochemistry* 54.28 (2015), pp. 4276–84. ISSN: 1520-4995 (Electronic) 0006-2960 (Linking). DOI: 10.1021/acs.biochem.5b00490. URL: <http://www.ncbi.nlm.nih.gov/pubmed/26098708>.
- [43] K. A. Dill and S. Bromberg. *Molecular driving forces : statistical thermodynamics in biology, chemistry, physics, and nanoscience*. 2nd. London ; New York: Garland Science, 2011, xx, 756 p. ISBN: 9780815344308 (pbk.) 0815344309 (pbk.)
- [44] C. M. Dobson. “Protein folding and misfolding”. In: *Nature* 426.6968 (2003), pp. 884–890.
- [45] C. M. Dobson, A. Šali, and M. Karplus. “Protein folding: a perspective from theory and experiment”. In: *Angewandte Chemie International Edition* 37.7 (1998), pp. 868–893.

- [46] C. M. Dreiza et al. “Transducible heat shock protein 20 (HSP20) phosphopeptide alters cytoskeletal dynamics”. In: *FASEB J* 19.2 (2005), pp. 261–3. ISSN: 1530-6860 (Electronic) 0892-6638 (Linking). DOI: 10.1096/fj.04-2911fje. URL: <http://www.ncbi.nlm.nih.gov/pubmed/15598710>.
- [47] M. L. Duennwald, A. Echeverria, and J. Shorter. “Small heat shock proteins potentiate amyloid dissolution by protein disaggregases from yeast and humans”. In: *PLoS Biol* 10.6 (2012), e1001346. ISSN: 1545-7885 (Electronic) 1544-9173 (Linking). DOI: 10.1371/journal.pbio.1001346. URL: <http://www.ncbi.nlm.nih.gov/pubmed/22723742>.
- [48] S. Dumont et al. “RNA translocation and unwinding mechanism of HCV NS3 helicase and its coordination by ATP”. In: *Nature* 439.7072 (2006), pp. 105–8. ISSN: 1476-4687 (Electronic) 0028-0836 (Linking). DOI: 10.1038/nature04331. URL: <http://www.ncbi.nlm.nih.gov/pubmed/16397502>.
- [49] M. Ehrnsperger et al. “Binding of non-native protein to Hsp25 during heat shock creates a reservoir of folding intermediates for reactivation”. In: *EMBO J* 16.2 (1997), pp. 221–9. ISSN: 0261-4189 (Print) 0261-4189 (Linking). DOI: 10.1093/emboj/16.2.221. URL: <http://www.ncbi.nlm.nih.gov/pubmed/9029143>.
- [50] H. El-Samad et al. “Surviving heat shock: control strategies for robustness and performance”. In: *Proceedings of the National Academy of Sciences of the United States of America* 102.8 (2005), pp. 2736–2741.
- [51] L. Ellgaard and A. Helenius. “Quality control in the endoplasmic reticulum”. In: *Nature reviews Molecular cell biology* 4.3 (2003), pp. 181–191.
- [52] S. Escusa-Toret, W. I. Vonk, and J. Frydman. “Spatial sequestration of misfolded proteins by a dynamic chaperone pathway enhances cellular fitness during stress”. In: *Nat Cell Biol* 15.10 (2013), pp. 1231–43. ISSN: 1476-4679 (Electronic) 1465-7392 (Linking). DOI: 10.1038/ncb2838. URL: <http://www.ncbi.nlm.nih.gov/pubmed/24036477>.
- [53] D.-J. Fan et al. “Thermal unfolding of Escherichia coli trigger factor studied by ultra-sensitive differential scanning calorimetry”. In: *Biochimica et Biophysica Acta (BBA)-Proteins and Proteomics* 1784.11 (2008), pp. 1728–1734.
- [54] B. Fauvet et al. “Alpha-synuclein in central nervous system and from erythrocytes, mammalian cells, and Escherichia coli exists predominantly as disordered monomer”. In: *J Biol Chem* 287.19 (2012), pp. 15345–64. ISSN: 1083-351X (Electronic) 0021-9258 (Linking). DOI: 10.1074/jbc.M111.318949. URL: <http://www.ncbi.nlm.nih.gov/pubmed/22315227>.
- [55] L. Ferbitz et al. “Trigger factor in complex with the ribosome forms a molecular cradle for nascent proteins”. In: *Nature* 431.7008 (2004), pp. 590–596.
- [56] A. W. Fitzpatrick et al. “Atomic structure and hierarchical assembly of a cross-beta amyloid fibril”. In: *Proc Natl Acad Sci U S A* 110.14 (2013), pp. 5468–73. ISSN: 1091-6490 (Electronic) 0027-8424 (Linking). DOI: 10.1073/pnas.1219476110. URL: <http://www.ncbi.nlm.nih.gov/pubmed/23513222>.

- [57] G. A. Frank et al. "Out-of-equilibrium conformational cycling of GroEL under saturating ATP concentrations". In: *Proceedings of the National Academy of Sciences* 107.14 (2010), pp. 6270–6274.
- [58] T. M. Franzmann et al. "Activation of the chaperone Hsp26 is controlled by the rearrangement of its thermosensor domain". In: *Mol Cell* 29.2 (2008), pp. 207–16. ISSN: 1097-2765 (Print) 1097-2765 (Linking). DOI: 10.1016/j.molcel.2007.11.025. URL: <http://www.ncbi.nlm.nih.gov/pubmed/18243115>.
- [59] D. N. Fuller et al. "A general method for manipulating DNA sequences from any organism with optical tweezers". In: *Nucleic Acids Research* 34.2 (2006). ISSN: 0305-1048. DOI: ARTNe1510.1093/nar/gnj016.
- [60] K. Furukawa et al. "Plasma membrane ion permeability induced by mutant alpha-synuclein contributes to the degeneration of neural cells". In: *J Neurochem* 97.4 (2006), pp. 1071–7. ISSN: 0022-3042 (Print) 0022-3042 (Linking). DOI: 10.1111/j.1471-4159.2006.03803.x. URL: <http://www.ncbi.nlm.nih.gov/pubmed/16606366>.
- [61] C. Garnier et al. "Binding of ATP to heat shock protein 90: evidence for an ATP-binding site in the C-terminal domain". In: *Journal of Biological Chemistry* 277.14 (2002), pp. 12208–12214.
- [62] R. C. Garratt, N. F. Valadares, and J. F. R. Bachega. "Oligomeric proteins". In: *Encyclopedia of Biophysics*. Springer, 2013, pp. 1781–1789.
- [63] C. Garrido et al. "The small heat shock proteins family: the long forgotten chaperones". In: *Int J Biochem Cell Biol* 44.10 (2012), pp. 1588–92. ISSN: 1878-5875 (Electronic) 1357-2725 (Linking). DOI: 10.1016/j.biocel.2012.02.022. URL: <http://www.ncbi.nlm.nih.gov/pubmed/22449631>.
- [64] E. Gazit. "The "Correctly Folded" state of proteins: is it a metastable state?" In: *Angew Chem Int Ed Engl* 41.2 (2002), pp. 257–9. ISSN: 1433-7851 (Print) 1433-7851 (Linking). URL: <http://www.ncbi.nlm.nih.gov/pubmed/12491403>.
- [65] O. Genest et al. "Heat shock protein 90 from Escherichia coli collaborates with the DnaK chaperone system in client protein remodeling". In: *Proceedings of the National Academy of Sciences of the United States of America* 108.20 (2011), pp. 8206–8211. ISSN: 0027-8424. DOI: 10.1073/pnas.1104703108.
- [66] K. Ghosh and K. A. Dill. "Theory for protein folding cooperativity: helix bundles". In: *Journal of the American Chemical Society* 131.6 (2009), pp. 2306–2312. ISSN: 0002-7863. DOI: 10.1021/ja808136x.
- [67] D. L. Goetsch and S. B. Davis. *Quality management for organizational excellence*. pearson, 2014.
- [68] N. M. Goodey and S. J. Benkovic. "Allosteric regulation and catalysis emerge via a common route". In: *Nature chemical biology* 4.8 (2008), pp. 474–482.
- [69] C. Graf et al. "Spatially and kinetically resolved changes in the conformational dynamics of the Hsp90 chaperone machine". In: *Embo Journal* 28.5 (2009), pp. 602–613. ISSN: 0261-4189. DOI: 10.1038/emboj.2008.306.

- [70] J. P. Grason, J. S. Gresham, and G. H. Lorimer. "Setting the chaperonin timer: a two-stroke, two-speed, protein machine". In: *Proceedings of the National Academy of Sciences* 105.45 (2008), pp. 17339–17344.
- [71] J. Gray. "Measurement of lipid oxidation: a review". In: *Journal of the American Oil Chemists' Society* 55.6 (1978), pp. 539–546. ISSN: 0003-021X.
- [72] W. J. Greenleaf et al. "Direct observation of hierarchical folding in single riboswitch aptamers". In: *Science* 319.5863 (2008), pp. 630–3. ISSN: 1095-9203 (Electronic) 0036-8075 (Linking). DOI: 10.1126/science.1151298. URL: <http://www.ncbi.nlm.nih.gov/pubmed/18174398>.
- [73] R. Gruber and A. Horovitz. "Allosteric Mechanisms in Chaperonin Machines". In: *Chemical reviews* (2016).
- [74] A. Gunnarsson et al. "Kinetic and thermodynamic characterization of single-mismatch discrimination using single-molecule imaging". In: *Nucleic Acids Research* 37.14 (2009). ISSN: 0305-1048. DOI: ARTNe9910.1093/nar/gkp487.
- [75] P. I. Hanson and S. W. Whiteheart. "AAA+ proteins: have engine, will work". In: *Nature Reviews Molecular Cell Biology* 6.7 (2005), pp. 519–529.
- [76] F. U. Hartl, A. Bracher, and M. Hayer-Hartl. "Molecular chaperones in protein folding and proteostasis". In: *Nature* 475.7356 (2011), pp. 324–32. ISSN: 1476-4687 (Electronic) 0028-0836 (Linking). DOI: 10.1038/nature10317. URL: <http://www.ncbi.nlm.nih.gov/pubmed/21776078>.
- [77] M. Haslbeck and E. Vierling. "A first line of stress defense: small heat shock proteins and their function in protein homeostasis". In: *J Mol Biol* 427.7 (2015), pp. 1537–48. ISSN: 1089-8638 (Electronic) 0022-2836 (Linking). DOI: 10.1016/j.jmb.2015.02.002. URL: <http://www.ncbi.nlm.nih.gov/pubmed/25681016>.
- [78] M. Haslbeck et al. "Disassembling protein aggregates in the yeast cytosol. The cooperation of Hsp26 with Ssa1 and Hsp104". In: *J Biol Chem* 280.25 (2005), pp. 23861–8. ISSN: 0021-9258 (Print) 0021-9258 (Linking). DOI: 10.1074/jbc.M502697200. URL: <http://www.ncbi.nlm.nih.gov/pubmed/15843375>.
- [79] M. Haslbeck et al. "Hsp26: a temperature-regulated chaperone". In: *EMBO J* 18.23 (1999), pp. 6744–51. ISSN: 0261-4189 (Print) 0261-4189 (Linking). DOI: 10.1093/emboj/18.23.6744. URL: <http://www.ncbi.nlm.nih.gov/pubmed/10581247>.
- [80] M. Haslbeck et al. "Some like it hot: the structure and function of small heat-shock proteins". In: *Nat Struct Mol Biol* 12.10 (2005), pp. 842–6. ISSN: 1545-9993 (Print) 1545-9985 (Linking). DOI: 10.1038/nsmb993. URL: <http://www.ncbi.nlm.nih.gov/pubmed/16205709>.
- [81] M. Haslbeck et al. "Hsp42 is the general small heat shock protein in the cytosol of *Saccharomyces cerevisiae*". In: *The EMBO journal* 23.3 (2004), pp. 638–649. ISSN: 0261-4189.
- [82] E. R. Henry and W. A. Eaton. "Combinatorial modeling of protein folding kinetics: free energy profiles and rates". In: *Chemical Physics* 307.2-3 (2004), pp. 163–185. ISSN: 0301-0104. DOI: 10.1016/j.chemphys.2004.06.064.

- [83] K. Henzler-Wildman and D. Kern. “Dynamic personalities of proteins”. In: *Nature* 450.7172 (2007), pp. 964–972.
- [84] K. A. Henzler-Wildman et al. “A hierarchy of timescales in protein dynamics is linked to enzyme catalysis”. In: *Nature* 450.7171 (2007), pp. 913–916.
- [85] K. A. Henzler-Wildman et al. “Intrinsic motions along an enzymatic reaction trajectory”. In: *Nature* 450.7171 (2007), pp. 838–844.
- [86] M. S. Hipp, S. H. Park, and F. U. Hartl. “Proteostasis impairment in protein-misfolding and -aggregation diseases”. In: *Trends Cell Biol* 24.9 (2014), pp. 506–14. ISSN: 1879-3088 (Electronic) 0962-8924 (Linking). DOI: 10.1016/j.tcb.2014.05.003. URL: <http://www.ncbi.nlm.nih.gov/pubmed/24946960>.
- [87] J. H. Hoffmann et al. “Identification of a redox-regulated chaperone network”. In: *Embo Journal* 23.1 (2004), pp. 160–168. ISSN: 0261-4189. DOI: 10.1038/sj.emboj.7600016.
- [88] A. Holmberg et al. “The biotin-streptavidin interaction can be reversibly broken using water at elevated temperatures”. In: *Electrophoresis* 26.3 (2005), pp. 501–510. ISSN: 0173-0835. DOI: 10.1002/elps.200410070.
- [89] I. Horvath et al. “Mechanisms of protein oligomerization: inhibitor of functional amyloids templates alpha-synuclein fibrillation”. In: *J Am Chem Soc* 134.7 (2012), pp. 3439–44. ISSN: 1520-5126 (Electronic) 0002-7863 (Linking). DOI: 10.1021/ja209829m. URL: <http://www.ncbi.nlm.nih.gov/pubmed/22260746>.
- [90] M. van den Hout et al. “End-joining long nucleic acid polymers”. In: *Nucleic Acids Res* 36.16 (2008), e104. ISSN: 1362-4962 (Electronic) 0305-1048 (Linking). DOI: 10.1093/nar/gkn442. URL: <http://www.ncbi.nlm.nih.gov/pubmed/18658247>.
- [91] Q.-X. Hua et al. “Structure of a protein in a kinetic trap”. In: *Nature Structural & Molecular Biology* 2.2 (1995), pp. 129–138.
- [92] K. A. Huey et al. “Inactivity-induced modulation of Hsp20 and Hsp25 content in rat hindlimb muscles”. In: *Muscle Nerve* 30.1 (2004), pp. 95–101. ISSN: 0148-639X (Print) 0148-639X (Linking). DOI: 10.1002/mus.20063. URL: <http://www.ncbi.nlm.nih.gov/pubmed/15221884>.
- [93] W. Hwang and M. J. Lang. “Mechanical design of translocating motor proteins”. In: *Cell biochemistry and biophysics* 54.1-3 (2009), pp. 11–22.
- [94] M. Ilbert et al. “The redox-switch domain of Hsp33 functions as dual stress sensor”. In: *Nature Structural & Molecular Biology* 14.6 (2007), pp. 556–563. ISSN: 1545-9985. DOI: 10.1038/nsmb1244.
- [95] U. Jakob et al. “Chaperone activity with a redox switch”. In: *Cell* 96.3 (1999), pp. 341–52. ISSN: 0092-8674 (Print) 0092-8674 (Linking). URL: <http://www.ncbi.nlm.nih.gov/pubmed/10025400>.
- [96] A. I. Jewett and J. E. Shea. “Folding on the chaperone: yield enhancement through loose binding”. In: *J Mol Biol* 363.5 (2006), pp. 945–57. ISSN: 0022-2836 (Print) 0022-2836 (Linking). DOI: 10.1016/j.jmb.2006.08.040. URL: <http://www.ncbi.nlm.nih.gov/pubmed/16987526>.

- [97] W. Jiao et al. "The dramatically increased chaperone activity of small heat-shock protein IbpB is retained for an extended period of time after the stress condition is removed". In: *Biochemical Journal* 410.1 (2008), pp. 63–70.
- [98] W. Jiao et al. "The essential role of the flexible termini in the temperature-responsiveness of the oligomeric state and chaperone-like activity for the polydisperse small heat shock protein IbpB from *Escherichia coli*". In: *Journal of molecular biology* 347.4 (2005), pp. 871–884.
- [99] B. D. Johnson et al. "Hop modulates hsp70/hsp90 interactions in protein folding". In: *Journal of Biological Chemistry* 273.6 (1998), pp. 3679–3686. ISSN: 0021-9258. DOI: DOI10.1074/jbc.273.6.3679.
- [100] J. L. Johnson. "Evolution and function of diverse Hsp90 homologs and cochaperone proteins". In: *Biochimica et Biophysica Acta (BBA) - Molecular Cell Research* 1823.3 (2012), pp. 607–613. ISSN: 0167-4889. DOI: <http://dx.doi.org/10.1016/j.bbamcr.2011.09.020>. URL: <http://www.sciencedirect.com/science/article/pii/S0167488911002795>.
- [101] N. W. S. Kam et al. "Nanotube molecular transporters: internalization of carbon nanotube-protein conjugates into mammalian cells". In: *Journal of the American Chemical Society* 126.22 (2004), pp. 6850–6851. ISSN: 0002-7863. DOI: 10.1021/ja0486059.
- [102] H. H. Kampinga and E. A. Craig. "The HSP70 chaperone machinery: J proteins as drivers of functional specificity". In: *Nat Rev Mol Cell Biol* 11.8 (2010), pp. 579–92. ISSN: 1471-0080 (Electronic) 1471-0072 (Linking). DOI: 10.1038/nrm2941. URL: <http://www.ncbi.nlm.nih.gov/pubmed/20651708>.
- [103] G. E. Karagoz et al. "Hsp90-Tau complex reveals molecular basis for specificity in chaperone action". In: *Cell* 156.5 (2014), pp. 963–974. ISSN: 0092-8674. DOI: 10.1016/j.cell.2014.01.037.
- [104] M. Kim et al. "A nanoscale force probe for gauging intermolecular interactions". In: *Angewandte Chemie-International Edition* 51.8 (2012), pp. 1903–1906. ISSN: 1433-7851. DOI: 10.1002/anie.201107210.
- [105] E. Kirschke et al. "Glucocorticoid receptor function regulated by coordinated action of the Hsp90 and Hsp70 chaperone cycles". In: *Cell* 157.7 (2014), pp. 1685–1697. ISSN: 0092-8674. DOI: 10.1016/j.cell.2014.04.038.
- [106] M. Kitagawa et al. "Escherichia coli small heat shock proteins, IbpA and IbpB, protect enzymes from inactivation by heat and oxidants". In: *European Journal of Biochemistry* 269.12 (2002), pp. 2907–2917.
- [107] T. P. Knowles, M. Vendruscolo, and C. M. Dobson. "The amyloid state and its association with protein misfolding diseases". In: *Nat Rev Mol Cell Biol* 15.6 (2014), pp. 384–96. ISSN: 1471-0080 (Electronic) 1471-0072 (Linking). DOI: 10.1038/nrm3810. URL: <http://www.ncbi.nlm.nih.gov/pubmed/24854788>.
- [108] V. S. Kokhan, M. A. Afanasyeva, and G. I. Van'kin. "Alpha-synuclein knockout mice have cognitive impairments". In: *Behav Brain Res* 231.1 (2012), pp. 226–30. ISSN: 1872-7549 (Electronic) 0166-4328 (Linking). DOI: 10.1016/j.bbr.2012.03.026. URL: <http://www.ncbi.nlm.nih.gov/pubmed/22469626>.

- [109] M. Kovermann et al. “Structural basis for catalytically restrictive dynamics of a high-energy enzyme state”. In: *Nature communications* 6 (2015).
- [110] K. A. Krukenberg et al. “Multiple conformations of E-coli Hsp90 in solution: insights into the conformational dynamics of Hsp90”. In: *Structure* 16.5 (2008), pp. 755–765. ISSN: 0969-2126. DOI: 10.1016/j.str.2008.01.021.
- [111] K. A. Krukenberg et al. “pH-Dependent conformational changes in bacterial Hsp90 reveal a Grp94-like conformation at pH 6 that is highly active in suppression of citrate synthase aggregation”. In: *Journal of Molecular Biology* 390.2 (2009), pp. 278–291. ISSN: 0022-2836. DOI: 10.1016/j.jmb.2009.04.080.
- [112] S. K. Kufer et al. “Covalent immobilization of recombinant fusion proteins with hAGT for single molecule force spectroscopy”. In: *Eur Biophys J* 35.1 (2005), pp. 72–8. ISSN: 0175-7571 (Print) 0175-7571 (Linking). DOI: 10.1007/s00249-005-0010-1. URL: <http://www.ncbi.nlm.nih.gov/pubmed/16160825>.
- [113] M. Kulig and H. Ecroyd. “The small heat-shock protein alphaB-crystallin uses different mechanisms of chaperone action to prevent the amorphous versus fibrillar aggregation of alpha-lactalbumin”. In: *Biochem J* 448.3 (2012), pp. 343–52. ISSN: 1470-8728 (Electronic) 0264-6021 (Linking). DOI: 10.1042/BJ20121187. URL: <http://www.ncbi.nlm.nih.gov/pubmed/23005341>.
- [114] S. Langereis et al. “Probing the interaction of the biotin-avidin complex with the relaxivity of biotinylated Gd-DTPA”. In: *Org Biomol Chem* 2.9 (2004), pp. 1271–3. ISSN: 1477-0520 (Print) 1477-0520 (Linking). DOI: 10.1039/b402917h. URL: <http://www.ncbi.nlm.nih.gov/pubmed/15105914>.
- [115] H. A. Lashuel and J. Lansbury P. T. “Are amyloid diseases caused by protein aggregates that mimic bacterial pore-forming toxins?” In: *Q Rev Biophys* 39.2 (2006), pp. 167–201. ISSN: 0033-5835 (Print) 0033-5835 (Linking). DOI: 10.1017/S0033583506004422. URL: <http://www.ncbi.nlm.nih.gov/pubmed/16978447>.
- [116] H. A. Lashuel et al. “The many faces of alpha-synuclein: from structure and toxicity to therapeutic target”. In: *Nat Rev Neurosci* 14.1 (2013), pp. 38–48. ISSN: 1471-0048 (Electronic) 1471-003X (Linking). DOI: 10.1038/nrn3406. URL: <http://www.ncbi.nlm.nih.gov/pubmed/23254192>.
- [117] C. Lavedan. “The synuclein family”. In: *Genome Res* 8.9 (1998), pp. 871–80. ISSN: 1088-9051 (Print) 1088-9051 (Linking). URL: <http://www.ncbi.nlm.nih.gov/pubmed/9750188>.
- [118] G. J. Lee et al. “A small heat shock protein stably binds heat-denatured model substrates and can maintain a substrate in a folding-competent state”. In: *EMBO J* 16.3 (1997), pp. 659–71. ISSN: 0261-4189 (Print) 0261-4189 (Linking). DOI: 10.1093/emboj/16.3.659. URL: <http://www.ncbi.nlm.nih.gov/pubmed/9034347>.
- [119] M. E. Leunissen et al. “Switchable self-protected attractions in DNA-functionalized colloids”. In: *Nature Materials* 8.7 (2009), pp. 590–595. ISSN: 1476-1122. DOI: 10.1038/Nmat2471.

- [120] S. Lifson and A Roig. "On the theory of helix—coil transition in polypeptides". In: *The Journal of Chemical Physics* 34.6 (1961), pp. 1963–1974. ISSN: 0021-9606.
- [121] C. X. Lin et al. "Functional DNA nanotube arrays: Bottom-up meets top-down". In: *Angewandte Chemie-International Edition* 46.32 (2007), pp. 6089–6092. ISSN: 1433-7851. DOI: 10.1002/anie.200701767.
- [122] J. Liphardt et al. "Reversible unfolding of single RNA molecules by mechanical force". In: *Science* 292.5517 (2001), pp. 733–7. ISSN: 0036-8075 (Print) 0036-8075 (Linking). DOI: 10.1126/science.1058498. URL: <http://www.ncbi.nlm.nih.gov/pubmed/11326101>.
- [123] O. R. Lorenz et al. "Modulation of the Hsp90 chaperone cycle by a stringent client protein". In: *Molecular Cell* 53.6 (2014), pp. 941–953. ISSN: 1097-2765. DOI: 10.1016/j.molcel.2014.02.003.
- [124] T. Luhrs et al. "3D structure of Alzheimer's amyloid-beta(1-42) fibrils". In: *Proc Natl Acad Sci U S A* 102.48 (2005), pp. 17342–7. ISSN: 0027-8424 (Print) 0027-8424 (Linking). DOI: 10.1073/pnas.0506723102. URL: <http://www.ncbi.nlm.nih.gov/pubmed/16293696>.
- [125] B. MA et al. "Transition-state ensemble in enzyme catalysis: possibility, reality, or necessity?" In: *Journal of theoretical biology* 203.4 (2000), pp. 383–397.
- [126] R. Maier et al. "Interaction of trigger factor with the ribosome". In: *Journal of molecular biology* 326.2 (2003), pp. 585–592.
- [127] R. Maillard et al. "ClpX(P) generates mechanical force to unfold and translocate its protein substrates". In: *Cell* 145.3 (2011), pp. 459–469. ISSN: 0092-8674. DOI: <http://dx.doi.org/10.1016/j.cell.2011.04.010>. URL: <http://www.sciencedirect.com/science/article/pii/S0092867411004296>.
- [128] J. van Mameren, E. J. G. Peterman, and G. J. L. Wuite. "See me, feel me: methods to concurrently visualize and manipulate single DNA molecules and associated proteins". In: *Nucleic Acids Research* 36.13 (2008), pp. 4381–4389. ISSN: 0305-1048. DOI: 10.1093/nar/gkn412.
- [129] I. Martin et al. "Screening and evaluation of small organic molecules as ClpB inhibitors and potential antimicrobials". In: *Journal of medicinal chemistry* 56.18 (2013), pp. 7177–7189.
- [130] E. Martinez-Hackert and W. A. Hendrickson. "Promiscuous substrate recognition in folding and assembly activities of the trigger factor chaperone". In: *Cell* 138.5 (2009), pp. 923–934.
- [131] A. T. Marttila et al. "Recombinant NeutraLite Avidin: a non-glycosylated, acidic mutant of chicken avidin that exhibits high affinity for biotin and low non-specific binding properties". In: *Febs Letters* 467.1 (2000), pp. 31–36. ISSN: 0014-5793. DOI: 10.1016/S0014-5793(00)01119-4.
- [132] A. Mashaghi, S. Mashaghi, and S. J. Tans. "Misfolding of luciferase at the single-molecule level". In: *Angewandte Chemie-International Edition* 53.39 (2014), pp. 10390–10393. ISSN: 1433-7851. DOI: 10.1002/anie.201405566.

- [133] A. Mashaghi, P. J. Vach, and S. J. Tans. “Noise reduction by signal combination in Fourier space applied to drift correction in optical tweezers”. In: *Rev Sci Instrum* 82.11 (2011), p. 115103. ISSN: 1089-7623 (Electronic) 0034-6748 (Linking). DOI: 10.1063/1.3658825. URL: <http://www.ncbi.nlm.nih.gov/pubmed/22129009>.
- [134] A. Mashaghi et al. “Chaperone action at the single-molecule level”. In: *Chem Rev* 114.1 (2014), pp. 660–76. ISSN: 1520-6890 (Electronic) 0009-2665 (Linking). DOI: 10.1021/cr400326k. URL: <http://www.ncbi.nlm.nih.gov/pubmed/24001118>.
- [135] A. Mashaghi et al. “Reshaping of the conformational search of a protein by the chaperone trigger factor”. In: *Nature* 500.7460 (2013), pp. 98–101. ISSN: 1476-4687 (Electronic) 0028-0836 (Linking). DOI: 10.1038/nature12293. URL: <http://www.ncbi.nlm.nih.gov/pubmed/23831649>.
- [136] R. U. Mattoo and P. Goloubinoff. “Molecular chaperones are nanomachines that catalytically unfold misfolded and alternatively folded proteins”. In: *Cellular and Molecular Life Sciences* 71.17 (2014), pp. 3311–3325.
- [137] M. M. Maye et al. “Switching binary states of nanoparticle superlattices and dimer clusters by DNA strands”. In: *Nature Nanotechnology* 5.2 (2010), pp. 116–120. ISSN: 1748-3387. DOI: 10.1038/Nnano.2009.378.
- [138] M. P. Mayer and L. Le Breton. “Hsp90: breaking the symmetry”. In: *Molecular Cell* 58.1 (2015), pp. 8–20. ISSN: 1097-2765. DOI: 10.1016/j.molcel.2015.02.022.
- [139] M. P. Mayer. “Gymnastics of molecular chaperones”. In: *Molecular cell* 39.3 (2010), pp. 321–331.
- [140] M. Mayer and B. Bukau. “Hsp70 chaperones: cellular functions and molecular mechanism”. In: *Cellular and molecular life sciences* 62.6 (2005), pp. 670–684.
- [141] I. G. McKeith et al. “Consensus guidelines for the clinical and pathologic diagnosis of dementia with Lewy bodies (DLB): report of the consortium on DLB international workshop”. In: *Neurology* 47.5 (1996), pp. 1113–24. ISSN: 0028-3878 (Print) 0028-3878 (Linking). URL: <http://www.ncbi.nlm.nih.gov/pubmed/8909416>.
- [142] I. L. Medintz and J. R. Deschamps. “Maltose-binding protein: a versatile platform for prototyping biosensing”. In: *Curr Opin Biotechnol* 17.1 (2006), pp. 17–27. ISSN: 0958-1669 (Print) 0958-1669 (Linking). DOI: 10.1016/j.copbio.2006.01.002. URL: <http://www.ncbi.nlm.nih.gov/pubmed/16413768>.
- [143] L. Mellblom and L. Enerbäck. “Protein content, dry mass and chemical composition of individual mast cells related to body growth”. In: *Histochemistry* 63.2 (1979), pp. 129–143.
- [144] S. B. Miller, A. Mogk, and B. Bukau. “Spatially organized aggregation of misfolded proteins as cellular stress defense strategy”. In: *J Mol Biol* 427.7 (2015), pp. 1564–74. ISSN: 1089-8638 (Electronic) 0022-2836 (Linking). DOI: 10.1016/j.jmb.2015.02.006. URL: <http://www.ncbi.nlm.nih.gov/pubmed/25681695>.

- [145] A. Mogk et al. "Refolding of substrates bound to small Hsps relies on a disaggregation reaction mediated most efficiently by ClpB/DnaK". In: *J Biol Chem* 278.33 (2003), pp. 31033–42. ISSN: 0021-9258 (Print) 0021-9258 (Linking). DOI: 10.1074/jbc.M303587200. URL: <http://www.ncbi.nlm.nih.gov/pubmed/12788951>.
- [146] Y. Morishima et al. "Stepwise assembly of a glucocorticoid receptor center dot hsp90 heterocomplex resolves two sequential ATP-dependent events involving first hsp70 and then hsp90 in opening of the steroid binding pocket". In: *Journal of Biological Chemistry* 275.24 (2000), pp. 18054–18060. ISSN: 0021-9258. DOI: DOI10.1074/jbc.M000434200.
- [147] M. T. Morita et al. "Translational induction of heat shock transcription factor sigma-32: evidence for a built-in RNA thermosensor". In: *Genes & development* 13.6 (1999), pp. 655–665.
- [148] A. Mossa et al. "Measurement of work in single-molecule pulling experiments". In: *Journal of Chemical Physics* 130.23 (2009). ISSN: 0021-9606. DOI: Artn23411610.1063/1.3155084.
- [149] Y. Motojima-Miyazaki, M. Yoshida, and F. Motojima. "Ribosomal protein L2 associates with E. coli HtpG and activates its ATPase activity". In: *Biochemical and Biophysical Research Communications* 400.2 (2010), pp. 241–245. ISSN: 0006-291x. DOI: 10.1016/j.bbrc.2010.08.047.
- [150] V. Munoz and W. A. Eaton. "A simple model for calculating the kinetics of protein folding from three-dimensional structures". In: *Proceedings of the National Academy of Sciences of the United States of America* 96.20 (1999), pp. 11311–11316. ISSN: 0027-8424. DOI: DOI10.1073/pnas.96.20.11311.
- [151] F. Neidhardt, J. Ingraham, and M. Schaechter. *Physiology of the bacterial cell: a molecular approach*. Wiley Online Library. 1992.
- [152] G. Neuert et al. "Dynamic force spectroscopy of the digoxigenin-antibody complex". In: *Febs Letters* 580.2 (2006), pp. 505–509. ISSN: 0014-5793. DOI: 10.1016/j.febslet.2005.12.052.
- [153] K. Neupane et al. "Diverse metastable structures formed by small oligomers of alpha-synuclein probed by force spectroscopy". In: *PLoS One* 9.1 (2014), e86495. ISSN: 1932-6203 (Electronic) 1932-6203 (Linking). DOI: 10.1371/journal.pone.0086495. URL: <http://www.ncbi.nlm.nih.gov/pubmed/24475132>.
- [154] A. O. Olivares et al. "Mechanochemical basis of protein degradation by a double-ring AAA+ machine". In: *Nature structural & molecular biology* 21.10 (2014), pp. 871–875.
- [155] D. R. Palleros, W. J. Welch, and A. L. Fink. "Interaction of hsp70 with unfolded proteins: effects of temperature and nucleotides on the kinetics of binding." In: *Proceedings of the National Academy of Sciences* 88.13 (1991), pp. 5719–5723.
- [156] D. R. Palleros et al. "Hsp70-protein complexes: complex stability and conformation of bound substrate protein". In: *Journal of Biological Chemistry* 269.18 (1994), pp. 13107–13114.

- [157] V. G. Panse et al. "Unfolding thermodynamics of the tetrameric chaperone, SecB". In: *Biochemistry* 39.9 (2000), pp. 2362–2369.
- [158] F. Patolsky, Y. Weizmann, and I. Willner. "Actin-based metallic nanowires as bio-nanotransporters". In: *Nature Materials* 3.10 (2004), pp. 692–695. ISSN: 1476-1122. DOI: 10.1038/nmat1205.
- [159] D. Poland and H. A. Scheraga. *Theory of helix-coil transitions in biopolymers: statistical mechanical theory of order-disorder transitions in biological macromolecules*. Molecular biology an international series of monographs and textbooks. New York: Academic Press, 1970, xvii, 797 p.
- [160] M. F. Princiotta et al. "Quantitating protein synthesis, degradation, and endogenous antigen processing". In: *Immunity* 18.3 (2003), pp. 343–354.
- [161] C. Prodromou et al. "Identification and structural characterization of the ATP/ADP-binding site in the Hsp90 molecular chaperone". In: *Cell* 90.1 (1997), pp. 65–75. ISSN: 0092-8674 (Print) 0092-8674 (Linking). URL: <http://www.ncbi.nlm.nih.gov/pubmed/9230303>.
- [162] M. E. van Raaij, I. M. Segers-Nolten, and V. Subramaniam. "Quantitative morphological analysis reveals ultrastructural diversity of amyloid fibrils from alpha-synuclein mutants". In: *Biophys J* 91.11 (2006), pp. L96–8. ISSN: 0006-3495 (Print) 0006-3495 (Linking). DOI: 10.1529/biophysj.106.090449. URL: <http://www.ncbi.nlm.nih.gov/pubmed/16997873>.
- [163] C Ratzke, B Hellenkamp, and T Hugel. "Four-colour FRET reveals directionality in the Hsp90 multicomponent machinery". In: *Nature communications* 5 (2014).
- [164] D. Reichmann et al. "Order out of disorder: working cycle of an intrinsically unfolded chaperone". In: *Cell* 148.5 (2012), pp. 947–957. ISSN: 0092-8674. DOI: 10.1016/j.cell.2012.01.045.
- [165] K. Richter, M. Haslbeck, and J. Buchner. "The heat shock response: life on the verge of death". In: *Molecular cell* 40.2 (2010), pp. 253–266.
- [166] A. D. Robertson and K. P. Murphy. "Protein structure and the energetics of protein stability". In: *Chemical reviews* 97.5 (1997), pp. 1251–1268.
- [167] T. G. Schmidt and A. Skerra. "The Strep-tag system for one-step purification and high-affinity detection or capturing of proteins". In: *Nat Protoc* 2.6 (2007), pp. 1528–35. ISSN: 1750-2799 (Electronic) 1750-2799 (Linking). DOI: 10.1038/nprot.2007.209. URL: <http://www.ncbi.nlm.nih.gov/pubmed/17571060>.
- [168] T. G. M. Schmidt and A. Skerra. "The random peptide library-assisted engineering of a C-terminal affinity peptide, useful for the detection and purification of a functional Ig Fv fragment". In: *Protein Engineering* 6.1 (1993), pp. 109–122. ISSN: 0269-2139. DOI: DOI10.1093/protein/6.1.109.
- [169] T. G. M. Schmidt et al. "Molecular interaction between the Strep-tag affinity peptide and its cognate target, streptavidin". In: *Journal of Molecular Biology* 255.5 (1996), pp. 753–766. ISSN: 0022-2836. DOI: DOI10.1006/jmbi.1996.0061.

- [170] J. D. Schmit, K. Ghosh, and K. Dill. “What drives amyloid molecules to assemble into oligomers and fibrils?” In: *Biophysical Journal* 100.2 (2011), pp. 450–458. ISSN: 0006-3495. DOI: 10.1016/j.bpj.2010.11.041.
- [171] M. Schröder and R. J. Kaufman. “ER stress and the unfolded protein response”. In: *Mutation Research/Fundamental and Molecular Mechanisms of Mutagenesis* 569.1 (2005), pp. 29–63.
- [172] S. Sharma et al. “Monitoring protein conformation along the pathway of chaperonin-assisted folding”. In: *Cell* 133.1 (2008), pp. 142–153.
- [173] A. K. Shiau et al. “Structural analysis of E-coli hsp90 reveals dramatic nucleotide-dependent conformational rearrangements”. In: *Cell* 127.2 (2006), pp. 329–340. ISSN: 0092-8674. DOI: 10.1016/j.cell.2006.09.027.
- [174] B. H. Shilton, H. A. Shuman, and S. L. Mowbray. “Crystal structures and solution conformations of a dominant-negative mutant of Escherichia coli maltose-binding protein”. In: *Journal of molecular biology* 264.2 (1996), pp. 364–376.
- [175] K. Singhal et al. “The trigger factor chaperone encapsulates and stabilizes partial folds of substrate proteins”. In: *PLoS Comput Biol* 11.10 (2015), e1004444. ISSN: 1553-7358 (Electronic) 1553-734X (Linking). DOI: 10.1371/journal.pcbi.1004444. URL: <http://www.ncbi.nlm.nih.gov/pubmed/26512985>.
- [176] R. Sitia and I. Braakman. “Quality control in the endoplasmic reticulum protein factory”. In: *Nature* 426.6968 (2003), pp. 891–894.
- [177] D. R. Southworth and D. A. Agard. “Species-dependent ensembles of conserved conformational states define the Hsp90 chaperone ATPase cycle”. In: *Molecular cell* 32.5 (2008), pp. 631–640.
- [178] S. Specht et al. “Hsp42 is required for sequestration of protein aggregates into deposition sites in *Saccharomyces cerevisiae*”. In: *The Journal of cell biology* 195.4 (2011), pp. 617–629. ISSN: 0021-9525.
- [179] F. Stengel et al. “Quaternary dynamics and plasticity underlie small heat shock protein chaperone function”. In: *Proceedings of the National Academy of Sciences* 107.5 (2010), pp. 2007–2012.
- [180] P. C. Stirling et al. “Convergent evolution of clamp-like binding sites in diverse chaperones”. In: *Nature structural & molecular biology* 13.10 (2006), pp. 865–870.
- [181] T. O. Street, L. A. Lavery, and D. A. Agard. “Substrate binding drives large-scale conformational changes in the Hsp90 molecular chaperone”. In: *Molecular Cell* 42.1 (2011), pp. 96–105. ISSN: 1097-2765. DOI: 10.1016/j.molcel.2011.01.029.
- [182] T. O. Street et al. “Elucidating the mechanism of substrate recognition by the bacterial Hsp90 molecular chaperone”. In: *Journal of Molecular Biology* 426.12 (2014), pp. 2393–2404. ISSN: 0022-2836. DOI: 10.1016/j.jmb.2014.04.001.

- [183] T. O. Street et al. "Osmolyte-induced conformational changes in the Hsp90 molecular chaperone". In: *Protein Science* 19.1 (2010), pp. 57–65. ISSN: 0961-8368. DOI: 10.1002/pro.282.
- [184] O. Suss and D. Reichmann. "Protein plasticity underlines activation and function of ATP-independent chaperones". In: *Frontiers in molecular biosciences* 2 (2015).
- [185] M. Taipale, D. F. Jarosz, and S. Lindquist. "HSP90 at the hub of protein homeostasis: emerging mechanistic insights". In: *Nature Reviews Molecular Cell Biology* 11.7 (2010), pp. 515–528. ISSN: 1471-0072. DOI: 10.1038/nrm2918.
- [186] J. L. Tang et al. "Recognition imaging and highly ordered molecular templating of bacterial s-layer nanoarrays containing affinity-tags". In: *Nano Letters* 8.12 (2008), pp. 4312–4319. ISSN: 1530-6984. DOI: 10.1021/nl802092c.
- [187] J. A. Tanner et al. "Investigation into the interactions between diadenosine 5', 5''-P 1, P 4-tetraphosphate and two proteins: molecular chaperone GroEL and cAMP receptor protein". In: *Biochemistry* 45.9 (2006), pp. 3095–3106.
- [188] J. G. Thomas and F. Baneyx. "ClpB and HtpG facilitate de novo protein folding in stressed *Escherichia coli* cells". In: *Molecular Microbiology* 36.6 (2000), pp. 1360–1370. ISSN: 0950-382x. DOI: DOI10.1046/j.1365-2958.2000.01951.x.
- [189] A. D. Thompson et al. "Visualization and functional analysis of the oligomeric states of *Escherichia coli* heat shock protein 70 (Hsp70/DnaK)". In: *Cell Stress and Chaperones* 17.3 (2012), pp. 313–327.
- [190] T. M. Treweek et al. "Small heat-shock proteins: important players in regulating cellular proteostasis". In: *Cell Mol Life Sci* 72.3 (2015), pp. 429–51. ISSN: 1420-9071 (Electronic) 1420-682X (Linking). DOI: 10.1007/s00018-014-1754-5. URL: <http://www.ncbi.nlm.nih.gov/pubmed/25352169>.
- [191] A. M. Tsai, T. J. Udovic, and D. A. Neumann. "The inverse relationship between protein dynamics and thermal stability". In: *Biophysical journal* 81.4 (2001), pp. 2339–2343.
- [192] J. Tyedmers, A. Mogk, and B. Bukau. "Cellular strategies for controlling protein aggregation". In: *Nat Rev Mol Cell Biol* 11.11 (2010), pp. 777–88. ISSN: 1471-0080 (Electronic) 1471-0072 (Linking). DOI: 10.1038/nrm2993. URL: <http://www.ncbi.nlm.nih.gov/pubmed/20944667>.
- [193] S. M. Ungelenk. "Structural features and interactions of substrates complexed with molecular chaperones". In: (2015).
- [194] V. N. Uversky. "A protein-chameleon: conformational plasticity of alpha-synuclein, a disordered protein involved in neurodegenerative disorders". In: *J Biomol Struct Dyn* 21.2 (2003), pp. 211–34. ISSN: 0739-1102 (Print) 0739-1102 (Linking). DOI: 10.1080/07391102.2003.10506918. URL: <http://www.ncbi.nlm.nih.gov/pubmed/12956606>.
- [195] R. D. Vale. "Millennial musings on molecular motors". In: *Trends in Biochemical Sciences* 24.12 (1999), pp. M38–M42.

- [196] L. Veinger et al. "The small heat-shock protein IbpB from *Escherichia coli* stabilizes stress-denatured proteins for subsequent refolding by a multichaperone network". In: *J Biol Chem* 273.18 (1998), pp. 11032–7. ISSN: 0021-9258 (Print) 0021-9258 (Linking). URL: <http://www.ncbi.nlm.nih.gov/pubmed/9556585>.
- [197] D. M. Walsh et al. "Naturally secreted oligomers of amyloid beta protein potently inhibit hippocampal long-term potentiation in vivo". In: *Nature* 416.6880 (2002), pp. 535–9. ISSN: 0028-0836 (Print) 0028-0836 (Linking). DOI: 10.1038/416535a. URL: <http://www.ncbi.nlm.nih.gov/pubmed/11932745>.
- [198] P. Walter and D. Ron. "The unfolded protein response: from stress pathway to homeostatic regulation". In: *Science* 334.6059 (2011), pp. 1081–1086.
- [199] M. J. Waner et al. "Thermal and sodium dodecylsulfate induced transitions of streptavidin". In: *Biophysical Journal* 87.4 (2004), pp. 2701–2713. ISSN: 0006-3495. DOI: 10.1529/biophysj.104.047266.
- [200] W. Wang et al. "A soluble alpha-synuclein construct forms a dynamic tetramer". In: *Proc Natl Acad Sci U S A* 108.43 (2011), pp. 17797–802. ISSN: 1091-6490 (Electronic) 0027-8424 (Linking). DOI: 10.1073/pnas.1113260108. URL: <http://www.ncbi.nlm.nih.gov/pubmed/22006323>.
- [201] C. Wasmer et al. "Amyloid fibrils of the HET-s(218-289) prion form a beta solenoid with a triangular hydrophobic core". In: *Science* 319.5869 (2008), pp. 1523–6. ISSN: 1095-9203 (Electronic) 0036-8075 (Linking). DOI: 10.1126/science.1151839. URL: <http://www.ncbi.nlm.nih.gov/pubmed/18339938>.
- [202] S. D. Weeks et al. "Molecular structure and dynamics of the dimeric human small heat shock protein HSPB6". In: *J Struct Biol* 185.3 (2014), pp. 342–54. ISSN: 1095-8657 (Electronic) 1047-8477 (Linking). DOI: 10.1016/j.jsb.2013.12.009. URL: <http://www.ncbi.nlm.nih.gov/pubmed/24382496>.
- [203] P. H. Weinreb et al. "NACP, a protein implicated in Alzheimer's disease and learning, is natively unfolded". In: *Biochemistry* 35.43 (1996), pp. 13709–15. ISSN: 0006-2960 (Print) 0006-2960 (Linking). DOI: 10.1021/bi961799n. URL: <http://www.ncbi.nlm.nih.gov/pubmed/8901511>.
- [204] W. Wickner, A. J. Driessen, and F. U. Hartl. "The enzymology of protein translocation across the *Escherichia coli* plasma membrane". In: *Annu Rev Biochem* 60 (1991), pp. 101–24. ISSN: 0066-4154 (Print) 0066-4154 (Linking). DOI: 10.1146/annurev.bi.60.070191.000533. URL: <http://www.ncbi.nlm.nih.gov/pubmed/1831965>.
- [205] M. Wolf-Watz et al. "Linkage between dynamics and catalysis in a thermophilic-mesophilic enzyme pair". In: *Nature structural & molecular biology* 11.10 (2004), pp. 945–949.
- [206] L. S. Wong, F. Khan, and J. Micklefield. "Selective covalent protein immobilization: strategies and applications". In: *Chemical Reviews* 109.9 (2009), pp. 4025–4053. ISSN: 0009-2665. DOI: 10.1021/cr8004668.

- [207] E. A. Yamada and V. C. Sgarbieri. “Yeast (*Saccharomyces cerevisiae*) protein concentrate: preparation, chemical composition, and nutritional and functional properties”. In: *Journal of agricultural and food chemistry* 53.10 (2005), pp. 3931–3936.
- [208] H. J. Yost, R. B. Petersen, and S. Linquist. “RNA metabolism: strategies for regulation in the heat shock response”. In: *Trends in Genetics* 6 (1990), pp. 223–227.
- [209] B. H. Zimm, P. Doty, and K. Iso. “Determination of the parameters for helix formation in poly-gamma-benzyl-L-glutamate”. In: *Proc Natl Acad Sci U S A* 45.11 (1959), pp. 1601–7. ISSN: 0027-8424 (Print) 0027-8424 (Linking). URL: <http://www.ncbi.nlm.nih.gov/pubmed/16590552>.
- [210] B. Zimm and J. Bragg. “Theory of the one-dimensional phase transition in polypeptide Chains”. In: *The Journal of Chemical Physics* 28.6 (1958), pp. 1246–1247. ISSN: 0021-9606.

Summary

Protein folding pathways are traditionally studied for isolated proteins, both in simulations and in experiments. However, folding in the cellular environment is critically guided by an array of chaperones. Without chaperones many proteins misfold and/or aggregate, which can for example in higher order organisms, lead to various neurodegenerative diseases and other disorders. Here we study chaperone-mediated protein folding at single molecule level, using optical tweezers. This approach allows a direct comparison of unfolding/refolding pathways and their transitions, in the presence and absence of chaperones.

Chapter 1 gives an overview of the functional and design principles of molecular chaperones. This chapter starts with introducing protein folding as a reaction and describes the role of chaperones in this context. Next, it discusses the structural principles of chaperone machinery, i.e. oligomerization, flexibility, and stability, in connection to the functional principles of chaperone actions. Chapter 1 attempts to map the tasks of molecular chaperones in different conditions and over different time scales.

Chapter 2 concerns the technical side of experiment and explores a new method to increase the stability and specificity of protein pulling experiments. . This chapter introduces a linkage between the protein StrepTactin (STN) and the peptide StrepTag II (ST) to join proteins and dsDNA molecule at their ends. Our results show this linkage provides high mechanical stability and specificity that is essential to make protein tethers for long pulling experiments.

Chapter 3-6 describe the chaperoning function of four different molecular chaperones, namely Hsp42, HspB6, Hsp33, and HtpG. Within these studies, four different model proteins are used which in principle can be divided to two groups; single proteins (e.g. MBP and Luciferase) and repeat proteins (e.g. 4MBP and 4 α -synuclein). By measuring on a single protein, folding can be assessed free of aggregation, whereas using constructs of protein repeats, aggregation and disaggregation can be followed in real time.

Chapter 3 and 4 investigate the functional role of Small Heat Shock Proteins (sHsps) in the prevention of aggregation. sHsps are known as holdases interacting with unfolded proteins and are believed to act at the front line of cellular defense mechanisms against protein aggregation. Using the 4MBP construct, the interaction of yeast Hsp42 with aggregates is studied in chapter 3. The findings reveal Hsp42 prevents tight intra-domain contacts and promotes native-like re-folding via interaction with the folded state. Investigating the folding of single domain

MBP suggests Hsp42 binds to the folded state, as destabilized refolded structures are detected in the presence of chaperone. The investigation of sHsps' function is followed in chapter 4, by probing the interaction of human HspB6 and a repeat construct of 4 α -synuclein. α -synuclein is known to form highly ordered aggregates and is expressed in the neural tissue of vertebrates, including humans. HspB6 also shows affinity to the folded state, as it stimulates the formation of compact structures and stabilizes them against force unfolding. Binding to the folded structures seems to be the generic feature of HspB6 functioning, as we observed HspB6 similarly stabilizes MBP folds with the known tertiary structure.

Chapter 5 addresses the molecular mechanism of yeast Hsp33, a redox-regulated chaperone that is also considered to be a holdase. At the single molecule level, Hsp33 stabilizes the protein chains in the unfolded and non-aggregated state, but also promotes partial refolding within monomers over aggregation between monomers. Mechanical perturbation of monomers that refold in the presence of chaperone indicates Hsp33 binds and deforms an intermediate refolded state, weakening it against unfolding and blocking transition to the native state. A statistical mechanics model is further used in this chapter to dissect the competition between folding, aggregation, and binding transitions, and to predict how Hsp33 affects the state of interacting MBP monomers without additional fitting.

Chapter 6 studies the mechanistic function of ATP dependent Hsp90 family, by focusing on the prokaryotic homologue, named as HtpG. The unfolding and refolding pathways of model protein Luciferase is probed in the presence of chaperone. The results show HtpG, in an ATP-dependent and step-wise manner, can promote chain structures that are stable in time and against force. Moreover, HtpG action suppresses the intra- and inter-domain misfoldings. This finding seems to be relevant to the many physiological roles of Hsp90.

Overall, our single molecules studies reveal new mechanistic information on the action of chaperones and represent a broader range of chaperone functions than previously assumed.

Samenvatting

Eiwitvouwing wordt traditioneel bestudeerd met geïsoleerde eiwitten, zowel in simulaties als in experimenten. Echter, chaperonne-eiwitten in de cel zijn van cruciaal belang om de eiwitvouwing in de cel te begeleiden. Zonder deze chaperonnes zouden veel van de eiwitten verkeerd vouwen of aggregeren. Dit kan leiden tot neurodegeneratieve ziekten en andere aandoeningen. In dit proefschrift bestudeer ik de door chaperonne-eiwitten begeleide eiwitvouwing op het niveau van een enkel eiwit met gebruik van een optische pincet. Met deze methode kunnen we de paden van het vouwen en ontvouwen van eiwitten vergelijken in situaties met en zonder de begeleiding van chaperonne-eiwitten.

In Hoofdstuk 1 geef ik een overzicht van de beginselen van de functies en het ontwerp van moleculaire chaperonne-eiwitten. Het hoofdstuk begint met de introductie van eiwitvouwen als een chemische reactie en beschrijft de rol van chaperonnes hierbij. Daarna bespreek ik de structurele principes van het chaperonne mechanisme, namelijk oligomerisatie, flexibiliteit en stabiliteit, in het licht van de functies van het chaperon. In hoofdstuk 1 breng ik de taken van moleculaire chaperonne-eiwitten in verschillende omstandigheden en tijdschalen in kaart.

Hoofdstuk 2 belicht het technisch aspect van het experiment waarin ik een nieuwe methode met een hogere efficiëntie onderzoek. In dit hoofdstuk introduceer ik een verbindingstuk tussen het eiwit StrepTacin (STN) en de peptide StrepTag II (ST) om de uiteinden van eiwitten en dsDNA te verbinden. Onze resultaten laten zien dat het verbindingstuk een hoge mechanische stabiliteit en specificiteit heeft. Deze eigenschappen zijn van cruciaal belang voor experimenten waarbij langdurig aan het eiwit getrokken wordt.

Hoofdstuk 3-6 beschrijft de chaperonnerende functie van vier verschillende moleculaire chaperonne-eiwitten: Hsp42, HspB6, Hsp33 en HtpG. Binnen dit onderzoek worden vier modeleiwitten gebruikt welke in twee groepen kunnen worden verdeeld: enkele eiwitten (bijv. MBP en Luciferase) en repeteereiwitten (bijv. 4MBP en 4 α -synuclein). Door te meten aan een enkel eiwit kan het vouwen worden bestudeerd zonder dat de eiwitten gaan aggregaten terwijl met repeteereiwitten juist de aggregatie en het uiteenvallen van het aggregaat rechtstreeks kan worden gevolgd.

In hoofdstukken 3 en 4 onderzoeken we de rol van kleine Hsps (sHsps) chaperonne-eiwitten bij het voorkomen van aggregatie. sHsps staan bekend als holdases welke een interactie met ongevouwen eiwitten aangaan en aan de frontlinie staan in het tegengaan van eiwitaggregatie. In hoofdstuk 3 bestuderen we de interactie tussen gist Hsp42 en eiwit aggregaten met behulp van het 4MBP construct. Mijn bevindingen

tonen aan dat Hsp42 de vorming van intra-domein verbindingen binnen het eiwit verhindert en het hervouwen naar de natuurlijke staat via de interactie met de gevouwen toestand bevordert. Onderzoek aan het vouwen van MBP bestaande uit een enkel domein suggereert dat Hsp42 bindt aan de gevouwen conformatie van MBP omdat er gedestabiliseerde hervouwen structuren worden gedetecteerd in een oplossing met Hsp42. Daarna, in hoofdstuk 4, wordt de functie van sHsps bepaald door onderzoek naar de interactie tussen het menselijke HspB6 en het repetiteer construct 4 α synuclein. α -synuclein is bekend om zijn vorming van zeer geordende aggregaten en komt tot uitdrukking in de zenuwweefsels van gewervelden, waaronder mensen. HspB6 heeft een hoge affiniteit voor de gevouwen toestand van 4 α synuclein omdat het de vorming van compacte structuren stimuleert en het geforceerd ontvouwen bemoeilijkt. Het binden aan de gevouwen toestand blijkt een algemeen kenmerk van HspB6 te zijn omdat het ook de gevouwen toestand van MBP met zijn bekende tertiaire structuur stabiliseert.

In Hoofdstuk 5 richt ik me op de moleculaire mechanismen achter de werking van gist Hsp33, een redox gereguleerd chaperonne-eiwit dat ook als een holdase bekend staat. Op het niveau van een enkel molecuul stabiliseert Hsp33 eiwitketens in de ongevouwen en niet geaggregeerde toestand, maar bevordert ook het gedeeltelijk hervouwen van monomeren boven de aggregatie tussen monomeren. Mechanische verstoring van hervouwende monomeren in de aanwezigheid van chaperonne-eiwitten toont aan dat Hsp33 bindt aan een toestand langs het pad tussen de gevouwen en ontvouwen conformaties en deze toestand vervormt. Daarbij voorkomt Hsp33 dat het eiwit ontvouwt en blokkeert het bovendien de transitie naar de natuurlijke toestand. We gebruiken een statistisch mechanisch model om de competitie tussen vouwen, aggregatie en binding transities te bepalen. Verder kunnen we met dit model, zonder fitten, het effect van de Hsp33 op de interacterende MBP moleculen voorspellen.

In hoofdstuk 6 bestudeer ik de mechanische functie van de ATP afhankelijke Hsp90 familie, waar ik de nadruk leg de prokaryotische homoloog HtpG. Het ontvouwen en hervouwen van het model eiwit Luciferase wordt onderzocht in de aanwezigheid van HtpG. Ik laat zien dat HtpG afhankelijk van ATP stapsgewijs ketting structuren kan bevorderen die voor langere tijd stabiel zijn en tegen externe krachten bestand zijn. Daarnaast onderdrukken de acties van HtpG het onjuiste vouwen van de intra- en inter-domeinen. Deze ontdekking is van groot belang voor de talrijke fysiologische functies van Hsp90.

Over het geheel genomen laat mijn onderzoek, op het niveau van een enkel eiwit, nieuwe mechanismen van de werking van chaperonne-eiwitten zien. Daarnaast toon ik aan dat chaperonnes een veel breder scala aan functies hebben dan eerder gedacht.

Acknowledgments

The names presented in this chapter are in no particular order.

مَنّتِ خدای را عزوجل که طاعتش موجب قُرْبَت و به شکر اندرش مزید نعمت. هر نفسی که
فرومی رود مدّ حیاتست و چون برمی آید مفرح ذات، پس در هر نفسی دو نعمت موجودست و
بر هر نعمت شُکری واجب.

سعدی علیه الرحمه

As a person, fascinated by science, doing a PhD was always a planned part of my life. However, I am not quite sure if I was truly aware of the real uncertainties and ups and downs that one typically encounters during the course of a PhD. Now, looking 4.5 years back, I think the place that I chose to do my PhD and the people that surrounded me during this time, made it possible for me to overcome these difficulties. Luckily, I came to Amolf, a great place to work at with many motivated, talented and supportive young scientists. The professional technical and administrative supports, beside the constructive atmosphere have made Amolf an amazing place to do science. First thanks to Amolf and all of the nice Amolfers!

Sander, you are the person who gave me the great opportunity of joining Amolf and your research group. I entered your group as an ambitious student without solid experimental background and I am now leaving the group as a scientist with many experimental and analytical experiences that knows how science works. Thank you for your support and all the essential skills you taught me.

Next, I want to thank all the current and former members of biophysics group, from the single-molecule to the single-cell part. **Alireza**, I have been always inspired by your attitude to science and also life. I believe that knowing you has been a great chance in my scientific life. I learned from you how to handle the tweezers experiments and wrote my first paper with you. Thank you for all the fruitful and motivating discussions during your stay at Amolf and also afterwards. **Sergey and Roeland**, I enjoyed working with you and I am thankful for all the great scientific input. **Arif**, you joined the lab during a frustrating time and we got many slaps in our faces from the single-molecule set-up. I admire all your efforts and the discussions that we had to get the experiment running again. **David**, you are a pool of information about proteins and biochemistry. To get a proper fish out of this pool, your colleagues should be really experienced in fishing. **Mario**, a good friend and a talented colleague with strong opinions, It was a pleasure to work with you. Thank you also for making nice figures for the HtpG paper. **Mohsin**, we had a short time to work together but it was productive. Thank you for all your help in finalizing the control experiments. **Eline and Florian**, I did not find the chance of working with you guys but I am sure you will make a great contribution to the group. **Noreen**, my lovely group-mate, office-mate, and friend we started this PhD adventure almost at the same time and went through so much together. Thank you for listening to me during the more difficult days of my PhD life and your support and empathy. **Katja**, I really love your critical way of thinking and independence. You were always my role model as a strong knowledgeable female scientist. **Vanda**, thank you for all your help and support in the lab and also your always positive vibes and willingness to listen to our never-ending PhD traumas. **Marjon, Phillippe, Sarah, Sebastian, Dimitry, Rutger, Martijn, and Donny** thank you all for the great moments together and helpful discussions during our group meetings.

During my PhD, I have had the chance of collaborating with outstanding researchers all over the world. **Bernd Bukau, Matthias Mayer, Guenter Kramer, Axel Mogk, and Sophia Mende**, from the University of Heidelberg, **Kingshuk Ghosh**, from the University of Denver, **Ursula Jakob**, from the University of Michigan, **Rachel Klevit**, from the University of Washington, **Michael Woodside** from the University of Alberta, **Vinod Subramaniam, and Aditya**

Iyer from the University of Twente (and Amolf), I am grateful to all your experimental contributions, scientific discussions, and critical input, without which the research in this thesis would not have been possible.

Joris, my Mathematica hero, thank you for always being kind and open in helping me solve the crazy equations. I enjoyed all the cuppa times and game nights that we had with you, **Martijn, Aditya V., Noreen and Stephen**. You guys have been kind to me during my stay at Amolf and I really appreciate it. Special thanks to **Martijn and Joris** for writing the dutch summary of my thesis. **Olga, Aditya V., and Cristina**, my lovely office-mates, thank you for keeping our office warm and welcoming.

Parisa K., Maga, Simone, Nuria, Agata, Ioanna, Milena, Feng, Clara, Johannes, Jacopo, Michele, Florian, Felipe, Jeanette, Tomak, Andrew, Aditya I., Yuval, Nicola, Poulomi, Keita, Pierre, Jose, Liselotte, Anders, Adelina, Corianne, Bob, Celine, Jenny, Baldo, Federica, Galja, Katharina, Viktoria, and Felicio, I spent a wonderful time at Amolf with you, shared a lot of laughs and enjoyed the coffee discussions. I am thankful for having met you.

Willem, Juliette, Wiebe, Henk-Jan, Peer, Marjolein, Yvonne, Silvia, and Andre, thank you for your support and big smiles that energized my days at Amolf.

Special thanks to my Iranian community in Amsterdam. **Sara and Vahid**, I really felt Amsterdam as home when I met you guys. I assume you as one of the valued things that I gained by moving to Amsterdam. **Marzi, Hodjat, Narges, Shayan** (remarkable thanks for teaching me how to use Latex and your self-made template), **Marzieh N., Mehdi H., Abbas, Danial** (especial thanks for designing the cover), **Sareh, Naser M.A., Saeideh, Mohammad-Ali, Azadeh, and Ali C.** (big thanks for fruitful discussions on quality control systems), you played the role of my family during past years and forced me to have a social life in the most intense days of the PhD. **Avid, Saba, Behsa, and Samin**, you little girls do not know how much happiness and joy you brought to our community. Love you all. **Maryam Babur** (no way to exclude you from my Iranian community ;)), **Mohammad Y., Elham, Seyyed Esmail, Samira, Mahdi J., Mahsa V., Mohammad R., Parisa K., Fatemeh S., Afshin, Zahra, Mohammad Hosein R., Aylar, Naser A., Mahdieh, Mahdi S., Fahimeh, Mohammad S., Andisheh, Saeed, Rokhsareh, Mehrsima, Marzieh F., Hammidreza, Parisa S., Seyyed Amin, Maryam P., Mohammad J., Jafar, Leila, Mina, Amir, Shima, Behrooz, Abolfazl, Fereshteh, Mahsa G., Farzin, Narges J., Nasibeh, Hoda A.**, (and others that I forgot to mention here,) you have supported me during my life in Amsterdam, maybe without even knowing it. I am truly happy to have you as friends.

Finally, I want to thank to my family! **Baba**, you are one of the kindest men I have ever met. With you, I have always felt supported in my life. **Maman**, you taught me to be strong and find a way to pass each and every difficulty. **Mojtaba**, my younger brother, you brought light and joy to our family life. We just ourselves know that our hot brother-sister discussions are our unique way of loving each other!

The most new member of our family, my little one **Dana**, I really cannot wait to

have you in my arms sweetie. Being your mother is a deep feeling of hopes and fears that I cannot explain it. I wish the world would be a better place for you and your generation.

And the last, but not the least, thanks to ***Mohammad-Amin***, my man of life, for infinitive love, no matter what. I love you with all my heart!

Fatemeh Moayed
March 2016, Amsterdam

Publications

1. **F. Moayed**, A. Mashaghi, S. J. Tans. *Functional and design principles of molecular chaperones*. Manuscript in preparation. Chapter 1.
2. **F. Moayed***, A. Mashaghi*, S. J. Tans. *A Polypeptide-DNA Hybrid with Selective Linking Capability Applied to Single Molecule Nano-Mechanical Measurements Using Optical Tweezers*. PloS one 8.1 (2013): e54440. Chapter 2.
3. S. Ungelenk, **F. Moayed**, A. Scharf, A. Mashaghi, S. J. Tans, M. Mayer, A. Mogk, B. Bukau. *Small heat shock proteins preserve aggregating proteins in native-like conformation*. Submitted to Nature Communications. Chapter 3.
4. S. Bezrukavnikova, **F. Moayed**, A. Iyer, V. Subramaniam, R. E. Klevit, M. Woodside, S. J. Tans. *Small heat shock protein HspB6 facilitates the compaction of α -synuclein*. Manuscript in preparation. Chapter 4.
5. **F. Moayed**, S. Bezrukavnikov, C. Cremers, G. Kramer, K. Ghosh, U. Jakob, S. J. Tans. *Aggregation suppression by the chaperone Hsp33 at the single molecule level*. Submitted to PNAS. Chapter 5.
6. **F. Moayed***, A. Mashaghi*, G. Kramer, M. Mayer, S. J. Tans. *Direct observation of Hsp90-induced conformational changes in a protein chain*. Manuscript in preparation. Chapter 6.

*Equal contributions

